

**The AMP activated protein kinase in the  
regulation of sodium coupled transporters  
(SGLT1, EAAT3 & EAAT4) and  
eryptosis**

der Fakultät für Biologie  
der **EBERHARD KARLS UNIVERSITÄT TÜBINGEN**  
zur Erlangung des Grades eines Doktors  
der Naturwissenschaften

von

**Mentor Sopjani**

aus Harilaq, Kosova

vorgelegte

**DISSERTATION**

2010

Tag der mündlichen Prüfung:

03. 03. 2010

Dekan:

**Prof. Dr. Hanspeter A. Mallot**

1. Berichterstatter:

**Prof. Dr. Florian Lang**

2. Berichterstatter:

**Prof. Dr. Friedrich Götz**

*“The miracle is not that we do this work, but that we are happy to do it“*

Mother Teresa (Agnesë Gonxhe Bojaxhiu)

# Table of contents

<b>Acknowledgements .....</b>	<b>8</b>
<b>List of figures and tables .....</b>	<b>10</b>
<b>List of abbreviations .....</b>	<b>13</b>
<b>1 Introduction .....</b>	<b>17</b>
1.1 General view of Red Blood Cells .....	17
1.1.1 Red blood cells regulation .....	18
1.1.2 Ionic distribution across the red cell membrane .....	20
1.1.3 Nonselective cation channels .....	21
1.1.4 $\text{Ca}^{2+}$ homeostasis of erythrocytes .....	21
1.1.5 Dehydration of erythrocytes .....	21
1.1.5.1 Gárdos $\text{K}^+$ channels activated by $\text{Ca}^{2+}$ .....	22
1.1.5.2 The erythrocytic $\text{KCl}$ cotransporter .....	23
1.1.5.3 $\text{Na}^+/\text{K}^+$ pump of the erythrocytes .....	24
1.2 Eryptosis signaling pathways .....	25
1.2.1 Cell death of nucleated cells .....	25
1.2.2 Mechanisms of eryptosis .....	25
1.2.2.1 $\text{PGE}_2$ formation by $\text{COX}$ activation and activation of the cation channel .....	26
1.2.2.2 Sphingomyelinase stimulation by $\text{PAF}$ formation .....	28
1.2.2.3 Phosphatidylserine movement .....	29
1.2.2.4 RBCs phosphatidylserine exposure recognized by macrophages .....	32
1.3 Glucose transporter families .....	33
1.3.1 Sodium-coupled Glucose (Co) Transporter (SGLT1) .....	33
1.4 Glutamatergic neurotransmission .....	35
1.4.1 Excitatory Amino Acid Transporters (EAATs) .....	37
1.4.1.1 Excitatory Amino Acid Transporter 3 (EAAT3) .....	39
1.4.1.2 Excitatory Amino Acid Transporter 4 (EAAT4) .....	39
1.5 AMP-activated protein kinase a key regulator of energy balance .....	41
1.5.1 Structure and regulation of AMP-activated protein kinase .....	41
1.5.2 Regulation of erythrocyte survival by AMP-activated protein kinase .....	44
1.5.3 Regulation of $\text{Na}^+$ -coupled glucose carrier by AMP-activated protein kinase .....	44
1.5.4 Downregulation of $\text{Na}^+$ -coupled glutamate transporter EAAT3 and EAAT4 by AMP-activated protein kinase .....	45
1.6 Aims of the study .....	47

<b>2</b>	<b>Materials and Methods.....</b>	<b>49</b>
2.1	Materials.....	49
2.1.1	Equipments.....	49
2.1.2	Chemicals.....	50
2.1.3	Antibodies.....	52
2.1.4	Kits.....	53
2.1.5	Stock materials.....	54
2.1.6	Human erythrocytes.....	54
2.1.7	Mice.....	54
2.1.8	<i>Xenopus laevis</i> .....	55
2.1.9	Software.....	55
2.2	Methods.....	56
2.2.1	Regulation of erythrocyte survival by AMP-activated protein kinase.....	56
2.2.1.1	Blood chemistry, blood count, and isolation of murine erythrocytes.....	56
2.2.1.2	Western blotting.....	56
2.2.1.3	Confocal microscopy and immunofluorescence.....	57
2.2.1.4	Incubations and solutions.....	57
2.2.1.5	Determination of the osmotic resistance.....	58
2.2.1.6	Phosphatidylserine exposure and forward scatter.....	58
2.2.1.7	Measurement of intracellular Ca <sup>2+</sup> .....	58
2.2.1.8	Measurement of the in vivo clearance of fluorescence-labeled erythrocytes ..	58
2.2.1.9	Statistics.....	59
2.2.2	Site Directed Mutagenesis.....	60
2.2.2.1	Transformation of E.coli XL1-Blue Supercompetent Cells.....	61
2.2.3	Preparation of cRNA.....	62
2.2.3.1	Plasmid DNA linearization.....	62
2.2.3.2	cRNA synthesis.....	63
2.2.3.3	<i>Xenopus laevis</i> oocyte preparation and maintenance.....	64
2.2.4	Protein expression in <i>Xenopus laevis</i> oocyte.....	66
2.2.5	Two-electrode-voltage clamp.....	67
2.2.6	Tracer flux measurements.....	68
2.2.7	Regulation of Na <sup>+</sup> -coupled glucose carrier SGLT1 by AMP-activated protein kinase.....	69
2.2.7.1	Constructs.....	69
2.2.7.2	Voltage clamp in <i>Xenopus</i> oocytes.....	69

2.2.7.3	Immunofluorescence .....	70
2.2.7.4	Biotinylation and Western blot analysis .....	71
2.2.7.5	Statistical analysis.....	72
2.2.8	Downregulation of Na <sup>+</sup> -coupled glutamate transporter EAAT3 and EAAT4 by AMP-activated protein kinase.....	72
2.2.8.1	Constructs.....	72
2.2.8.2	Voltage clamp in <i>Xenopus</i> oocytes .....	72
2.2.8.3	Immunohistochemistry.....	73
2.2.8.4	Detection of EAAT cell surface expression by chemiluminescence .....	74
2.2.8.5	Statistical analysis.....	75
<b>3</b>	<b>Results .....</b>	<b>76</b>
3.1	AMP-activated protein kinase regulates erythrocyte survival.....	76
3.1.1	Expression of AMP-activated protein kinase in erythrocytes .....	76
3.1.2	Compound C increased cytosolic Ca <sup>2+</sup> concentration and caused eryptosis in glucose depletion of RBCs .....	77
3.1.3	AICAR decreased while compound C increased phosphatidylserine exposure in ionomycin treated erythrocytes .....	79
3.1.4	AMPK-deficient mice exhibit anemia .....	80
3.1.5	AMPK $\alpha$ 1-deficient mice enhanced suicidal erythrocyte death.....	82
3.1.6	Accelerated erythrocyte clearance in AMPK $\alpha$ 1-deficient mice.....	83
3.1.7	Splenomegaly in AMPK $\alpha$ 1-deficient mice .....	84
3.2	AMP activated protein kinase regulate Na <sup>+</sup> -coupled glucose carrier SGLT1 .....	86
3.2.1	Constitutively active AMPK stimulates SGLT1-mediated electrogenic glucose transport.....	86
3.2.2	The dead mutant <sup>K45R</sup> AMPK did not stimulate SGLT1 and blunted the stimulating effect of AMPK.....	87
3.2.3	AMPK enhanced the maximal current.....	88
3.2.4	SGLT1 protein abundance is enhanced by activation of AMPK .....	89
3.3	AMPK downregulates Na <sup>+</sup> -coupled glutamate transporter EAAT3 and EAAT4 .....	92
3.3.1	Constitutively active AMPK downregulated EAAT3-mediated electrogenic glutamate transport .....	92
3.3.2	AMPK decreased the maximal glutamate-induced current in EAAT3-expressing oocytes .....	94
3.3.3	AMPK decreased the EAAT3 cell plasma membrane protein abundance .....	94
3.3.4	Constitutively active AMPK downregulated EAAT4-mediated electrogenic glutamate transport .....	95

3.3.5	AMPK decreased the maximal glutamate-induced current in EAAT4-expressing oocytes .....	98
3.3.6	AMPK decreased the EAAT4 cell plasma membrane protein abundance .....	98
<b>4</b>	<b>Discussion.....</b>	<b>100</b>
4.1	Regulation of erythrocyte survival by AMP-activated protein kinase.....	100
4.2	Upregulation of Na <sup>+</sup> -coupled glucose carrier SGLT1 by AMPK.....	102
4.3	Downregulation of Na <sup>+</sup> -coupled glutamate transporter EAAT3 and EAAT4 by AMP-activated protein kinase .....	103
<b>5</b>	<b>Conclusions .....</b>	<b>105</b>
<b>6</b>	<b>Summary .....</b>	<b>106</b>
<b>7</b>	<b>Zusammenfassung .....</b>	<b>108</b>
<b>8</b>	<b>References .....</b>	<b>110</b>
<b>9</b>	<b>Publications.....</b>	<b>129</b>
<b>10</b>	<b>Curriculum vitae .....</b>	<b>132</b>

## **Acknowledgements**

I hereby wish to express my deep recognition and appreciation for the tremendous opportunity to complete my thesis at the Institute of Physiology of the Eberhard-Karls-University in Tübingen, Germany.

I am especially indebted to my supervisor Prof. Dr. **Florian Lang** for introducing me in the fascinating topics of both eryptosis and electrophysiology in the exciting field of molecular cell biology. Furthermore, I wish to express my deep sense of gratitude to him for his scientific guidance, mentoring, critical review, encouraging and support throughout my Ph.D. at the Institute of Physiology.

I acknowledge my sincere thanks to my wife Mrs. **Miribane Dërmaku-Sopjani** for her support, understanding, encouragement, and her scientific advice during our daily work.

I am greatly indebted to Dr. **Michael Föller** for provoking suggestions and stimulating discussions during the progress of the research and his help to overcome all experimental difficulties during our almost daily discussions.

I would like to thank Prof. Dr. **Friedrich Götz**, Dept. of Microbial Genetics, Faculty of Biology for accepting and giving me an opportunity to present the dissertation at the Faculty of Biology, Eberhard Karls Universität Tübingen, Germany.

My heartfelt thanks go to Dr. **Rexhep Rexhepaj**, especially for his scientific support and useful criticism, as well as for his encouragement throughout my work.

My special thanks go to Prof. Dr. **Monica Palmada** and Dr. **Ekaterina Shumilina**, for their thesis corrections, suggestions, criticism and scientific support.

I thank my lab. colleagues Mrs. **Iris Brillhaus**, Miss. **Ioana Alesutan**, Dr. **Saisudha Koka**, Dr. **Shafalee K. Bhavsar**, Dr. **Oana Ureche**, Mr. **Jan Wilmes**, Mr. **Carlos Muñoz**, Mr. **Gulab Siraskar** and Miss. **Shuchen Gu** for their help, supportive suggestions, and encouragement.

Finally, I would like to thank all other colleagues of the Institute of Physiology as well as technical staff of the institute, especially Mrs. **Elfirade Faber**, Mr. **Uwe Schüller**, Miss **Vanessa Schnor**, Mr. **Peter Durr**, Mrs. **Lejla Subasic**, Mrs. **Tanja Loch**, Mrs. **Sari Rube** and Mr. **Faruk Subasic** for their kind cooperation, valuable help and support.



I wish to express my deep sense of gratitude to Prof.Dr. **Muharrem Jakupaj** as well as to my friend Mr.sc. **Ramadan Sopi** for their support, and encouragement throughout all of my research.

This task never completes without the mention of my loving family. I am deeply indebted for being a constant source of inspiration, support and endless love for me.

I dedicate my thesis to my family!

## **List of figures and tables**

### **Introduction**

1. Table 1.1.1<sub>Introd.</sub> Normal values of major electrolytes in human plasma.
2. Figure 1.21.1<sub>Introd.</sub> A. Heterotetrameric structure of hemoglobin. B. Heme group.
3. Figure 1.2.2.1<sub>Introd.</sub> Synopsis of eryptosis signaling.
4. Figure 1.2.2.3<sub>Introd.</sub> Phospholipids are arranged asymmetrically in the most membranes, including the human RBCs membrane leaflets, as shown here. Values are mole percentage.
5. Figure 1.2.2.4<sub>Introd.</sub> The regulation and physiology of membrane phospholipids asymmetry.
6. Figure 1.3.1<sub>Introd.</sub> Role of SGLT1 symporter in a model for glucose (and galactose) absorption across a mature enterocyte from the upper villus of the small intestine.
7. Figure 1.4.1<sub>Introd.</sub> Glutamate transporters and glutamatergic synapses.
8. Figure 1.5.1<sub>Introd.</sub> Subunit interactions involved in the activation of AMPK by phosphorylation and by allosteric regulation by 5'-AMP as well as its structure and regulation of AMPK.

### **Materials and methods**

9. Table 2.2.2.A<sub>Method.</sub> Forward and reverse primers used to generate EAAT4-HA.
10. Table 2.2.2.B<sub>Method.</sub> Polymerase Chain Reaction mixture for two-stage PCR site-directed mutagenesis.
11. Table 2.2.3.1A<sub>Method.</sub> Plasmids containing the desired genes encoding for specific proteins and restriction endonuclease enzymes used to linearize each plasmid.
12. Table 2.2.3.1.B<sub>Method.</sub> Reaction mixture used to linearize DNA plasmid.
13. Table 2.2.3.2.A<sub>Method.</sub> Reaction mixture used to synthesize RNA from the linearized DNA.
14. Table 2.2.3.2.B<sub>Method.</sub> RNA polymerases used to prepare cRNA and amount of cRNA injected into oocytes.

15. Figure 2.2.3.3<sub>Method</sub>. An overview of oocytes preparation, cRNA injection, protein expression in oocytes, and TEVC measurement.
16. Table 2.2.6<sub>Method</sub>. Types of solutions used in two electrode voltage clamp experiments. Figure
17. Figure 2.2.8.3<sub>Method</sub>. Overall view of an immunohistochemistry based cell membrane transporter abundance experiment.
18. Figure 2.2.8.4<sub>Method</sub>. General view of a chemiluminescence-based cell surface experiment.

## **Results**

19. Figure 3.1.1. Expression of AMPK in erythrocytes.
20. Figure 3.1.2. Cytosolic Ca<sup>2+</sup> concentration and eryptosis with or without glucose depletion in the presence and absence of compound C.
21. Figure 3.1.3. Phosphatidylserine exposure of erythrocytes with or without ionomycin in the presence and absence of AICAR and compound C.
22. Figure 3.1.4. Anemia in AMPK $\alpha$ 1-deficient mice.
23. Figure 3.1.5. Enhanced eryptosis of erythrocytes from AMPK $\alpha$ 1-deficient mice.
24. Figure 3.1.6. Accelerated erythrocyte clearance of erythrocytes in AMPK $\alpha$ 1-deficient mice.
25. Figure 3.1.7. Splenomegaly associated with increased erythroid cell mass in AMPK $\alpha$ 1-deficient mice.
26. Figure 3.2.1. Coexpression of  $\gamma^{R70Q}$ AMPK stimulated electrogenic glucose transport in SGLT1-expressing *Xenopus* oocytes.
27. Figure 3.2.2. The catalytically inactive mutant  $K^{45R}$ AMPK did not stimulate SGLT1
28. Figure 3.2.3. AMPK enhanced the maximal current without appreciably affecting affinity.
29. Figure 3.2.4. Cell surface SGLT1 protein abundance in Caco2 cells was upregulated by the AMPK activator AICAR.
30. Figure 3.2.5. Cell surface SGLT1 protein abundance in Caco2 cells was similarly upregulated by phenformin and A-769662.

31. Figure 3.3.1. Coexpression of <sup>R70Q</sup>AMPK decreased electrogenic glutamate transport in EAAT3-expressing *Xenopus* oocytes.
32. Figure 3.3.2. AMPK decreased the EAAT3 maximal current without appreciably affecting affinity.
33. Figure 3.3.3. Coexpression of <sup>R70Q</sup>AMPK decreased cell surface EAAT3 protein abundance.
34. Figure 3.3.4. Coexpression of <sup>R70Q</sup>AMPK decreased electrogenic glutamate transport in EAAT4-expressing *Xenopus* oocytes.
35. Figure 3.3.5. AMPK decreased the EAAT4 maximal current without appreciably affecting affinity.
36. Figure 3.3.6. Coexpression of <sup>R70Q</sup>AMPK decreased cell surface EAAT4 protein abundance.

## **List of abbreviations**

[Ca <sup>2+</sup> ] <sub>i</sub>	(free) cytosolic ionic calcium concentration
μg	Micro gram
μl	Micro liter
μM	Micro molar
ACC	Acetyl-CoA carboxylase
ADP	Adenosine di phosphate
Akt/PKB	Protein kinase B
AMP	Adenosine mono phosphate
AMPK	AMP-activated protein kinase
Annexin	Annexin V-Fluos
ASM	Acid sphingomyelinase
ATP	Adenosine tri phosphate
BPG	1.3-bisphosphoglycerate
BSA	Bovine serum albumin
bw	Body weight
CaMKK	Ca <sup>2+</sup> /calmodulin-dependent protein kinase kinase
cAMP	Cyclic adenosine monophosphate
CBS	Cystathionine β-synthase
CFSE	Carboxyfluorescein Succinimidyl Ester
COX	Cyclooxygenase
cRNA	Complementary ribonucleic acid
Ctr	Control
Da	Dalton
DAG	Diacylglycerol
EAAT	Excitatory amino acid transporter/s
EDTA	Ethylenediaminetetraacetic acid
EIPA	5-(N-ethyl-N-isopropyl) Amiloride
ENaC	Epithelial sodium channel

FACS	Fluorescence-activated cell sorting
FITC	Fluorescein isothiocyanate
Fluo	Fluo-3/AM
FSC	Forward scatter
FSH	Follicle stimulating hormone
G6PDH	Glucose-6-phosphate dehydrogenase
GAPDH	Glycerinaldehyd-3-phosphat-dehydrogenase
Gárdos channel	Calcium activated potassium channel
Gcat	Nonselective cation conductance
Glc	Glucose
Gln	Glutamine
Glu	Glutamate
GSH	Gluthathione
GSSG	Oxidized gluthathione
GTP	Guanosine triphosphate
h	Hour/s
HA	Haemagglutinin
Hb	Hemoglobin
HCT	Hematocrit
HEK	Human embryonic kidney cells
HEPES	4-(2-Hydroxyethyl)-1-Piperazineethanesulfonic acid
HGB	Hemoglobin concentration
HMG-CoA reductase, HMGR	3-hydroxy-3-methylglutaryl-CoA reductase
i.v.	Intravenous
Ig	Immunoglobulin
IGF-1	Insulin-like growth factor-1
IL	Interleukin
IONO	Ionomycin
K <sub>M</sub>	Michaelis constant
KO	Knockout

LKB1	Serine/threonine kinase 11
MCH	Mean corpuscular hemoglobin
MCHC	Mean corpuscular hemoglobin concentration
MCV	Mean corpuscular volume
ND-96	Physiological solution
Nedd4-2	Neuronal cell expressed developmentally downregulated 4-2
NFDM/TBS	Non-fat dried milk in Tris-buffered saline
NMDA	N-methyl-D-aspartate
NO	Nitric oxide
NSC	Nonselective cation
NSM	Neutral sphingomyelinase
°C	Degree(s) celsius (centigrade)
OR2	Solution
<i>P</i>	Permselectivity
P2X7	Purinergic receptor P2X, ligand-gated ion channel, 7
PAF	Platelet activation factor
PBS	Phosphate buffered saline
PC	Phosphatidylcholine
PC	Purkinje cells
PCR	Polymerase chain reaction
PDGF	Platelet derived growth factor
PDK	3-phosphoinositide-dependent protein kinase
PE	Phosphatidylethanolamine
PG	Prostaglandin
PGE <sub>2</sub>	Prostaglandin E <sub>2</sub>
PI3K	Phosphatidylinositol 3-kinase
PK	Protein kinase
PKA	Protein kinase A
PKC	Protein kinase C
PL	Phospholipase
PS	Phosphatidylserine

PVDF	Polyvinylidene difluoride
RBC	Red blood cell
RDW	Red cell distribution width
Ringer	Buffer solution
RT	Room temperature
SDS-PAGE	Sodium dodecyl sulfate polyacrylamide gel electrophoresis
SEM	Standard error of the mean
SGK	Serum and glucocorticoid inducible protein kinase
SLC	Solute carrier
SM	Sphingomyelin
SS cells	Sickle-cell (disease) cells
TAK1	Transforming growth factor- $\beta$ -activated kinase 1
TM	Transmembrane domain
TRPC6	Transient receptor potential cation channel, subfamily C, member 6
VGLUT	Vesicular glutamate transporter
WBC	White blood cells
WT	Wild type



# 1 Introduction

## 1.1 General view of Red Blood Cells

Among any cell type of the human body, human erythrocytes have the highest soluble protein concentrations. The major intracellular protein of RBCs is hemoglobin with an intracellular concentration of approximately 7.2 mM Hb/l cell water <sup>1</sup>. The ability of normal erythrocytes to rapidly change their shape in response to fluid shear stresses is governed by cytoplasm viscosity, which is determined by intracellular hemoglobin concentration <sup>2</sup>. In humans, as in all mammals, the mature RBCs are *enucleated* when mature (they lack a cell nucleus and have no DNA). They also lose their other organelles such as mitochondria, endoplasmic reticulum and ribosome's. An advantage of enucleating is that the cell now has increased space to store hemoglobin, the oxygen-binding protein, enabling the RBC to transport additional oxygen. Disadvantages center around the inability to produce and repair structural proteins or enzymes which limits their lifespan. The morphology of RBCs is similar to biconcave discs (flattened and depressed in the center, with a dumbbell-shaped cross section) with an impressive mechanical flexibility of RBC morphology. Additionally, this shape increases surface area (app. 40% compared with a sphere of the same volume) and allows better diffusion of oxygen across the surfaces <sup>2-5</sup>.

Erythrocytes produce energy by fermentation via glycolysis. Their glucose uptake (by Glut1) is not regulated by insulin due to the lack of insulin-dependent transporters <sup>4,5</sup>.

Erythrocytes are highly water-permeable sacs ensuring continued osmotic equilibrium in plasma. Volume changes, such as shrinking or swelling only occur by the loss or gain of a fluid isosmotically exchanged with surrounding plasma, resulting in additional mechanical flexibility. Since the plasma protein concentration is more than 1 mM, a powerful oncotic pressure drives water into the cells. To remain osmotically stable over their app. 120-day circulatory life-span, mature RBCs have evolved a strategy of homeostatic balance in order to regulate and maintain their cell volume with minimal energy expenditure <sup>1,6</sup>.

### 1.1.1 Red blood cells regulation

Erythrocytes are suspended in plasma, its electrolyte compositions is as represented in Table nr. 1.1.1.

**Table 1.1.1** Introd. Normal values of major electrolytes in human plasma <sup>7</sup>.

<b>Cations</b>	<b><i>mM</i></b>	<b>Anions</b>	<b><i>mM</i></b>
Na <sup>+</sup>	142	Cl <sup>-</sup>	104
K <sup>+</sup>	4.5	HCO <sub>3</sub> <sup>-</sup>	24
Ca <sup>2+</sup>	2.5	HPO <sub>4</sub> <sup>2-</sup>	2
Mg	1	Proteins	14 (66-83g/l)
<b>Total</b>	<b>150</b>	Other	6
		<b>Total</b>	<b>150</b>

The diameter of a typical human erythrocyte is 6-8 μm. They are small enough to pass through the smallest blood vessels. A typical erythrocyte contains about 270 million hemoglobin molecules with each carrying four heme groups. The tetrameric hemoglobin molecule (Figure 1.1.1.A), makes up to 97.5% of the total cell protein by weight <sup>8</sup>.

Tetrameric hemoglobin molecules consist of four polypeptide chains: 2 α chains (141 amino acids each) and 2 β chains (each 146 amino acids). Each chain contains an iron molecule known as heme that binds oxygen. (Fig. 1.1.1. B) <sup>9</sup>.

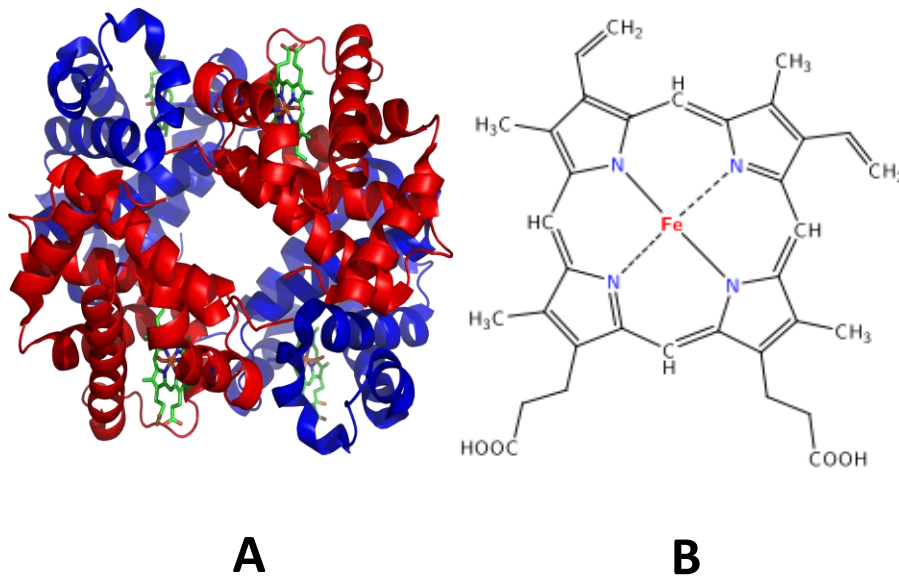


**Figure 1.1.1** Introd. **A. Heterotetrameric structure of hemoglobin.** The protein subunits are in red ( $\alpha$  chains) and blue ( $\beta$  chains), and the iron containing heme groups in green<sup>10</sup> **B. Heme group.**

The red blood cells of an average adult human male store collectively about 2.5 g of iron, representing about 65% of the total iron contained in the body. Throughout erythropoiesis (RBCs production process), erythrocytes are continuously produced in the red bone marrow of large bones at a rate of about 2-3 million per second (in the embryo, RBCs production is mainly localized in the liver). The production can be stimulated by the hormone erythropoietin (EPO), synthesized and secreted by kidney cells as a response to a lack of oxygen or a shortage of erythrocytes. In the transition stage in and out of the bone marrow, the RBCs are known as reticulocytes, which constitute about 1% of circulating RBCs. Erythrocytes develop from committed stem cells through reticulocytes to mature erythrocytes in about 7 days and live about 120 days. Aging erythrocytes undergo changes in their plasma membrane, making them susceptible to phagocyte recognition and subsequent phagocytosis in the spleen, liver and bone marrow. Young erythrocytes have a surface protein that binds to an inhibitory receptor on macrophages and thereby prevents phagocytosis<sup>4,8</sup>.

### 1.1.2 Ionic distribution across the red cell membrane

The transmembrane ionic distribution of an erythrocyte is accomplished by various pumps, transporters and cation channels. Ion distribution is intimately linked to various functional characteristics. Erythrocytes maintain high intracellular  $K^+$  and  $Cl^-$  concentrations whereas the intracellular  $Na^+$  and  $Ca^{2+}$  concentrations are low. The cation gradients across the erythrocyte membrane are set up by the two ATP-dependent pumps  $Na^+/K^+$  ATPase and the  $Ca^{2+}$  ATPase<sup>11</sup>.

The list below contains the transport pathways that facilitate and assist transmembrane transport of  $K^+$  ions<sup>2,11</sup>:

- $Na^+/K^+$  ATPase
- $Na^+/K^+/2Cl^-$  cotransporter
- $K^+/Cl^-$  cotransporter
- The Gárdos channel
- $Na^+-K^+$  cotransporter
- $Ca^{2+}$  ATPase
- Band 3 anion exchanger
- Glut1 (glucose and L-dehydroascorbic acid transporter)

Membrane proteins with transport function include also<sup>2</sup>:

- Aquaporin 1 (water transporter)
- Kidd antigen protein (urea transporter)
- RhAG (gas transporter, probably of carbon dioxide)
- $Na^+-Cl^-$  cotransporter

The unidirectional fluxes in mature normal erythrocyte membrane for  $Na^+$  and  $K^+$  are extremely low ( $\sim 2-3 \text{ mmol} \cdot \text{l original cells}^{-1} \cdot \text{h}^{-1}$ , “*Original*” means that measured fluxes are referred to as 1 liter of normal, packed RBCs at the beginning of an experiment), whereas in reticulocytes membrane permeability may be 10 to 30 times higher. As a consequence, a relatively small number of ATP-driven  $Na^+/K^+$  pumps per cell are sufficient to counteract the basal cation gradient-driven “leaks”<sup>1</sup>.

Moreover, based on high  $Cl^-$  and  $HCO_3^-$  exchange and electrodiffusional fluxes, the erythrocytes anion permeability can serve as an extremely efficient  $CO_2$  carrier to transport  $CO_2$  between tissues and lungs (referred to as the Jacobs-Stewart cycle). Due to the high

electrodiffusional anion permeability, the membrane potential of the erythrocyte is very near the equilibrium potentials of  $\text{Cl}^-$  and  $\text{HCO}_3^-$  which is about  $-10 \text{ mV}$  <sup>1,12,13</sup>.

This delicate homeostatic balance is characteristic in the normal state of erythrocytes. It is markedly changed in SS cells (Sickle-cell disease cells) due to a mutation in the hemoglobin gene, resulting in a disruption of ion fluxes, ion content regulation, and hydration state in the circulation <sup>1</sup>.

### 1.1.3 Nonselective cation channels

Nonselective cation (NSC) channels in the human RBC membrane are voltage-gated channels <sup>14</sup>, which are stimulated through nicotinic acetylcholine <sup>15</sup> and PGE2 receptors, as well as, activated by strong depolarization of the membrane potential <sup>16,17</sup>. They are permeable to divalent cations such as  $\text{Ca}^{2+}$ ,  $\text{Mg}^{2+}$ , and  $\text{Ba}^{2+}$  <sup>14,18</sup>.

$\text{Ca}^{2+}$  may enter via nonselective cation channels, which involve TRPC6<sup>19</sup> and P2X7-dependent pathways<sup>20</sup>. These channels are stimulated by oxidative stress, hyperosmotic shock, and  $\text{Cl}^-$  removal (extracellular  $\text{Cl}^-$  concentration to 27 mM half-maximally activates these cation channels). The cation channels are activated by PGE2 <sup>21,22</sup>. Activation also occurs within minutes upon replacement of extracellular  $\text{Cl}^-$  by gluconate.

### 1.1.4 $\text{Ca}^{2+}$ homeostasis of erythrocytes

Compared to nucleated cell types, human RBCs have a low amount of  $[\text{Ca}^{2+}]_i$ , (below 100 nM) <sup>23</sup> due to the absence of  $\text{Ca}^{2+}$  storage in endoplasmic reticulum and mitochondria and to low cytoplasmic  $\text{Ca}^{2+}$  buffering capacity <sup>24,25</sup>.

Furthermore, the strong  $\text{Ca}^{2+}$  efflux by the P type ATP-dependent  $\text{Ca}^{2+}$  ATPase pump <sup>26,27</sup>, and the low  $\text{Ca}^{2+}$  influx (passive or through a non-selective cation channels) of non-stressed RBCs, physiological free  $[\text{Ca}^{2+}]_i$  lower the intracellular  $\text{Ca}^{2+}$  concentration <sup>24,27</sup>.

### 1.1.5 Dehydration of erythrocytes

Most of the erythrocyte membrane proteins are involved in active and passive ion transport *i.e.* they maintain erythrocyte homeostasis <sup>1,28</sup>.

Erythrocyte dehydration (loss of water) *in vivo* may result from the activation of one or more of three transporters expressed in their plasma membranes <sup>1</sup>:

- 1) the  $\text{Ca}^{2+}$ -sensitive, small-conductance,  $\text{K}^+$ -selective channel (Gárdos channel, IK1 or hSK4), This channel is also expressed in many other cell types <sup>1,29</sup>;
- 2) the  $\text{K}^+$ - $\text{Cl}^-$  cotransporter (KCC), regulated by internal pH and cell volume is functionally active in reticulocytes and much less in mature erythrocytes <sup>1,30</sup>;
- 3) the  $\text{Na}^+/\text{K}^+$  pump <sup>1,31</sup>.

The three mentioned transporters differ considerably in their dehydrating modalities, potencies, and distributions among erythrocytes <sup>1</sup>.

#### 1.1.5.1 Gárdos $\text{K}^+$ channels activated by $\text{Ca}^{2+}$

$\text{Ca}^{2+}$ -dependent  $\text{K}^+$  efflux from human erythrocytes, first described in the 1950s by Gárdos, is dependent on a membrane protein with channel activity (Gárdos channel) responsible for the *Gárdos effect* phenomenon. The basic Gárdos channel topology is predicted to be a homotetramer of six-transmembrane-domain polypeptides, with the pore (“p”) region between the membrane domains of s5 and s6. The  $\text{K}^+$  selectivity is mediated by the carbonyl oxygen atoms within the selectivity filter protruding from the backbone of the polypeptides from each of the four identical subunits <sup>11</sup>.

Gárdos channels (app. 100-200 channels per erythrocyte) are located in RBCs membrane and play an important role in the regulation of cell volume <sup>1,32-35</sup>; their activity is dependent upon the free  $\text{Ca}^{2+}$  concentration at the cytoplasmatic membrane face.  $\text{Ca}^{2+}$  acts on Gárdos channels by binding to calmodulin which is tightly associated with the cytoplasmic domain of the Gárdos channel creating a mechanical alteration, which is responsible for pore openings <sup>11,36</sup>. Gárdos channels are highly  $\text{K}^+$  over  $\text{Na}^+$ -selective ( $PK/PNa > 100$ ). In addition, a dramatic enhancement of Gárdos channel activity induces protein kinase A (PKA), possibly by modulating the  $\text{Ca}^{2+}$  sensitivity <sup>35,37</sup>.

Furthermore, intracellular  $\text{Cl}^-$  concentrations in human erythrocytes is high (around 80 mM <sup>38,39</sup> resulting in a very low membrane potential ( $\leq -10$  mV) <sup>40</sup> close to the  $\text{Cl}^-$  equilibrium (zero current, reversal, Nernst) potential <sup>39</sup>.

In non-stimulated and non-stressed human RBCs, the fractional Gárdos  $K^+$  channel activity is low. The number of  $Ca^{2+}$  ions per channel required for opening the channel is a matter of controversy. It is reported to be either 1<sup>41</sup> or 2<sup>42</sup>.

The normal intracellular  $Ca^{2+}$  concentration of human erythrocytes is 20-50 nM, at this concentration, Gárdos channels are closed. Activation occurs if the intracellular  $Ca^{2+}$  concentration is increased<sup>1</sup>. A wide range of values of intracellular  $Ca^{2+}$  concentration required for the Gárdos channel activation are reported. According to some studies, an intraerythrocytic  $Ca^{2+}$  level increase  $\geq 150$  nM<sup>43</sup>, is sufficient, while others suggest 2-4  $\mu$ M<sup>42,44</sup> levels are required for Gárdos channels activation<sup>45,46</sup> which leads to erythrocyte membrane hyperpolarization, due to efflux of potassium ions that are close to the  $K^+$  equilibrium potential. This consequently creates the potential for the loss of anions, such as chloride or bicarbonate via parallel voltage-sensitive pathways, due to an outwardly directed electrochemical anion gradient across the RBC membrane. The resulting net loss of KCl and  $KHCO_3$  is coupled by osmotically-driven water efflux resulting in RBCs dehydration and shrinkage (Gárdos effect) which when at physiological  $Cl^-$  and  $HCO_3^-$  concentrations, full dehydration created by maximally activated Gárdos channels, may take over 1 hour<sup>1,46</sup>. Thus, the Gárdos effect is dependent on the extracellular  $Ca^{2+}$  concentration.

### 1.1.5.2 The erythrocytic KCl cotransporter

KCC mediates a strictly coupled electroneutral transport of  $K^+$  and  $Cl^-$ , independent of the membrane potential<sup>47</sup>. KCCs are expressed in a large variety of eukaryotic cell types, including erythroid precursors<sup>30</sup>. While in mature erythrocytes, KCl cotransporter activity is substantially reduced<sup>1</sup>. KCl cotransporter is a multi-regulated transporter influenced by several factors. Factors such as the oxidation state of Hb<sup>48</sup>, increased cell volume, intracellular acidification, and to a lesser extent by low intracellular  $Mg^{2+}$  concentrations<sup>1,13,49,50</sup>.

Its functional state is reported to be regulated by phosphorylation and dephosphorylation of serine/threonine and tyrosine residues. Activation of KCC follows dephosphorylation of a serine/threonine residue by PP1<sup>51</sup> and/or PP2A<sup>52</sup>. In RBCs with active KCC, acidification may induce dehydration<sup>53</sup>.

Similar to the loss of cell volume via the Gárdos channel, the driving force for erythrocyte dehydration through the KCC cotransporter occurs by  $K^+$  permeabilization which is based on an outward electrochemical gradient of  $K^+$ . Cell acidification is an important side effect of isotonic dehydration by the loss of KCl and  $KHCO_3$ <sup>1</sup>, which was fully confirmed experimentally<sup>54</sup>. Its mechanism is as follows: The positive charges within an erythrocyte are due to the positive ion charges on  $Na^+$ ,  $K^+$ ,  $Ca^{2+}$ ,  $Mg^{2+}$ , in a density of 150 meq/l cell water, balanced by negative charges on  $Hb^-$  (50 meq/l cell water),  $Cl^-$ , and  $HCO_3^-$  (the later at a concentration together of 100 meq/l cell water). If the erythrocytes lose water isotonically due to efflux of 150 meq/l KCl and  $KHCO_3$ , the concentrations of  $Cl^-$  and  $HCO_3^-$  are higher in the effluent as compared to the cell. Thus, with proceeding efflux, the intracellular concentrations of chloride and bicarbonate decrease while the extracellular concentrations approximately remain the same<sup>1</sup>. The erythrocytic membrane bicarbonate/chloride exchanger together with the  $CO_2$  shunt in the RBC membrane, known as the Jacobs-Stewart mechanism<sup>55</sup>, ensure rapid equilibrium by increasing the intracellular  $H^+$  concentration as a consequence of the decreased intracellular bicarbonate concentration<sup>1</sup>.

### 1.1.5.3 $Na^+/K^+$ pump of the erythrocytes

The  $Na^+/K^+$  pump is an ion-transporting enzyme dependant on ATP, and is therefore an active energy-requiring process. The pump is located in the plasma membrane that builds up and maintains a low intracellular  $Na^+$  ( $[Na^+]_i$ ) and a high intracellular  $K^+$  ( $[K^+]_i$ ) concentration<sup>56,57</sup>. The RBCs has approximately 400 molecules of the membrane sodium-potassium pump per cell, which when bound with ATP, pumps 2  $K^+$  ions into the cell and removes 3  $Na^+$  out of the cell, thereby generating opposing chemical gradients for both ions. While doing this, cellular electroneutrality is mainly maintained by anion efflux balancing the extra  $Na^+$  efflux. If the resulting increase of NaCl efflux, is not compensated by changes in passive fluxes, it will induce cell dehydration<sup>1,58</sup>.

The  $Na^+/K^+$  pump process helps to build up the membrane potential, avails transport and regulates cellular volume. The intraerythrocytic concentrations of  $Na^+$  are between 10 to 20 mM and the concentrations of  $K^+$  is approximately 140 mM<sup>59-62</sup>.



## 1.2 Eryptosis signaling pathways

### 1.2.1 Cell death of nucleated cells

The most widely mammalian cell death classification recognizes two types: **apoptosis** and **necrosis**. A third mode of cell death has been proposed named **autophagy**, which is the process used by starving cells, digesting their own macromolecules and organelles, generating energy and metabolites. Autophagy allows cells to survive if they do not receive nutrients for extended periods. They ultimately digest all available substrates and die (autophagy-associated cell death)<sup>63</sup>. Cell death is “programmed” if it is genetically controlled; therefore, apoptosis and autophagy-associated cell deaths are the two basic types of programmed types of cell deaths<sup>64</sup>.

The term apoptosis is derived from an ancient Greek word that suggests “*leaves falling from a tree*”<sup>63</sup>. Apoptosis is a form of cell death in which a programmed sequence of events leads to the elimination of cells without releasing harmful substances into the surrounding area. Two distinct, but convergent, apoptotic pathways are known: the death receptor and mitochondrial pathways. Without apoptosis, 2 tons of bone marrow and lymph nodes and a 16 km intestine would probably accumulate in a human by the age of 80<sup>65</sup>. This programmed cell death includes some key features: cleavage of cytoskeleton proteins by aspartate-specific proteases, which thereby collapse subcellular components, chromatin condensation, DNA fragmentation, cell shrinkage, breakdown of the phosphatidylserine asymmetry of the plasma membrane and the formation of plasma-membrane blebs<sup>63-65</sup>.

A cell suicide mechanism or a programmed cell death is initiated by unique sensors on the cell membrane surface, termed death receptors<sup>66</sup>. These receptors trigger the apoptosis machinery of the cell by detecting the presence of extracellular death signals (stressors) such as energy depletion<sup>67</sup>, osmotic shock<sup>68</sup>, oxidants and radiation<sup>69</sup>, or chemotherapeutics<sup>70,71</sup>.

### 1.2.2 Mechanisms of eryptosis

Erythrocytes have been considered unable to undergo programmed cell death like other cells, since they lack mitochondria and nuclei (key organelles in the apoptotic machinery of nucleated cells).

According to one theory, erythrocyte aging is a form of apoptosis<sup>72,73</sup> based on the elimination of injured or senescent erythrocytes after their physiological life span. Erythrocyte degradation by macrophages is mediated by a  $\beta$ -galactoselectin present in the macrophage membrane<sup>74</sup>. It has been shown that sialic acid residues of membrane glycoconjugates control the life span of erythrocytes through desialylation of glycans and therefore responsible for the clearance of senescent erythrocytes after  $\beta$ -galactoselectin mediated capture<sup>72-74</sup>.

Similar to apoptosis, the suicidal death of erythrocytes or eryptosis is characterized by cell shrinkage, membrane blebbing, activation of proteases and phospholipids scrambling of the cell membrane with subsequent phosphatidylserine exposure at the cell surface<sup>72,75-79</sup>. Eryptosis leads to rapid clearance of circulating erythrocytes<sup>80-83</sup>, as phosphatidylserine exposing erythrocytes are rapidly engulfed and degraded by macrophages<sup>84</sup>. Eryptosis is triggered by erythrocyte injury following several stressors including osmotic shock, oxidative stress, ligation of cell membrane antigens, and energy depletion (glucose or ATP)<sup>6</sup>. This process is termed “*eryptosis*” by prof. F. Lang<sup>6,85</sup>.

Two signaling pathways have been identified which trigger eryptosis (fig. 1.2.2.1). Both weaken the antioxidative erythrocyte defense. One pathway involves the activation of the cyclooxygenase (COX) which in turn triggers prostaglandin E2 formation and leads to activation of a  $\text{Ca}^{2+}$ -permeable cation channel. The other pathway comprises the activation of a phospholipase A2 (PLA2s) leading to the release of platelet activating factor (PAF), which in turn activates a sphingomyelinase resulting in the formation of the proapoptotic sphingolipid ceramide<sup>6,77</sup>.

### 1.2.2.1 PGE2 formation by COX activation and activation of the cation channel

This mechanism includes the release of arachidonate (omega-6 fatty acids) present in the membrane phospholipids and cyclooxygenase (COX) activation which triggers PGE2 formation. PGE2 in turn, activates a  $\text{Ca}^{2+}$ -permeable cation channels (NSC channels) with subsequent cellular  $\text{Ca}^{2+}$  accumulation<sup>46,86,87</sup>.  $\text{Ca}^{2+}$  activates  $\text{Ca}^{2+}$ -sensitive  $\text{K}^+$  channels leading to  $\text{K}^+$  exit, resulting in hyperpolarisation,  $\text{Cl}^-$  exit, loss of osmotically obliged water, and thus cell shrinkage (Gárdos effect (at free  $[\text{Ca}^{2+}]_i \geq 150 \text{ nM}$ ))<sup>88,89</sup>.

$\text{Ca}^{2+}$  activates a membrane-bound polyphosphoinositide phosphodiesterase (at free  $[\text{Ca}^{2+}]_i \approx 2 \mu\text{M}$ )<sup>79</sup>, an endogenous transamidase<sup>90</sup>, and the cysteine endopeptidase calpain (at free  $[\text{Ca}^{2+}]_i \geq 10 \mu\text{M}$ )<sup>6,91-94</sup>, causing proteolysis, breakdown of polypeptides and membrane proteins aggregation<sup>79</sup>.

The Calpain effect is apparently not required for PS exposure but plays a role in the degradation of the cytoskeleton. In particular, it degrades the cytoskeleton by ankyrin R, fodrin (spectrin) and polypeptide 4.1 cleavages<sup>6,91</sup> which leads to membrane budding<sup>6,79,91-94</sup> and decreases cellular flexibility<sup>95</sup>. Most important, an increase in intracellular free  $[\text{Ca}^{2+}]_i$  results in PS asymmetry breakdown by inhibition of the translocase (ATP-dependent amino-phospholipid) and activation of the non-specific lipid scramblase. Thus,  $\text{Ca}^{2+}$  further triggers cell membrane scrambling<sup>96</sup> leading to translocation of phospholipids from the inner cell membrane leaflet to the erythrocyte surface<sup>46,86,87,91,97-99</sup>. As macrophages are equipped with receptors specific for phosphatidylserine<sup>100-102</sup>, erythrocytes exposing phosphatidylserine at their surface will be rapidly recognized, engulfed and degraded<sup>84,103</sup> and are thus expected to be rapidly eliminated from circulating blood.

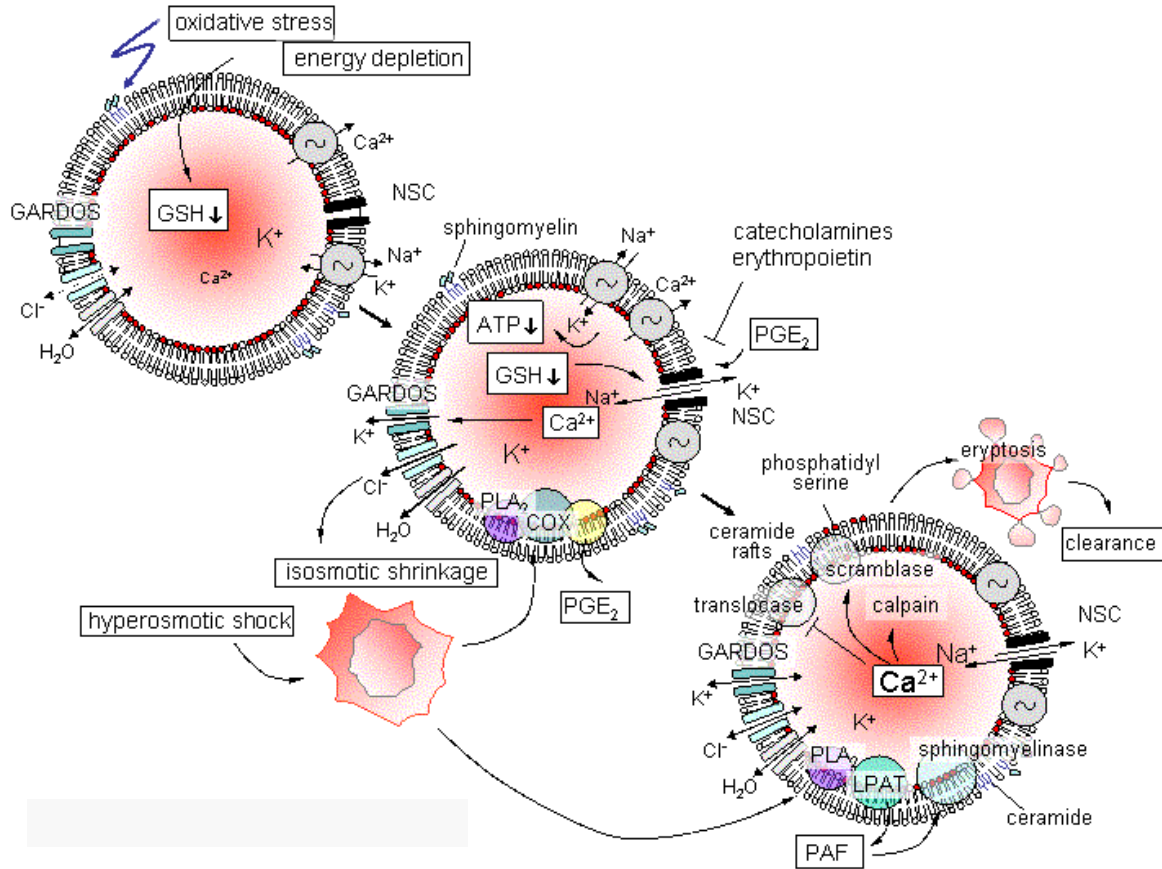


**Figure 1.2.2.1<sub>Introd.</sub> Synopsis of eryptosis signaling**<sup>6</sup>

### 1.2.2.2 Spingomyelinase stimulation by PAF formation

Breakdown of the membrane phospholipid asymmetry causes cell volume loss<sup>91,104,105</sup>, which is a prerequisite and an early and fundamental feature of programmed cell death<sup>106-109</sup>. In erythrocytes, PAF formation, upon cell shrinkage, stimulates the activation of sphingomyelinase. The Sphingomyelinase cleaves the phosphorylcholine unit of sphingomyelin and releases the proapoptotic sphingolipid ceramide (ceramide formation) consisting of the sphingosine backbone and the fatty acid unit of sphingomyelin (SM). Ceramide appearance at the erythrocyte membrane or/and increase of  $[Ca^{2+}]_i$  results in activation of the scramblase and inhibition of the translocase. This enhances PS migration from the inner to the outer leaflet of the bilayer cell membrane<sup>6,46</sup>. Moreover, the scramblase is sensitized to  $Ca^{2+}$  by ceramide which is formed following activation of a sphingomyelinase (fig. 1.2.2.1)<sup>110</sup>.

Besides increase in scramblase activity,  $Ca^{2+}$  activates the  $Ca^{2+}$ -sensitive  $K^+$  channels<sup>32,111</sup>, which similarly favors eryptosis<sup>89</sup>.  $Ca^{2+}$  activity may be increased by activation of a  $Ca^{2+}$

permeable cation conductance which is activated by osmotic shock, oxidative stress and energy depletion<sup>22,46,112,113</sup>.

Eryptosis may participate in the machinery leading to erythrocyte senescence<sup>114,115</sup> and neocytolysis<sup>116</sup>.

Enhanced eryptosis has been observed in a variety of anemic conditions. Wide variety of environmental pollutants, drugs, and further xenobiotics, as well as endogeneous substances, clinical conditions and diseases trigger eryptosis<sup>6,21</sup>.

### 1.2.2.3 Phosphatidylserine movement

In human erythrocytes, within the transversal membrane plane, lipids are usually asymmetrically distributed, choline-containing phospholipids *i.e.* sphingomyelin (82%) and phosphatidylcholine (76%), are mostly located in the outer leaflet, whereas amino phospholipids are either mostly phosphatidylethanolamine (80 %) or exclusively phosphatidylserine (100%) localized in the inner membrane leaflet<sup>117</sup> (Fig. 1.2.2.3).

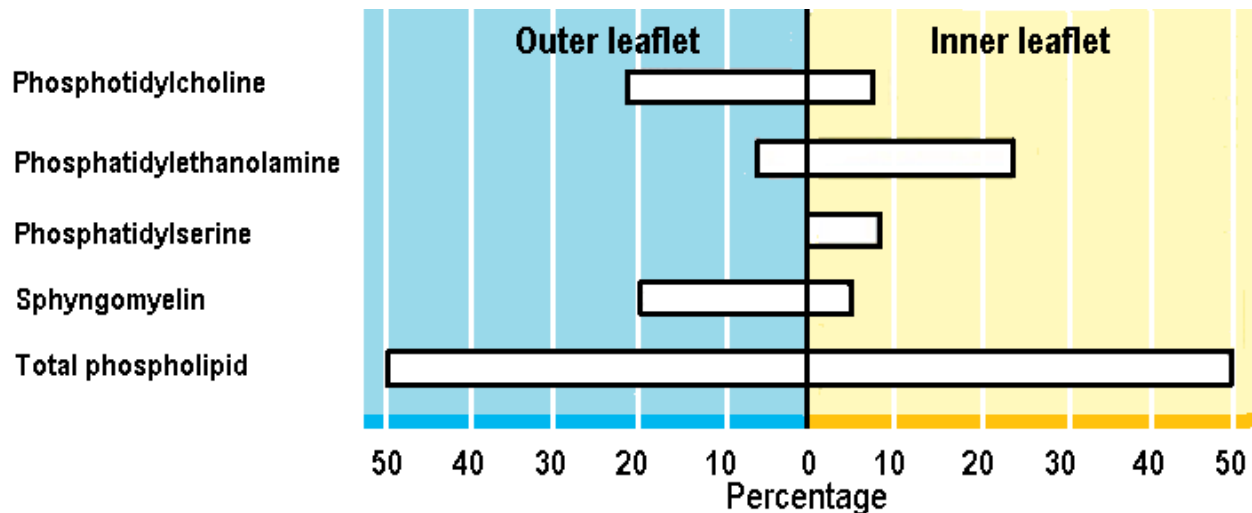


**Figure 1.2.2.3<sub>introd</sub>.** Phospholipids are arranged asymmetrically in the most membranes, including the human RBCs membrane leaflets, as shown here. Values are in mole percentage<sup>118</sup>.

This selective localization dictates that asymmetric biomembranes are assembled and maintained by specific mechanisms that control transbilayer lipid sidedness and any change of this composition might lead to physiological and pathophysiological consequences<sup>84</sup>. Thus, asymmetry of the cell membranes is the rule for normal cells, loss of asymmetry, especially the

appearance of PS at the cell surface, is associated with many physiologic and pathologic phenomena<sup>105</sup>.

In the outer leaflet of the plasma membrane of younger erythrocytes, PS is present only in a few cells, however, increasing with erythrocyte age<sup>81,119</sup>.

**Aminophospholipid translocase** (or flipase), it appear to belong to a subfamily of P-type ATPases<sup>120</sup>. Flipase is a ubiquitous  $Mg^{2+}$ -ATP-dependent aminophospholipid translocase, is responsible for active translocation of amino phospholipids from the outer to the inner leaflet of the cell membrane against their concentration gradient, whereas cholinephospholipids are not moved.<sup>96,121</sup> The same protein transports both PS and PE, although PS is transported much faster with half-times of 5 to 10 minutes. This process consumes one molecule of ATP per molecule of phospholipids transported<sup>105,122</sup>. Micro molar concentrations of  $[Ca^{2+}]_i$  reversibly inhibit the flipase<sup>123</sup>. Treatment of RBCs with ionomycin, a  $Ca^{2+}$  ionophore, leads to exposure of up to 300000 PS sites per cell<sup>124</sup>. Accordingly, the aminophospholipid translocase builds up the phospholipids asymmetry of the RBC membrane (fig. 1.2.2.4).

**ATP-dependent floppase** belongs to a superfamily of ABC transporters which transports both cholinephospholipids and amino phospholipids to the outer from the inner leaflet. Its transport rate is about 10 times slower than the inward movement of aminophospholipids by aminophospholipid translocase. Thus, its influence on the membranes phospholipids composition is small<sup>105,120</sup> (fig. 1.2.2.4).

Because rapid inward translocation of aminophospholipids does not accelerate outward migration of all phospholipids, both processes may be mediated by independent mechanisms<sup>122</sup>.

Both floppase and flipase appear to be permanently active in normal quiescent cells<sup>120</sup>. Through these two processes all phospholipids are slowly but continuously moved to the outer membrane surface, whereas the aminophospholipids are shuttled rapidly back to the inner leaflet thus securing a dynamic asymmetric steady state.

**Lipid scramblase**, lipid randomization induced by  $Ca^{2+}$  is likely to depend on a protein or proteins with lipid scramblase activity.<sup>125</sup> Unlike the energy-dependent translocase and floppase, the lipid scramblase does not require hydrolysable ATP. However, during prolonged ATP depletion its activity partially is decreased<sup>126</sup>. For its activity scramblase requires the continuous presence of  $[Ca^{2+}]_i$ <sup>105,126</sup>. Ceramide further stimulates scramblase activity<sup>127</sup>.

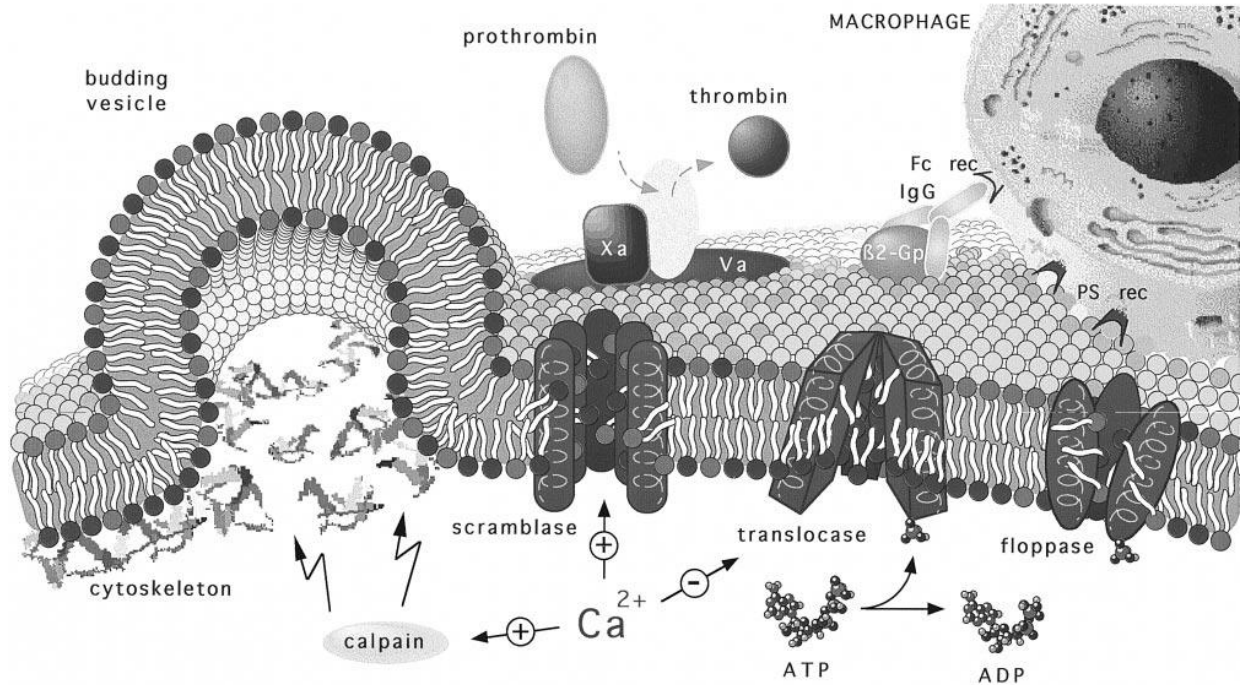


**Figure 1.2.2.4<sub>introd.</sub> The regulation and physiology of membrane phospholipid asymmetry.**

Membrane lipid asymmetry is regulated by the cooperative activities of three transporters. The ATP-dependent aminophospholipid-specific translocase, which rapidly transports PS and PE from the cell's outer-to-inner leaflet; the ATP-dependent nonspecific lipid floppase, which slowly transports lipids from the cell's inner-to-outer leaflet; and the  $\text{Ca}^{2+}$ -dependent nonspecific lipid scramblase, which allows lipids to move randomly between both leaflets. The model predicts that the translocases are targets for  $\text{Ca}^{2+}$  that directly regulates the transporter's activities. Elevated intracellular  $\text{Ca}^{2+}$  induces PS randomization across the cell's plasma membrane by providing a stimulus that positively and negatively regulates scramblase and translocase activities, respectively. At physiologic  $\text{Ca}^{2+}$  concentrations, PS asymmetry is promoted because of an active translocase and floppase but inactive scramblase. Increased cytosolic  $\text{Ca}^{2+}$  can also result in calpain activation, which facilitates membrane blebbing and the release of PS-expressing procoagulant microvesicles. Exposure of PS at the cell's outer leaflet marks the cell as a pathologic target for elimination by phagocytes. (*Aminophospholipids are shown with black polar headgroups and cholinephospholipids with light polar headgroups*)<sup>105</sup>.

Increase in the free  $[\text{Ca}^{2+}]_i$  levels between 63-88  $\mu\text{M}$  half-maximally activates the phospholipid scramblase<sup>91,128</sup> (and block the cooperative action of translocase and floppase), which catalyzes bi-directional migration (flip-flop) of all major phospholipids classes at comparable rates across the lipid bilayer in a largely non-selective manner<sup>123</sup> leading within minutes a loss of membrane phospholipid asymmetry<sup>120,129</sup>. Whereas,  $\text{Ca}^{2+}$  efflux can lead to restoration of lipid asymmetry<sup>130</sup>.

In addition,  $\text{Ca}^{2+}$  stimulates the cysteine endopeptidase **calpain**, which by catalyzing the controlled proteolysis of its cytoskeletal target proteins, degrades them, and thus initiates cell membrane blebbing<sup>21</sup>.

Taken together, these data strongly suggest that the activity of the NSC channels does regulate free  $[\text{Ca}^{2+}]_i$  in intact RBCs. All stress stimuli that induce cation channel activation also stimulate PS exposure. Furthermore PS exposure is inhibited by blockage of the non selective cation channels by the inhibitors ethylisopropylamiloride (EIPA), and amiloride<sup>46,86,93</sup>.

Accordingly, transamidase, phosphodiesterase, calpain and scramblase probably execute an erythrocyte death program<sup>99</sup> followed by phagocytic clearance. Externalization of PS even precedes DNA fragmentation, loss of membrane integrity, and cell lysis<sup>131</sup> in nucleated cells.

#### **1.2.2.4 RBCs phosphatidylserine exposure recognized by macrophages**

Senescent or injured erythrocytes exposing PS are rapidly recognized, engulfed and degraded by macrophages<sup>6,84,100,104,119</sup>. Hence, defective or old RBCs are rapidly removed from circulation, accumulating in spleen macrophages and liver Kupffer cells<sup>84</sup>.



### 1.3 Glucose transporter families

Glucose is the fuel that provides energy for normal activity in humans and the major component of carbohydrates in food. The amount of glucose stored in the body is ~450g and thereof ~250 g are turned over daily. To ensure that an adequate amount of energy is provided, homeostatic mechanisms maintain blood glucose within narrow limits, 4 to 12 mM. Glucose uptake, from food sources, is usually in the form of complex carbohydrates, which are broken down enzymatically and are then absorbed completely in the small intestine. The kidneys glomeruli continuously reabsorb app. ~180 g glucose (in 24 hours) from primary urine and keep the blood glucose levels normal <sup>132</sup>.

There are two gene families that encode proteins responsible for the absorption of glucose across the small intestine, uptake in the brain across the blood–brain barrier, the reabsorption of glucose from the glomerular filtrate, and the uptake and release of glucose from all cells in the body:

- 1) **SLC2 gene family** (SLC2A1-13) or facilitated **glucose** **t**ransporters (the GLUT1-12 and the H<sup>+</sup>/myo-inositol transporter HMIT) - responsible for the downhill, passive transport of glucose (or myo-inositol respectively) across cell membranes <sup>133</sup>;
- 2) **SLC5 gene family** or **s**odium-coupled **glucose** **c**o**t**ransporters (the SGLTs) - secondary active Na<sup>+</sup>/glucose symporters, SGLT1 and SGLT2. These transporters use the energy released by transporting Na<sup>+</sup> ions along its electrochemical gradient to move glucose inside the cell <sup>134</sup>.

Over 230 known members of the Sodium Substrate Symporter gene Family (SSSF) are known, but only 11 are identified members of the SLC5 human gene subfamily. These include proteins that transport sugars (SLC5A1, 2, 9 and 11), myo-inositols (SLC5A3 and 11), anions (SLC5A5 and SLC5A8), vitamins (SLC5A6) and choline (SLC5A7). Also one orphan (SLC5A10) and one glucose sensor (SLC5A4) are known <sup>132,134</sup>.

#### 1.3.1 Sodium-coupled Glucose (Co) Transporter (SGLT1)

SGLT1 is a transporter, utilizing the Na<sup>+</sup> gradient as a driving force, cotransporting Na<sup>+</sup> and sugar (into the cell), a transport referred to as secondary active transport. The driving force - Na<sup>+</sup> gradient - is maintained by the primary active Na/K-pump, or Na/K-ATPase. SGLT1 is

different from SGLT2, it has a higher affinity for glucose and it does transport galactose which is not the case for SGLT2<sup>132</sup>.

Although SGLT1 is prominently expressed in the small intestine, the gene is also transcribed in the renal proximal tubule and other organs such as the brain and heart, as well as, the trachea, testis and prostate. The natural substrates are glucose and galactose with apparent affinities ( $K_{0.5}$ ) of 0.5 mM. Mutations in the SGLT1 gene cause malabsorption of glucose and galactose<sup>132,134</sup>.

SGLT1 couples the transport of two sodium ions per one glucose molecule across the brush border membrane in the small intestine. Energy is provided by the sodium electrochemical potential gradient across the brush border membrane. Sodium that enters the cell along with glucose is then exported into blood vessels by the Na/K-pump in the basolateral membrane, thereby maintaining the driving force for glucose transport. As the sugar accumulates within enterocytes, this generates a driving force to transport glucose out of the cells into the blood via GLUT2 expressed in the basolateral membranes. A fraction of the intracellular glucose, in the form of glucose-6-phosphate, appears to be taken up into endosomes and delivered to the blood by exocytosis through the basolateral membrane<sup>133</sup>. The net result is that 1 mole of glucose and two moles of sodium are transported across the enterocyte from gut lumen into blood, and this is followed by two moles of anions to ensure electroneutrality, and water (fig. 1.3.1). The energy for the overall process comes from the ATP consumed by the basolateral Na/K-pump<sup>132</sup>.

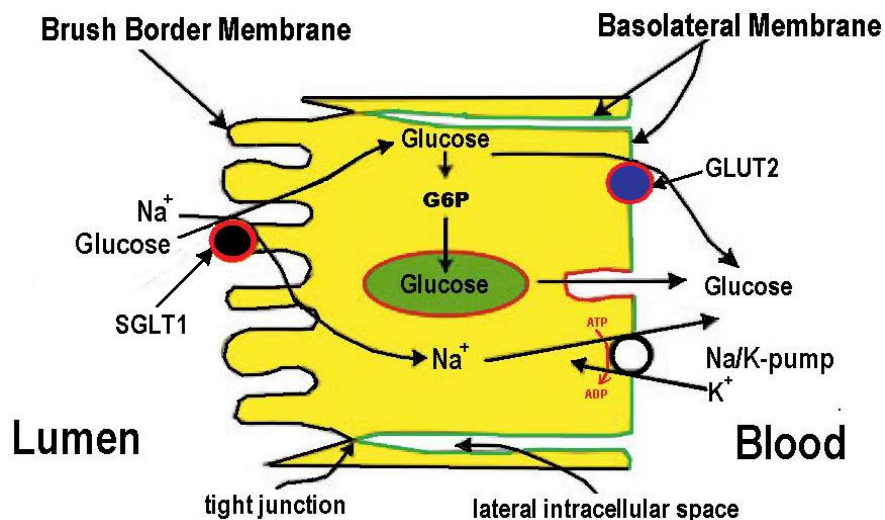


**Figure 1.3.1**<sup>Introd.</sup> Role of SGLT1 symporter in a model for glucose (and galactose) absorption across a mature enterocyte from the upper villus of the small intestine<sup>132</sup>.

## 1.4 Glutamatergic neurotransmission

Excitatory amino acids (EAA), especially L-Glutamate (Glu) are the major brain excitatory neurotransmitter; as well as, an important neurotoxin. When its concentration in the extracellular fluid increases this could result in damage of the neurons through a massive calcium entry into the cell or a swelling process leading to cell death <sup>135</sup>.

The glutamatergic neurotransmission involves the so-called “*Glutamate-glutamine cycle*“, and begins with the release of glutamate from the synaptic vesicles to the synaptic cleft by exocytosis (ATP and  $\text{Ca}^{2+}$  dependent process). When released in the synaptic space, glutamate diffuses to the post-synaptic element to act on different subsets of glutamatergic receptors (ionotropic and metabotropic subtypes, see below) and to transfer excitatory transmission. The glutamate neurotransmission is terminated by uptake of excessive glutamate from the synaptic cleft <sup>135-137</sup>. Since the synaptic clefts are in continuity with the general extracellular space in the brain, it is not only a question of keeping a low resting concentration inside the synaptic clefts, but also outside the clefts (extrasynaptically) <sup>136</sup>. Therefore, the concentration of L-glutamate in the extracellular fluid is kept low (1-3 mM), even though there is 12 mM of L-glutamate per gram of whole brain which is almost completely intracellularly located <sup>138,139</sup>. There is no evidence for any extracellular enzyme that can metabolize glutamate to any significant degree; thereby the only rapid way to remove glutamate from the extracellular fluid is by cellular uptake. Although simple diffusion appears to be an important mechanism for glutamate removal, it is far too slow to maintain low extracellular levels <sup>136</sup>. Glutamate uptake is accomplished by means of glutamate transporter proteins expressed in both neurons and glial cells (presynaptically, postsynaptically and extrasynaptically) <sup>135,136</sup>. Glutamate transporters use the electrochemical gradient across the plasma membrane as driving force for glutamate uptake. Sodium is required for glutamate binding while potassium is required for net transport. The process is electrogenic (net positive charge moving into the cell) and it is thereby stimulated by a negative membrane potential. Astroglia (in an ATP-dependent process) detoxify glutamate by converting it to glutamine which is subsequently released from the glial cells by means of glutamine transporters and taken up by presynaptic terminals of neurons by means of another glutamine transporter. Neurons metabolize glutamine by converting it back to glutamate using mitochondrial enzyme glutaminase. Synaptic vesicles are loaded with glutamate from cytosol by means of a vesicular glutamate transporter. It is commonly referred to as the glutamine-glutamate cycle <sup>135,136</sup>.

Glutamine is normally present in the extracellular fluid at around 200–500  $\mu\text{M}$ . In contrast to glutamate, glutamine is nontoxic and does not activate glutamate receptors. Thus it does not compromise neurotransmission<sup>140</sup>.

This description of glutamate and glutamine metabolism represents an oversimplification because transmitter glutamate is not necessarily derived from glutamine nor is transmitter glutamate necessarily converted into glutamine but may serve as a nutrient for neurons.

Three different families of glutamate receptor proteins have been identified<sup>136,137</sup>.

- **Ionotropic glutamate receptors** are all glutamate gated ion channels (conducting only  $\text{Na}^+$  or both  $\text{Na}^+$  and  $\text{Ca}^{2+}$ ) that activates when glutamate binds to the receptor. They belong to two receptor families:
  - **NMDA-receptor family** of glutamate receptors, activated by the glutamate analogue *N*-methyl-D-aspartate (NMDA) (receptors NR1, NR2A, NR2B, NR2C and NR2D). To be activated they need both depolarized membrane and glutamate binding. These receptors have high affinities and are slowly inactivated.
  - **AMPA/kainate-receptor family** based to their preference for AMPA or kainite (further subdivided into AMPA-receptors (GluR1-4) and kainate receptors (GluR5-9, KA1 and KA2)). Upon glutamate exposure they readily open, but desensitize quickly and, compared to NMDA receptors, have low affinity to glutamate.
- **Metabotropic glutamatergic receptors** (mGluR1-8) consist of G-protein-coupled receptors which are subdivided into groups I (mGluR1 and mGluR5), II (mGluR2 and mGluR3) and III (mGluR4, mGluR6, mGluR7 and mGluR8).

A common property of all these synaptic receptors is a fast desensitization rate. Consequently, for maintaining the efficacy of excitatory transmission a key mechanism is considered to be the uptake of Glu from the synaptic space through the highly efficient glial transporters, namely GLAST/EAAT1 and especially GLT1/EAAT2, present on the astrocytes. However, neurons have also been shown to contribute efficiently to the clearance of EAA from the synaptic cleft through the specific transporters EAAC1/EAAT3, EAAT4 and EAAT5 whose exact significance has yet to be determined<sup>135,136</sup>.

There are two classes of glutamate transporters<sup>136</sup>:

- **Dependent on electrochemical gradient sodium ions** (also dependent on  $\text{K}^+$  concentrations) in humans, “Excitatory Amino Acid Transporters“(EAATs). Some  $\text{Na}^+$ -

dependent transporters have also been called “high-affinity transporters“, though their glutamate affinity actually varies widely, and

- **Sodium independent transporters** (Vesicular **G**lutamate **T**ransporters known as VGluTs) some of which are localized to cell plasma membrane while others in synaptic vesicles being dependent on the proton gradient.

#### 1.4.1 Excitatory Amino Acid Transporters (EAATs)

The solute carrier family 1 (SLC1) includes five high-affinity glutamate transporters, EAAT3, EAAT2, EAAT1, EAAT4, EAAT5 (SLC1A1, SLC1A2, SLC1A3, SLC1A6, and SLC1A7, respectively) as well as the two neutral amino acid transporters, ASCT1, ASCT2 (SLC1A4 and SLC1A5) <sup>141</sup>. Five members of the EAATs family (EAAT1-EAAT5) are expressed in different cellular localizations: EAAT1 and EAAT2 are astroglial, whereas EAAT3, EAAT4, and EAAT5 are neuronal (fig. 1.4.1) <sup>142</sup>.

EAAT dysfunctions have been associated generally with serious brain damage and thus implicate an impairment of brain functions. They are involved in acute brain lesions related to ischemia, in different states of epilepsy and traumatic events, etc. Excitotoxicity could also be involved in other neurodegenerative diseases such as Parkinson’s disease, Huntington’s chorea or even Alzheimer’s disease, although direct evidence for the contribution of EAA is still lacking. Consequently, the basic knowledge gained about glutamatergic synapses will further contribute to the development of new strategies aimed at limiting such pathological changes associated with EAA dysfunctions <sup>135,138</sup>.

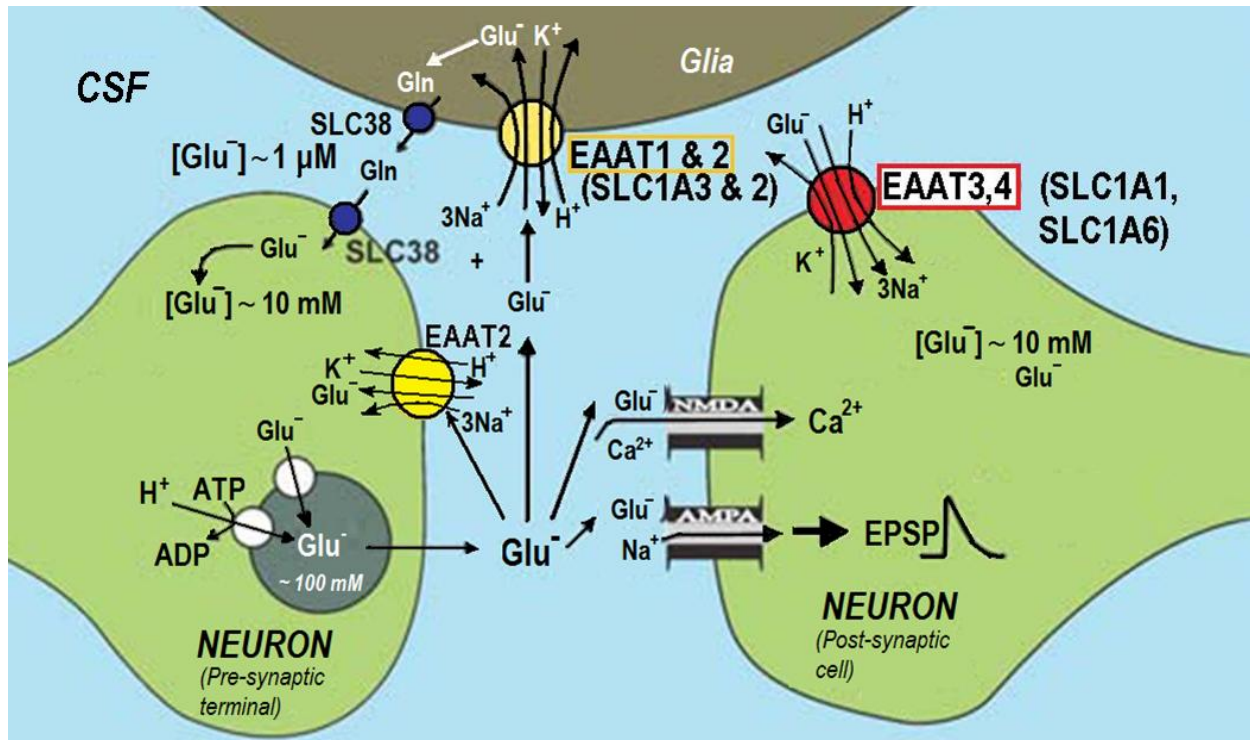


**Figure 1.4.1<sup>Introd.</sup> Glutamate transporters and glutamatergic synapses.** Glutamate is stored in synaptic vesicles at presynaptic terminals. Glutamate is transported into these vesicles by the vesicular glutamate transporters VGluT1-3 (or SLC17A6-8, respectively). Glutamate is released into the synaptic cleft to act on glutamate receptors. The AMPA receptors mediate fast excitatory postsynaptic potentials, whereas the NMDA receptors possess a cation channel which is permeable to  $\text{Ca}^{2+}$ . EAA transporters are crucial for maintaining the extracellular glutamate concentration of the cerebrospinal fluid (CSF) below neurotoxic levels by removing it from synaptic cleft. The power of glutamate transporters is provided by the coupling transport to the co- or countertransport of the ions  $\text{Na}^+$ ,  $\text{H}^+$  and  $\text{K}^+$ . The figure shows the EAAT3 & 4 and the glial glutamate transporter EAAT1 & 2 (or SLC1A3 & SLC1A2). Much of the glutamate taken up into glial cells via EAAT2 or EAAT1 is metabolized to glutamine by glutamine synthase (in an ATP-dependant process). On the other hand, glial cells in turn supply the nerve terminal with glutamine which serves as precursors of glutamate synthesis. Glutamine exits astrocytes via an SLC38 (system N) transporter and then enters neurons via another SLC38 (system A) transporter<sup>141</sup>.

EAATs mediate transport of l-glutamate, l-aspartate and d-aspartate, accompanied by the cotransport of  $3 \text{Na}^+$  and  $1 \text{H}^+$ , and the countertransport of  $1 \text{K}^+$ , whereas, ASC transporters mediate  $\text{Na}^+$ -dependent exchange of small neutral amino acids such as Ala, Ser, Cys and Thr<sup>141</sup>.

EAATs show a substrate-gated anion conductance. The anion permeability of glutamate transporters decreases in the order EAAT4/5>EAAT1>EAAT3>>EAAT2. The anion conductance has the characteristics of a substrate-gated anion channel with a selectivity order  $\text{NO}_3^- > \text{I}^- > \text{Br}^- > \text{Cl}^- > \text{F}^-$ .  $\text{Cl}^-$  is mainly translocated in the presence of glutamate or related substrates, and  $\text{Cl}^-$  movement is not thermodynamically coupled to the substrate transport.  $\text{Cl}^-$  is therefore

not necessary for substrate translocation<sup>143</sup>. Thus, glutamate transporters appear to possess structures that can function as chloride channels.

#### **1.4.1.1 Excitatory Amino Acid Transporter 3 (EAAT3)**

The molecular weight of the EAAC1/EAAT3 proteins are generally accepted to be around 64 kDa, the transport complex is a pentamer forming a pore with Cl<sup>-</sup> channel activity. The stoichiometry has been determined by studies using the cell expression of EAAC1/EAAT3, three sodium ions and one hydrogen ion which enter the cell together with one glutamate, in exchange for one potassium ion<sup>135</sup>.

Most of the studies published to date on the localization of EAAC have used specific antibodies. In the brain, the high-affinity transporter protein for anionic amino acids, originally called EAAC1, and now mostly referred to as EAAT3 (SLC1A1) is found in highest concentrations in the hippocampus, cerebellum and basal ganglia<sup>136</sup>. EAAC proteins and associated mRNA have a wide distribution in the brain and may be found in most (if not all) glutamatergic neurons, as well as in hippocampal interneuron's and GABAergic neurons like the cerebellar Purkinje cells. It is also detected in peripheral neurons (spinal ganglia) and in oligodendrocytes in various white matter regions of the CNS, in ependymal cells, and in epithelial cells of the plexus choroideus of the four ventricles, as well as, in satellite cells of spinal ganglia<sup>144</sup>. EAAC is also found outside the CNS, it is expressed in the intestine and kidney (localized in the proximal tubule brush border membrane with an axial gradient: low amounts in S1 and highest levels in the later segments S2 and S3)<sup>145</sup>.

Once L-glutamic acid has reached the inside of the cell via EAAT3, it can be interconverted and/or metabolized to produce energy, ammonia, and bicarbonate and thus play an important role in the context of pH regulation<sup>145</sup>.

#### **1.4.1.2 Excitatory Amino Acid Transporter 4 (EAAT4)**

Purkinje cells (PC) of the cerebellum in addition to EAAT3, express EAAT4, a transporter that exhibits a 10-fold higher affinity for glutamate than other glutamate transporters. Purkinje

cells remove the majority of glutamate released at climbing fiber (CF) synapses in the cerebellum<sup>146</sup>.

Using highly specific antibodies and immunohistochemistry it has been shown that EAAT4 protein was largely expressed in the somatodendritic compartment of Purkinje cells, especially in dendrites and spines. Unlike EAAT4, EAAT3 was found in Purkinje cell axons and presynaptic terminals. Immunogold staining revealed that EAAT4 was localized at the plasma membrane. Regional immunoblot analysis confirmed that a small amount of EAAT4 protein is expressed by cells in the forebrain albeit at much lower protein levels than in cerebellum, as well as, less expressed compared to EAAT3. EAAT4 is expressed mainly in small-caliber dendrites in neocortex and hippocampus. EAAT4 was also rarely found in forebrain astrocytes<sup>147</sup>.

EAAT4 possess both glutamate transport activity and potent chloride conductance properties which compared to other glutamate transporter subtypes are significantly higher. Obviously this may serve to modulate neuronal depolarization. Interestingly, because EAAT4 may serve to both clear extracellular glutamate and increase postsynaptic hyperpolarization, defects in, or a loss of, EAAT4 could have serious pathological consequences. Failure to transport glutamate via EAAT4 could lead to both excessive extracellular levels of glutamate and diminished postsynaptic inhibition; potentially resulting in selective Purkinje cell degeneration<sup>136,147</sup>.



## 1.5 AMP-activated protein kinase a key regulator of energy balance

The AMP-activated protein kinase (AMPK) system was discovered in mammalian cell extracts as activities that phosphorylate and inactivate key enzymes of lipid biosynthesis, that is, acetyl-CoA carboxylase (ACC) and 3-hydroxy-3-methylglutaryl-CoA reductase (HMG-CoA reductase, HMGR), which regulate fatty acid and cholesterol synthesis, respectively. These activities are functions of AMPK. AMP-activated protein kinase induces a cascade of events within cells in response to the ever changing energy charge of the cell and thus this enzyme plays a central control role in *maintaining energy homeostasis*. This kinase is allosterically activated by 5'-AMP and is also activated through phosphorylation by upstream kinases, and was named as AMPK in 1988<sup>148,149</sup>.

### 1.5.1 Structure and regulation of AMP-activated protein kinase

One of the most profound features of AMPK as a metabolic sensor is its sensitivity to the cellular energy status, which results from its unique biochemical properties. In humans and rodents AMPK is a trimeric enzyme composed of a catalytic  $\alpha$  subunit and the non-catalytic  $\beta$  and  $\gamma$  subunits (fig. 1.5.1A). Humans and rodents express two genes encoding  $\alpha$  ( $\alpha_1$ ,  $\alpha_2$ ) and  $\beta$  ( $\beta_1$ ,  $\beta_2$ ) isoforms and three genes encoding  $\gamma$  isoforms ( $\gamma_1$ ,  $\gamma_2$  and  $\gamma_3$ ). All possible combinations of isoforms appear to be able to form complexes. The  $\alpha_2$  isoform is the subunit of AMPK found predominantly within skeletal and cardiac muscle, whereas, approximately equal distribution of both the  $\alpha_1$  and  $\alpha_2$  isoforms are present in hepatic AMPK. Within pancreatic islet  $\beta$ -cells the  $\alpha_1$  isoform predominates<sup>148-150</sup>.

The N-terminal half of the  $\alpha$  subunits contains a conserved threonine residue (Thr-172) in the catalytic domain whose phosphorylation by upstream kinases is absolutely required for their activity (fig.1.5.1B). Interaction to form a complex with the  $\beta$  and  $\gamma$  subunits occurs via the C-terminal regions of the  $\alpha$  subunits. The  $\alpha_1$  is predominantly cytoplasmic, whereas  $\alpha_2$  isoform is enriched in the nucleus of several cell types, including pancreatic  $\beta$  cells, neurons, and skeletal muscle. The  $\beta$  subunits contain 2 conserved regions, located in the central (the core of the  $\beta$  subunits) and C-terminal regions. The central conserved region is recognized to be a glycogen-binding domain (GBD). However, functions of this domain remain unclear. The C-terminal domain is required to form a functional  $\alpha\beta\gamma$  complex that is regulated by AMP. The  $\gamma$  subunits

( $\gamma 1$ ,  $\gamma 2$ , and  $\gamma 3$ ) contain variable N-terminal regions followed by 4 tandem repeats of a 60 amino acids sequence as a CBS motif (termed by Bateman), which are nucleotide binding sites with similarity to cystathionine  $\beta$ -synthase (CBS) domains. CBS motifs act in pairs to form 2 domains (named Bateman domains), each of which binds one molecule of AMP. As AMP binds both Bateman domains the  $\gamma$  subunit undergoes a conformational change which exposes the catalytic domain found on the  $\alpha$  subunit where AMPK becomes activated when it is phosphorylated by upstream kinases. Mutations in these domains lead to a variety of human hereditary diseases caused by defective ligand binding which reduce both AMP binding and allosteric activation, proving that these are the regulatory binding sites for the nucleotides. The Bateman domains also antagonistically bind ATP with a lower affinity than AMP. The tandem domains bind AMP with a high degree of cooperativity suggesting that the second site is inaccessible until AMP has bound at the first domain. This represents yet another potential mechanism to increase the sensitivity of the AMPK system to small changes in AMP<sup>148,149,151,152</sup>.

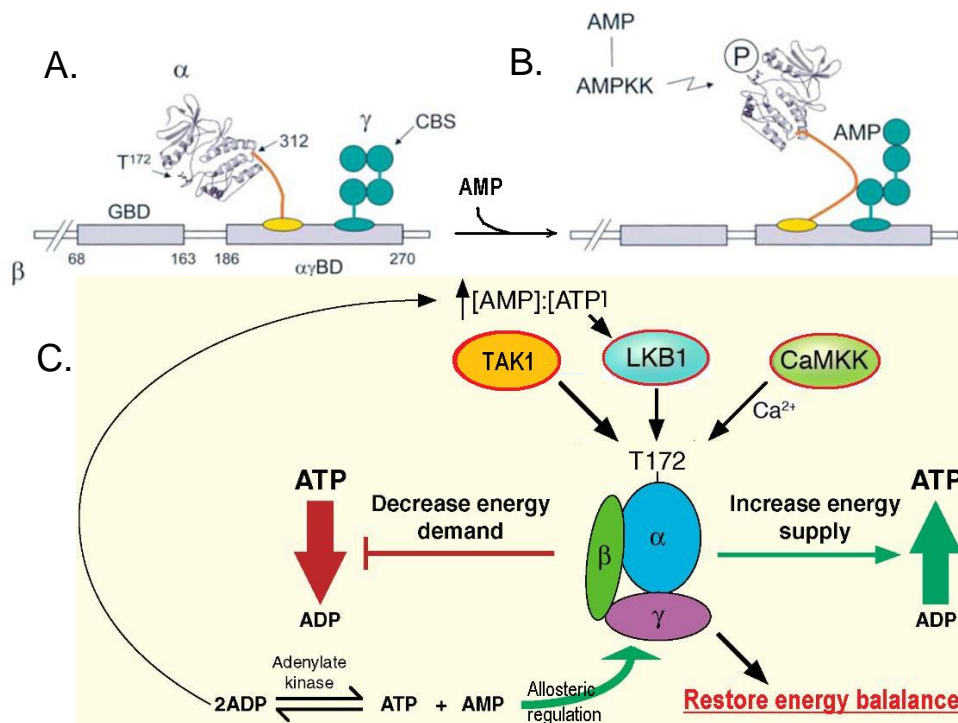


**Figure 1.5.1<sup>Introd.</sup> Subunit interactions involved in the activation of AMPK by phosphorylation and by allosteric regulation by 5'-AMP as well as its structure and regulation.**

**A.** The  $\beta$  subunit may act as a scaffold, binding  $\alpha$  and  $\gamma$  subunits via a C-terminal binding domain ( $\alpha\gamma$ BD).

**B.** Phosphorylation of the  $\alpha$  subunit at Thr-172 by AMPKK may lead to a conformational change in the  $\alpha$  subunit autoinhibitory domain (brown), altering its interaction with CBS domains of the  $\gamma$  subunit (green), relieving inhibition of catalytic activity in the  $\alpha$  subunit. GBD, glycogen binding domain of  $\beta$  subunit<sup>153</sup>.

C. Heterotrimeric ( $\alpha$ ,  $\beta$ , and  $\gamma$  subunit) complex of AMPK is activated through allosteric regulation by AMP, or by phosphorylation of Thr-172 by the upstream kinases CaMKK (dependent on the intracellular calcium), LKB1 (dependent on AMP/ATP ratio, which occurs following a drop in the ATP concentration as a consequence of the reaction catalyzed by adenylate kinase) and TAK1, thus AMPK restores energy homeostasis by activating energy producing processes (e.g., lipid oxidation and glucose uptake) while inhibiting those that consume energy (e.g., protein synthesis). These combined roles of AMPK ensure that the energy status of the cell is finely balanced<sup>151,154</sup>.

Any metabolic stress that inhibits ATP production, or that accelerates ATP consumption, will tend to increase the AMP:ATP ratio. An increased AMP to ATP ratio leads to a conformational change in the  $\gamma$ -subunit leading to increased phosphorylation and decreased dephosphorylation of AMPK, with consequent activation of AMPK. AMP-activated protein kinase activity is regulated acutely by AMP both (a) through a direct, allosteric mechanism, and (b) by making the enzyme a poorer substrate for dephosphorylation through protein phosphatases. These two effects of AMP effectively multiply together, so that a small increase in AMP can produce a much larger effect, so that AMPK is activated in a sensitive manner by a small rise in the AMP/ATP ratio<sup>148,149</sup>.

AMPK is phosphorylated by at least three different upstream AMPK kinases (AMPKKs) effect<sup>148,149</sup>.

The primary upstream kinase was recently identified to be a complex between the tumor suppressor, **LKB1** (also called serine-threonine kinase 11, STK11), and two accessory subunits, STRAD (STE-20 related adaptor protein) and MO25 (fig.1.5.1C). LKB1 is a classical tumor suppressor. There is evidence that activation of AMPK inhibits cell growth and proliferation. This makes it likely that the ability of LKB1 to activate AMPK explains much of its tumor suppressor effect<sup>148,149,151</sup>.

Some cells express an alternate pathway for AMPK activation, that is triggered by increases in cytoplasmic  $\text{Ca}^{2+}$ , leading to activation of calmodulin-dependent kinase kinase- $\beta$  (**CaMKK $\beta$** ) which, like LKB1, can phosphorylate Thr-172 on the AMPK  $\alpha$ -subunit (fig.1.5.1C). However, unlike the effect of LKB1, phosphorylation by CaMKK $\beta$  appears to be AMP-independent. The tissue distribution of CaMKK $\beta$  is more restricted than that of LKB1, with the former being most abundant in neurones and cells of the endothelial/haemopoietic lineage<sup>148,149</sup>.

Transforming growth factor- $\beta$ -activated kinase 1 (**TAK1**) is a serine/threonine protein kinase that is a third AMPK phosphorylating kinase. TAK1 form the heterotrimeric complexes with TAK1-binding protein 1 and 2 or 3 (TAB1, TAB2 or TAB3). As LKB1 and CaMKK $\beta$  it

phosphorylates Thr-172 on the AMPK  $\alpha$ -subunit (fig.1.5.1C). However, the normal physiological conditions under which TAK1 phosphorylates AMPK are still not clear<sup>154</sup>.

### 1.5.2 Regulation of erythrocyte survival by AMP-activated protein kinase

Cellular energy status is sensed by the AMP-activated protein kinase, which is activated on increase in the cytosolic AMP-to-ATP concentration ratio<sup>149,155</sup>. Effects of AMPK include stimulation of cellular glucose uptake, glycolysis, stimulation of fatty acid oxidation, and expression of enzymes required for ATP production<sup>155-158</sup>. On the other hand, AMPK down regulates energy-utilizing mechanisms, including protein synthesis, gluconeogenesis, and lipogenesis<sup>155,156,159</sup>. Through appropriate modulation of gene transcription, AMPK enhances the capacity of the cell to generate ATP<sup>159</sup>. The regulation of metabolism by AMPK thus ensures cell survival during energy depletion<sup>159,160</sup>. Moreover, AMPK inhibits cell growth and protects against suicidal cell death or apoptosis<sup>160</sup>.

Similar to nucleated cell survival, erythrocyte survival could be limited by suicidal cell death or eryptosis<sup>161</sup>. Similar to apoptosis of nucleated cells, eryptosis involves cell shrinkage, cell membrane blebbing, and cell membrane scrambling, leading to exposure of phosphatidylserine at the erythrocyte surface<sup>85,91,99,162,163</sup>. The cell membrane scrambling could be stimulated by cytosolic  $\text{Ca}^{2+}$ <sup>85,91,99</sup>, which may enter erythrocytes through  $\text{Ca}^{2+}$ -permeable cation channels<sup>22,46,112,113</sup>. The channels are activated by PGE2<sup>164</sup>. Cell shrinkage is similarly triggered by  $\text{Ca}^{2+}$ , which activates  $\text{Ca}^{2+}$ -sensitive  $\text{K}^+$  channels<sup>32,111</sup>, leading to the exit of KCl with osmotically obliged water<sup>89</sup>. The cellular loss of KCl contributes to suicidal erythrocyte death<sup>165</sup>. The  $\text{Ca}^{2+}$  sensitivity of erythrocytes is enhanced by ceramide<sup>110,166</sup>, which similarly stimulates eryptosis<sup>167,168</sup>.

Whether AMPK is expressed and plays a functional role in erythrocytes has never been tested.

### 1.5.3 Regulation of $\text{Na}^+$ -coupled glucose carrier by AMP-activated protein kinase

The AMP-activated protein kinase is activated upon increase in the cytosolic AMP/ATP concentration ratio and thus senses the energy status of the cell<sup>149,155,169</sup>. Functionally, AMPK

has been demonstrated to play roles in regulation of cellular glucose uptake, glycolysis, fatty acid oxidation and of enzymes required for ATP production<sup>155-158</sup>. Accordingly, AMPK enhances the capacity of the cell to generate ATP<sup>159</sup>. By the same token, AMPK downregulates energy-utilizing mechanisms including protein synthesis, gluconeogenesis and lipogenesis<sup>155,156,159</sup>. Thus through its roles in promoting ATP production and conservation AMPK supports cell survival during energy deprivation<sup>159,160,170</sup>.

Cellular glucose uptake is mediated by two families of glucose transporters; the GLUT family that facilitates the passive transport of glucose across the membrane and the Na<sup>+</sup>-glucose cotransporters which mediate secondary active transport driven by the coupling of glucose uptake with Na<sup>+</sup>. It is widely accepted that acute activation of AMPK leads to increased glucose transport in a variety of cells predominantly through the stimulation of the GLUT family of transport<sup>171-182</sup>.

However, during prolonged ischemia low oxygen supply is paralleled by decreased extracellular glucose concentrations. Thus, the nutrient uptake with facilitative glucose carriers alone may fail to provide the cell with sufficient glucose supply in ischemic tissue. Alternatively, in response to chronic hypoxia cellular glucose transport may be achieved by Na<sup>+</sup>-coupled transporters, such as SGLT1<sup>134</sup>. Transport through SGLT1 is indirectly energy-consuming as transport is facilitated through energy maintained through the active transport of Na<sup>+</sup> across the basolateral membrane by the energy-consuming Na<sup>+</sup>/K<sup>+</sup> ATPase. At least in some cells, AMPK inhibits Na<sup>+</sup>,K<sup>+</sup> ATPase activity, which would partially dissipate the electrochemical Na<sup>+</sup> gradient<sup>183-185</sup>.

The present study thus explored whether the metabolic-sensing kinase AMPK similarly stimulates electrogenic uptake of glucose.

#### **1.5.4 Downregulation of Na<sup>+</sup>-coupled glutamate transporter EAAT3 and EAAT4 by AMP-activated protein kinase**

Clearance of extracellular glutamate in the brain may be compromised by ischemia, which may be followed by an increase in the extracellular glutamate concentration, thus enhancing glutamate action and triggering excitotoxicity<sup>186,187</sup>.

Cellular glutamate uptake is accomplished in part by EAAT3, a Na<sup>+</sup>-coupled glutamate transporter expressed in a variety of tissues including blood-brain barrier<sup>138</sup>, neurons<sup>135,146,147,188-192</sup>,

retinal ganglion cells<sup>193</sup> and glial cells<sup>139,192,194,195</sup>. Glutamate uptake into cerebellar Purkinje cells is accomplished by the glutamate transporter EAAT4<sup>146,196</sup>.

EAAT3 has been implicated in the pathophysiology of schizophrenia<sup>142,197-202</sup>, epilepsy<sup>203-207</sup> and hepatic encephalopathy<sup>208</sup>. Malfunction of the carrier is considered to impair the clearance of excitatory transmitters and thus to cause neuroexcitotoxicity in those clinical conditions. Gene targeted mice lacking EAAT3 (EAAC1) develop dicarboxylic aminoaciduria and display a significantly reduced spontaneous locomotors activity<sup>209</sup>.

Deregulated function of EAAT4 has similarly been implicated in schizophrenia<sup>142,199</sup>. Glutamate transporter currents recorded at climbing fiber (CF)-PC synapses are absent in gene targeted mice lacking EAAT4, indicating that the carrier is responsible for clearance of glutamate at this site<sup>210</sup>.

The cellular energy depletion following ischemia is expected to increase the cytosolic AMP/ATP concentration ratio thus leading to activation of the AMP-activated protein kinase, a kinase known to sense the energy status of the cell<sup>149,155,169</sup>. AMPK regulates cellular glucose uptake, glycolysis, fatty acid oxidation and enzymes required for ATP production<sup>149,155,156,158,211</sup>. Accordingly, AMPK increases cellular ATP formation<sup>159</sup>. On the other hand, AMPK inhibits energy-utilizing mechanisms, such as protein synthesis, gluconeogenesis and lipogenesis<sup>155,156,159</sup>. The AMPK-dependent regulation of cell function thus fosters cell survival during energy depletion<sup>160,170</sup>. AMPK may decrease<sup>170</sup> or increase<sup>212</sup> the cytosolic Ca<sup>2+</sup> activity, depending on the cell type.

The present study thus explored whether AMPK influences the function of the Na<sup>+</sup>-coupled glutamate transporters EAAT3 and EAAT4. AMPK dependent regulation of those transporters could be considered a paradigm for altered regulation of neurotransmitter metabolism during energy depletion.

## 1.6 Aims of the study

This study aims at elucidating the role of AMP-activated protein kinase in the erythrocytes' mechanisms of eryptosis, which regulate and control erythrocyte survival. In addition, the study focuses on defining the impact and role of AMPK in modulating the carriers SGLT1, EAAT3 and EAAT4 expressed in *Xenopus* oocytes.

Whether AMPK is expressed and plays a functional role in erythrocytes has never been tested before. Cellular energy status is sensed by the AMP-activated protein kinase activated upon increases in the cytosolic AMP-to-ATP concentration ratio<sup>149,155</sup>. Effects of AMPK include upregulation of energy producing mechanisms and downregulation of energy-utilizing mechanisms<sup>155-158</sup>. Moreover, AMPK inhibits cell growth and protects suicidal cell death or apoptosis<sup>160</sup>.

As already described above, energy depletion of erythrocytes by withdrawal of glucose increases cytosolic  $\text{Ca}^{2+}$  concentration, which in turn triggers scrambling of the cell membrane with subsequent phosphatidylserine exposure at the erythrocyte surface.  $\text{Ca}^{2+}$  activates  $\text{Ca}^{2+}$ -sensitive  $\text{K}^+$  channels leading to the efflux of  $\text{K}^+$ ,  $\text{Cl}^-$ , and osmotically obliged water subsequently further decreasing cell volume. Increase in cytosolic  $\text{Ca}^{2+}$  activity, cell membrane scrambling, and cell shrinkage are hallmarks of eryptosis, the suicidal death of erythrocytes<sup>6</sup>. The present study addresses the expression of the AMP-dependent kinase in erythrocytes and a functional role of AMPK in the regulation of suicidal erythrocyte death during energy depletion and increase in cytosolic  $\text{Ca}^{2+}$  activity.

The AMP-activated protein kinase senses energy status of the cell<sup>149,155</sup>. It is widely accepted that acute activation of AMPK leads to increased glucose transport in a variety of cells predominantly through the stimulation of the GLUT family of transporters. However, during prolonged ischemia (low oxygen supply paralleled by decreased extracellular glucose concentrations) nutrient uptake by facilitative glucose carriers alone may fail. Alternatively, in response to chronic hypoxia cellular glucose transport and thus energy maintenance may be achieved by  $\text{Na}^+$ -coupled transporters (indirectly energy-consumption), such as SGLT1<sup>134</sup>. The present study thus explored whether the metabolic sensing kinase, AMPK, would similarly stimulate electrogenic uptake of glucose by SGLT1.

Clearance of extracellular glutamate in the brain may be compromised by ischemia, which may be followed by an increase in the extracellular glutamate concentration, thus enhancing glutamate action and triggering excitotoxicity<sup>186,187</sup>. Cellular glutamate uptake is accomplished in part by EAAT3, a Na<sup>+</sup>-coupled glutamate transporter expressed in a variety of tissues<sup>135,136,194</sup>. Whereas Glutamate uptake into cerebellar Purkinje cells is accomplished by the glutamate transporter EAAT4<sup>146,196</sup>. Malfunction of the carriers EAAT3 and EAAT4 have been implicated in the various pathophysiological conditions<sup>142,199,206,213</sup> by impairing the clearance of glutamate and thus causing neuroexcitotoxicity in those clinical conditions. The AMPK-dependent regulation of cell function fosters cell survival during energy depletion<sup>160,170</sup>. The present study thus explored whether AMPK influences the function of the Na<sup>+</sup>-coupled glutamate transporters EAAT3 and EAAT4.



## 2 Materials and Methods

### 2.1 Materials

#### 2.1.1 Equipments

8-channel-multi-pipette Research pro	Eppendorf, Hamburg, Germany
Autoclave HICCAVE HV-50 HMC	Systemec Labor Systemtechnik, Wettenberg, Germany
Berthold Biolumat LB9500	Bad Wildbad, Germany
Digitizer Digidata 1322A	Axon instruments. USA
DMZ Universal Puller	Zeitz-Instruments, Martinsried, Germany
Electronic Hematology Particle Counter	Scil Vet abc, Weinheim, Germany
Eppendorf Biophotometer	Eppendorf AG, Hamburg, Germany
Eppendorf Centrifuge 5415R	Hinz GmbH. Hamburg, Germany
Eppendorf Pipettes 0.1-1000µl	Eppendorf, Hamburg, Germany
FACS-Calibur from Becton Dickinson	Heidelberg, Germany
Fluorescence laser scanning microscope (LSM 510)	Carl Zeiss MicroImaging GmbH, Germany
Fluorescence microscope	Axiovert, Zeiss, Jena, Germany
Gene clamp 500 amplifier	Axon Instruments, Foster City, CA, USA
Hera cell incubator 37 °C	Kendro Laboratory Products, Langenselbold, Germany
Hettich zentrifugen Rotanta 460R	Andreas Hettich GmbH & Co. KG, Tuttlingen, Germany
KL1500 LCD	Carl Zeiss MicroImaging, Oberkochen, Germany

Luminometer (Walter Wallac 2 plate reader)	Perkin Elmer, Juegesheim, Germany
Luminometer TD20/20	Bad Wildbad, Germany
MacLab D/A converter	AD Instruments, Castle Hill, Australia
Microscope Stemi 200	Carl Zeiss MicroImaging, Oberkochen, Germany
Nanoliter Injector 2000	World Precision Instruments, Berlin, Germany
Nitrocellulose membrane	Millipore GmbH, Schwalbach/Ts., Germany
pH Meter 646	Carl Zeiss , Oberkochen, Germany
Photometer Tecan Sunrise Remote	Tecan, Männedorf, Switzerland
Safety cabinet class II (Hera Safe)	Kendro Laboratory Products, Langenselbold, Germany
Stereomicroscope	Wetzlar/Munich, Germany
Using micromanipulators	Leitz, Wetzlar, Germany
VX-100 Vortex Mixer	Labned, Langenfeld, Germany
WPI microinjector	WPI, Sarasota, FL, USA
Zeiss LSM 5 EXCITER Confocal Laser Scanning Microscope, equipped with a 405–633 nm laser	Carl Zeiss MicroImaging GmbH, Germany

### **2.1.2 Chemicals**

A-769662	Tocris Biosciences, Ellisville, USA
Acetone	Sigma, Taufkirchen, Germany
AICAR	Calbiochem, Bad Soden, Germany
Annexin V-Fluos	Roche, Mannheim, Germany
Annexin V-APC	BD, Heidelberg, Germany
BSA	Sigma, Taufkirchen, Germany
CaCl <sub>2</sub> x 2H <sub>2</sub> O	Carl Roth, Karlsruhe, Germany

CFSE	Molecular Probes, Leiden, Netherlands
Collagenase	Worthington Biochemical Corp., NJ, USA
Compound C	Calbiochem, Bad Soden, Germany
D-(+) Glucose	Sigma, Taufkirchen, Germany
DMEM medium	Invitrogen Carlsbad, USA
DRAQ-5 dye	Biostatus, Leicestershire, UK
ECL detection reagent	Amersham, Freiburg, Germany
EZ-link Sulfo-NHS-Biotin	Pierce protein research products, Thermo Scientific, USA
Fluo-3/AM	Calbiochem; Bad Soden, Germany
Gentamicin solution	Sigma, Taufkirchen, Germany
Glucose	Carl Roth Karlsruhe Germany
HEPES	Sigma, Taufkirchen, Germany
Ionomycin	Sigma, Schnelldorf, Germany
KCl	Carl Roth Karlsruhe Germany
KCl solution 3M, AgCl saturated	Carl Roth, Karlsruhe, Germany
Laemmli buffer	Sigma, Taufkirchen, Germany
L-Glutamic acid, non animal source	Sigma, Taufkirchen, Germany
Lysis buffer	Sigma, Taufkirchen, Germany
Methanol	Sigma, Taufkirchen, Germany
MgSO <sub>4</sub>	Sigma, Taufkirchen, Germany
NaCl	Sigma, Taufkirchen, Germany
NeutrAvidin Agarose Resin	Thermo Scientific, USA
Nonfat milk in TBS	Cell Signaling Technology, Inc. Danvers, USA
Normal goat serum	Invitrogen, Paisley, UK
Ouabain	Sigma, Schnelldorf, Germany
Paraffin	MERCK, Darmstadt, Germany
Paraformaldehyde	Sigma, Schnelldorf, Germany

Pavidon-Iod	Braun, Melsungen AG, Germany
PBS	Sigma, Taufkirchen, Germany
Phenformin hydrochloride	Sigma, Taufkirchen, Germany
Prolong Gold antifade reagent	Invitrogen, Carlsbad, USA
Protease inhibitor cocktail	Sigma, Schnellendorf, Germany
Sodium piruvate	Sigma, Taufkirchen, Germany
Theophylin	Sigma, Taufkirchen, Germany
Water immersion Plan-Neofluar 63/1.3 NA DIC	Carl Zeiss MicroImaging GmbH, Germany

### 2.1.3 Antibodies

Anti-ceramide antibody (clone MID 15B4)	Alexis, Grünberg, Germany
Anti-rabbit IgG antibody (Secondary)	Cell Signaling, Danvers, MA, USA
Anti-SGLT1 antibody (rabbit polyclonal antibody)	Millipore GmbH, Schwalbach/Ts., Germany
Cy5 anti-rabbit	Jackson ImmunoResearch Laboratories, W Baltimore, USA
FITC anti-goat antibody	Invitrogen, Carlsbad, USA
FITC-conjugated goat anti-rabbit	Invitrogen, Carlsbad, USA
Goat anti-EAAT3 antibody	Millipore, Chemicon International, USA
Goat anti-SGLT1	Santa Cruz Biotechnology, Inc., Santa Cruz, USA
Primary mouse monoclonal anti-EAAC1/EAAT3 antibody	Zymed Laboratories, Invitrogen, USA
Primary rat monoclonal anti-HA antibody (clone 3 F10)	Boehringer, Biberach, Germany
Rabbit AMPK $\alpha$ antibody	Cell Signaling, Danvers, MA, USA
Rabbit anti-alpha tubulin	Cell Signalling Technology, Danvers, USA

Rabbit anti-AMPK $\alpha$ antibody	Cell Signaling, Danvers, MA, USA
Secondary, anti-rabbit antibody	Cell Signaling, Danvers, MA, USA
Secondary, goat anti-rat conjugated Alexa488 antibody	Invitrogen Carlsbad, USA
Secondary, peroxidase-conjugated affinity-purified F(ab') <sub>2</sub> goat anti-rat IgG antibody	Jackson ImmunoResearch, West Grove, PA, USA
Secondary, peroxidase-conjugated sheep anti-mouse IgG antibody	GE Healthcare, Amersham, UK
Secondary, swine anti-goat conjugated FITC antibody	Invitrogen Carlsbad, USA
$\alpha$ -actin antibody (rabbit polyclonal antibody)	Cell Signaling, Danvers, MA, USA

#### **2.1.4 Kits**

Competitive immunoassays (B <sub>12</sub> and folate)	R&D Systems, Inc., Minneapolis, USA
Erythropoietin immunoassay kit	R&D Systems, Wiesbaden, Germany
Immunoassay kit	R&D Systems, Wiesbaden, Germany
Luciferin–luciferase assay kit	Roche Diagnostics, Mannheim, Germany
Nuceobond Xtra Midi	MACHEREY-NAGEL, Dürren, Germany
Site Directed Mutagenesis Kit	Stratagene, Heidelberg, Germany
SuperSignal ELISA Femto Maximum Sensitivity Substrate	Pierce, Rockford, IL, USA

### 2.1.5 Stock materials

12-mm glass coverslips in 12-well plates	neoLab Migge Laborbedarf- Vertriebs GmbH, Heidelberg, Germany
96-well plates	Greiner Bio-One, Frickenhausen
Borosilicate glass capillaries	Harvard APPARATUS. USA
Bottle-top filters for 0.125 l	Millipore, Schwalbach, Germany
Bottle-top filters for 0.25 and 0.5 l	Carl Roth, Karlsruhe, Germany
Combitips plus 2.5 ml	Eppendorf, Hamburg, Germany
Disposable cuvettes (12 x 50 mm)	Promega corporation, USA
Eppendorf tubes	Eppendorf, Hamburg, Germany
FACS tubes	Greiner Bio-One, Frickenhausen
Falcon tubes (15 and 50 ml)	Greiner Bio-One, Frickenhausen
Glass replacement	World Precision Instruments, Inc. Sarasota, FL, USA
Tissue Culture Dish (60 x 15mm) Style medium	Carl Roth Karlsruhe Germany
Vicryl (P-3, 13mm, 3/8c)	Ethicon, Norderstedt, Germany

### 2.1.6 Human erythrocytes

Experiments were performed at 37°C with isolated leukocyte-depleted erythrocytes from concentrates provided by the blood bank of the University of Tübingen. The volunteers providing erythrocytes gave informed consent.

The study has been approved by the ethical Commission of the University of Tübingen (184/2003V).

### 2.1.7 Mice

Experiments were performed in 6- to 12-wk-old male AMPK $\alpha$ 1-deficient mice (*ampk*  $-/-$ ) and their wild-type littermates (*ampk*  $+/+$ ). The *ampk*  $-/-$  mice have been described previously

214.

All animal experiments were conducted according to the guidelines of the American Physiological Society as well as the German law for the welfare of animals and were approved by local authorities.

### **2.1.8 *Xenopus laevis***

Female *X. laevis* frogs were maintained at the animal facility of the Physiological Institute, University of Tübingen. Frogs were kept humanely in accordance with the German law for the welfare of animals and were approved by local authorities.

### **2.1.9 Software**

CellQuest Version 9 and 10	BectonDickinson, Heidelberg, Germany
InStat statistic program	GraphPad Software San Diego, California, USA
pClamp 9.0 software package	Axon instruments, USA
Quantity one software (Biorad gel doc system, Chemidoc XRS)	Bio-Rad Laboratories GmbH, München, Germany

## **2.2 Methods**

### **2.2.1 Regulation of erythrocyte survival by AMP-activated protein kinase**

#### ***2.2.1.1 Blood chemistry, blood count, and isolation of murine erythrocytes***

For all experiments except for the blood count, heparin blood was retrieved from the mice. The plasma concentrations of erythropoietin were determined using an immunoassay kit according to the manufacturer's instructions (R&D Systems, Wiesbaden, Germany). Vitamin B<sub>12</sub> and folate were determined by competitive immunoassays according to clinical standards in the laboratory of the University Hospital Tübingen. For the blood count, EDTA blood was analyzed using an electronic hematology particle counter (scil Vet abc, Weinheim, Germany). Murine erythrocytes were isolated by being washed two times with Ringer solution containing (in mM): 125 NaCl, 5 KCl, 1 MgSO<sub>4</sub>, and 32 HEPES/NaOH (pH 7.4), 5 glucose, and 1 CaCl<sub>2</sub>.

#### ***2.2.1.2 Western blotting***

To examine the expression of AMPK $\alpha$  in human or murine erythrocytes, 150  $\mu$ l erythrocyte pellets was lysed in 50 ml of 20 mM HEPES/NaOH (pH 7.4). Ghost membranes were pelleted (15,000 g for 20 min at 4°C) and lysed in 200  $\mu$ l lysis buffer (50 mM Tris-HCl, pH 7.5; 150 mM NaCl; 1% Triton X-100; 0.5% SDS; 1 mM NaF; 1 mM Na<sub>3</sub>VO<sub>4</sub>; and 0.4%  $\beta$ -mercaptoethanol) containing protease inhibitor cocktail (Sigma, Schnellendorf, Germany). In all cases, 60  $\mu$ g of protein was solubilized in Laemmli sample buffer at 95°C for 5 min and resolved by 10% SDS-PAGE. For immunoblotting, proteins were electrotransferred onto a polyvinylidene difluoride (PVDF) membrane and blocked with 5% nonfat milk in TBS-0.10% Tween 20 at room temperature for 1 h. Then, the membrane was incubated with affinity purified rabbit AMPK $\alpha$  antibody (1:1000; 62 kDa; Cell Signaling, Danvers, MA, USA) at 4°C overnight. After being washed (in TBS-0.10% Tween 20) and subsequently blocked, the blots were incubated with secondary anti-rabbit antibody (1:2000; Cell Signaling) for 1 h at room temperature. After being washed, the antibody binding was detected with the ECL detection reagent (Amersham, Freiburg, Germany).



### 2.2.1.3 Confocal microscopy and immunofluorescence

For the detection of AMPK $\alpha$ , erythrocytes were resuspended in PBS at  $5 \times 10^7$  cells/ml, and 20  $\mu$ l was smeared onto a glass slide. After being air dried for 30 min and fixed with methanol for 2 min, the slide was rinsed 4 times over 10 min with PBS. Then, the slide was blocked with 10% normal goat serum (Invitrogen, Paisley, UK) for 10 min and again rinsed 3 times with PBS for 5 min each. After incubation with rabbit anti-AMPK $\alpha$  antibody (1:200; Cell Signaling) diluted in PBS at 4°C overnight, the slide was again rinsed 3 times with PBS for 5 min each time. Subsequently, the slide was incubated with FITC-conjugated goat anti-rabbit (1:500; Invitrogen) antibody diluted in PBS for 1.5 h at room temperature. Then, the slide was rinsed 3 times with PBS for 10 min each time and mounted with Prolong Gold antifade reagent (Invitrogen).

Images were taken on a Zeiss LSM 5 EXCITER confocal laser scanning microscope (Carl Zeiss MicroImaging, Oberkochen, Germany) with a water immersion Plan-Neofluar 63/1.3 NA DIC. For the detection of annexin V binding and carboxyfluorescein-diacetate-succinimidyl-ester (CFSE)-dependent fluorescence of erythrocytes from murine spleens, the spleens of AMPK $\alpha$ -deficient mice and their wild-type littermates were homogenized mechanically in 1ml cold PBS. The suspension was then centrifuged at 500 g for 10 min at 4°C. The cell pellet was resuspended in 200  $\mu$ l cold PBS. Five microliters of annexin V-APC (BD, Heidelberg, Germany) was added, and incubation was carried out for 20 min at 37°C protected from light. Then, the suspension was transferred onto a glass slide and mounted with Prolong Gold antifade reagent (Invitrogen).

Images were taken as described above.

### 2.2.1.4 Incubations and solutions

For the *in vitro* experiments on suicidal death of erythrocytes incubations were carried out at 37°C in Ringer solution at a hematocrit of 0.4% in a total volume of 200  $\mu$ l. Where indicated, glucose-free Ringer was used. One mM 5-aminoimidazole-4-carboxamide-1- $\beta$ -d-ribofuranoside (AICAR), 20  $\mu$ M compound C (both from Calbiochem, Bad Soden, Germany) or 0.1  $\mu$ M calcium ionophore ionomycin (Sigma, Schnellendorf, Germany) were added to the respective solution, where indicated.

### **2.2.1.5 Determination of the osmotic resistance**

Two microliters of blood was added to 200  $\mu$ l of PBS solutions with decreasing osmolarity. After centrifugation for 5 min at 500 g, the supernatant was transferred to a 96-well plate, and the absorption at 405 nm was determined as a measure of hemolysis. Absorption of the supernatant of erythrocytes lysed in pure distilled water was defined as 100% hemolysis.

### **2.2.1.6 Phosphatidylserine exposure and forward scatter**

FACS analysis was performed as described earlier<sup>215</sup>. After incubation, erythrocytes were washed in Ringer solution containing 5 mM CaCl<sub>2</sub>. The cells were then stained with annexin V-Fluos (Roche, Mannheim, Germany) at a 1:500 dilution. After 15 min, samples were measured by flow cytometric analysis (FACS-Calibur). Cells were analyzed by forward scatter, and annexin-V-fluorescence intensity was measured in fluorescence channel FL-1 with an excitation wavelength of 488 nm and an emission wavelength of 530 nm.

### **2.2.1.7 Measurement of intracellular Ca<sup>2+</sup>**

Intracellular Ca<sup>2+</sup> ([Ca<sup>2+</sup>]<sub>i</sub>) measurements were performed as described previously<sup>93</sup>. Briefly, erythrocytes were washed in Ringer solution and then loaded with Fluo-3/AM (Calbiochem) in Ringer solution containing 5 mM CaCl<sub>2</sub> and 2  $\mu$ M Fluo-3/AM. The cells were incubated at 37°C for 20 min and washed twice in Ringer solution containing 5 mM CaCl<sub>2</sub>.

The Fluo-3/AM-loaded erythrocytes were resuspended in 200  $\mu$ l Ringer. Then, Ca<sup>2+</sup>-dependent fluorescence intensity was measured in fluorescence channel FL-1 in FACS analysis.

### **2.2.1.8 Measurement of the in vivo clearance of fluorescence-labeled erythrocytes**

The experiment was performed as described previously<sup>94</sup>. Briefly, erythrocytes (obtained from 200  $\mu$ l bloods) were fluorescence labeled by staining with 5  $\mu$ M CFSE (Molecular Probes, Leiden, Netherlands) in PBS and incubated for 30 min at 37°C. After washing twice in PBS containing 1% FCS, the pellet was resuspended in Ringer solution (37°C), and 100  $\mu$ l of the CFSE-labeled erythrocytes was injected into the tail vein of the recipient mouse. Every day,

blood was retrieved from the tail veins of the mice, and CFSE-dependent fluorescence intensity of the erythrocytes was measured in FL-1 as described above. The percentage of CFSE-positive erythrocytes was calculated as percentage of the total labeled fraction determined 5 min after injection.

#### **2.2.1.9 Statistics**

Data are expressed as arithmetic means  $\pm$  SEM and statistical analysis was made by paired or unpaired t-test, by u-test, or by ANOVA, as appropriate. Values of  $P < 0.05$  were considered as statistically significant.

### 2.2.2 Site Directed Mutagenesis

For surface abundance quantification of EAAT4 transporters on the oocytes membrane, a hemagglutinin tag (HA-tag) was introduced in an extracellular loop of transporters by two-stage Polymerase Chain Reaction (PCR) site-directed mutagenesis. The expression of HA-tagged transporters then was detected using an anti-HA antibody by a chemiluminescence assay.

At the first stage of the two-stage PCR site-directed mutagenesis, two separate PCR reactions were performed, one with the forward primer and another with the reverse primer (Table 2.2.2.A) containing the HA sequence flanked for EAAT4 specific sequences. The first PCR consisted of 4 cycles of 30s at 94°C; 30s at 95°C; 1min at 55°C; 2 min at 68°C. In the second stage, the PCR products were mixed and further amplified as a single reaction, and the PCR consisted of 18 cycles of 30s at 94°C; 30s at 95°C 1min at 55°C; 2 min at 68°C.

**Table 2.2.2.A<sub>Method</sub>. Forward and reverse primers used to generate EAAT4-HA.**

Protein	Forward Primer	Reverse Primer
EAAT4-HA	5' GGGTCAGAGTTGGGG TACGACGTACCAGATTAC GCTGCCTCCATTTCTCC 3'	5' GGAGAAATGGAGG CAGCGTAATCTGGTAC GTCGTACCCCAACTCT GACCC 3'

In the table 2.2.2.B is given the composition of the PCR mixture as suggested by Stratagene (Heidelberg, Germany).

**Table 2.2.2.B<sub>Method</sub>. Polymerase Chain Reaction mixture for two-stage PCR site-directed mutagenesis.**

PCR reaction mixture	Quantity
10X Pfu buffer	5 µl
10 mM primer	1 µl
Plasmid template	0.1 – 0.2 µl
10 mM dNTP mix	1 µl
H <sub>2</sub> O	Final volume of 50 µl
Pfu turbo polymerase	1 µl

Since the product of final PCR contains a mixture of mutated and wild type plasmid DNA, in order to get rid of DNA wild type, the product was treated with 1  $\mu$ l of *Dpn* I enzyme (10U/ $\mu$ l) which digests only methylated parent (template) DNA. Then, by using the heat shock method, the subsequent product was transformed into *E.coli* XL1-Blue Supercompetent cells and plated onto LB plates to grow bacteria. Grown bacteria were picked and inoculated into LB media then used for further DNA isolation and RNA synthesis. To confirm the presence of desired mutation, mutants were sequenced.

This EAAT4-HA mutant was used to study the modulation of EAAT4 activity, cell surface expression and plasma membrane abundance by AMPK.

The mutants of  $\gamma^{R70Q}$ AMPK, and  $\alpha^{K45R}$ AMPK were prepared by other collaborators.

### **2.2.2.1 Transformation of *E.coli* XL1-Blue Supercompetent Cells**

After *E.coli* XL1-Blue Supercompetent cells from Stratagene (Heidelberg, Germany) were thawed with the usage of ice, 50  $\mu$ l of the supercompetents cells were taken into a prechilled Falcon 2059 polypropylene tube. 1  $\mu$ l of *Dpn* I-treated DNA sample was added to the aliquots of supercompetent cells. To mix the content, the tube was gently vortexed and incubated for 30 minutes on ice.

The transformation reaction was started by keeping the tube at 42°C for 45 seconds which causes the bacteria to open their cell wall pores, thus enabling entry of DNA inside the bacteria cells. The tube was then suddenly placed on ice for 2 minutes allowing bacteria to close their pores of the cell wall.

0.5 ml of preheated (42°C) NZY broth was added to the heat-shock treated supercompetent cells and incubated at 37°C for 1 hour shaking at 220 rpm. Then, 250  $\mu$ l of DNA transformed bacterial cells were plated on agar plates. These LB plates were incubated overnight at 37°C.

Bacterial cells needed to be multiplied for transformed plasmids isolation were used for further experiments.

### 2.2.3 Preparation of cRNA

Mutant DNAs including EAAT4-HA,  $\gamma^{R70Q}$ AMPK, and  $\alpha^{K45R}$ AMPK were used as a template to synthesize cRNA. Also, using the same method, cRNAs of AMPK $\alpha$ 1, AMPK $\beta$ 1, AMPK $\gamma$ 1, SGLT1, EAAT1, EAAT2, EAAT3, and EAAT4 were synthesized. The RNA synthesis protocol possesses two steps:

1. Linearization of the plasmid DNA containing the sequence of interest;
2. Generation of cRNA itself.

#### 2.2.3.1 Plasmid DNA linearization

Endonucleases were used to obtain a cut at 3' end of the insert. Specific restriction enzymes as shown in table 2.2.3.1A were used to linearize specific plasmids.

**Table 2.2.3.1A<sub>Method</sub>. Plasmids containing the desired genes encoding for specific proteins and restriction endonuclease enzymes used to linearize each plasmid.**

Protein	Plasmid	Restriction Endonuclease
Human SGLT1	pBluescript	EcoRI
Human EAAT1	pOTV	SmaI, BamHI, Spe I, NotI
Human EAAT2	pOTV	SmaI, BamHI, Spe I, NotI
Human EAAT3	pBluescript SK+	NotI
Human EAAT4	pGHJ	XbaI/NotI
Human EAAT4-HA	pGHJ	Xba I
AMPK $\alpha$ 1-HA	PolI	NheI
$\alpha^{K45R}$ AMPK $\alpha$ .1-HA	PolI	NheI
AMPK $\beta$ 1-flag	PolI	NheI
AMPK $\gamma$ 1-HA	PolI	NheI
$\gamma^{R70Q}$ AMPK $\gamma$ 1-HA	PolI	NheI

The reaction mixture as presented in the table below (table 2.2.3.1A) was prepared and incubated for 2 hours at 37°C. Afterwards DNA was precipitated with 1 volume of isopropanol (50  $\mu$ l) and 1/10 volume (5  $\mu$ l) of 3 M sodium acetate, at a pH of 5.2, and incubated for 10

minutes at room temperature. The reaction mixture was centrifuged at 17,000 rpm for 15 minutes at 4°C. After removal of the supernatant, the pellet was washed twice with 70 % ethanol (100 µl) at 17,000 rpm for 10 minutes. Ethanol was removed from the last wash and the pellet was dried using the Eppendorf Concentrator (Eppendorf, Hamburg, Germany) at 35-45° C for 5 minutes.

**Table 2.2.3.1.B<sub>Method</sub>. Reaction mixture used to linearize DNA plasmid.**

<b>Reaction mixture</b>	<b>Quantity</b>
10X Buffer	5 µl
Plasmid DNA (10 µg)	20 µl
Restriction enzymed (20U)	2 µl
Water	23 µl

### **2.2.3.2 cRNA synthesis**

The linearized DNA produced by the method mentioned above was used as a template to generate cRNA. The reaction mixture listed below (table 2.2.3.2.A) was put in a sterile eppendorf tube.

**Table 2.2.3.2.A<sub>Method</sub>. Reaction mixture used to synthesize RNA from the linearized DNA.**

<b>Reaction mixture</b>	<b>Quantity</b>
Linearized DNA (1 µg)	10 µl
10 X Buffer	2.5 µl
rNTPs	1 µl
Cap analogue	2.5 µl
RNase inhibitor	1 µl
Water	8 µl

The reaction mixture was gently spanned and the appropriate RNA polymerase (Table 2.2.3.2.B) was added and pulse spanned again. RNA polymerases T3 or T7 were used, and the mixture was then incubated at 37°C for 1 hour. 1 µl of DNase was added in the reaction mixture afterwards to remove the possible DNA contamination. Finally the reaction mixture was incubated at 37°C for 15 min by shaking.

**Table 2.2.3.2.B<sub>Method</sub>** RNA polymerases used to prepare cRNA and amount of cRNA injected into oocytes.

Protein	RNA Polymerase	cRNA (ng/oocyte)	Exp. time (days)
Human SGLT1	T3	5	3
Human EAAT1	T7	2	5
Human EAAT2	T7	2	5
Human EAAT3	T7	2	3
Human EAAT4	T7	6	3-5
Human EAAT4-HA	T7	6	3-5
AMPK $\alpha$ 1-HA	T7	4.6	3
$\alpha$ K45R AMPK $\alpha$ .1-HA	T7	4.6	3
AMPK $\beta$ 1-flag	T7	4.6	3
AMPK $\gamma$ 1-HA	T7	4.6	3
$\gamma$ R70Q AMPK $\gamma$ 1-HA	T7	4.6	3

To purify the generated RNA, 125  $\mu$ l of phenol chloroform mixture was mixed with 100  $\mu$ l DEPC water and centrifuged at a maximum speed for 2 minutes. After that the upper inorganic phase was carefully taken into a new eppendorf tube, 12.5  $\mu$ l of 3 M sodium acetate (pH 5.2) was added, as well as, 375  $\mu$ l of ethanol (100% concentration) then mixed by pulse vortex and further incubated at -70 °C overnight.

After incubation, the mixture was centrifuged at 17000 rpm for 15 minutes at 4 °C. The supernatant was removed and the pellet was washed twice with 200  $\mu$ l of 70% ethanol. Finally the pellet was left to dry at room temperature and reconstituted in 25  $\mu$ l of DEPC water and vortexed. Then cRNA concentration was measured by taking 1  $\mu$ l of cRNA in 69  $\mu$ l water using an Eppendorf Biophotometer (Hamburg, Germany). Finally, to confirm quality of generated cRNA its quality was checked by gel electrophoresis.

### 2.2.3.3 *Xenopus laevis* oocyte preparation and maintenance

To study function and plasma membrane abundance of transporters *Xenopus laevis* oocytes were used. Prior to operation the frogs were anaesthetized by submersion in a 0.1% 3-



aminobenzoic acid ethyl ester solution (Sigma, St. Louis, Mo, USA) and placed on ice for surgery. Through a small abdominal incision (1-2 cm in length) small pieces of ovary were removed carefully and the wound was subsequently closed with a reabsorbable suture. To prevent drowning, frogs were kept wet but not under water until reflexes were fully recovered. The ovarian sacs were manually separated and oocytes enzymatically defolliculated and thus singularized by treatment of ovarian lobes with a  $\text{Ca}^{2+}$ -free OR2- collagenase solution (OR2 supplemented with 1-2mg/ml collagenase (Worthington Biochemical Corp., NJ, USA)) for about 2 h at room temperature (at app. 22°C), then slightly shaken in the flask to ensure even digestion. To remove all degraded elements obtained at this point, the oocytes were washed in a  $\text{Ca}^{2+}$ -free OR2- solution. To stop defolliculation, oocytes were repeatedly washed with ND96 solution (96 mM NaCl, 2 mM KCl, 1.8 mM  $\text{CaCl}_2$ , 1 mM  $\text{MgCl}_2$ , and 5 mM HEPES, pH 7.4) and singularized oocytes were stored in a ND-96 storage solution (complemented after sterilization with 5 mM Sodium pyruvate, 50  $\mu\text{g/ml}$  gentamycin and staurosporine (to prevent infections) and 0.5 mM theophylline (inhibits the further maturation)). Large oocytes (stage V-VI) showing evenly colored poles and a sharp border between both poles were selected and microinjected with an appropriate amount of cRNA using a nanoliterinjector 2000 (World Precision Instruments, Berlin, Germany) with glass capillaries (WPI, Sarasota, FL, USA) mounted in a micromanipulator controlled by nanoliterinjector 2000. During injection permanent care was taken to avoid contamination of cRNA with RNases (by cleaning the space around, as well as, by using sterile pipettes, gloves, and DEPC water for dilution of cRNA) or small particles which could clog the injection capillaries. A glass capillary tip was manually broken under the microscope to provide an orifice with a diameter of about 10-20  $\mu\text{m}$  and in order to seal the pipette from air it was backfilled with paraffin oil. Then cRNA was loaded into the capillary (usually  $\sim 2 \mu\text{l}$ ) by suction and oocytes were placed into a 35 mm petri dish with a polypropylene mesh glued to the bottom to fix the oocytes. A certain amount of cRNA was injected in each oocyte (see Table 2.2.3.2.B). After injection, oocytes were kept in petri dishes containing app. 3 ml ND 96 storage solution (see Table 2.2.6) in an incubator at about 15° C. Oocytes were also separated to each others. Daily, dead and damaged oocytes were removed and the sterile ND-96 storage solution which had been exchanged using a sterile pipette. Under these conditions oocytes were kept stored as long as 3-5 days after injection until the cRNA was expressed. Thereafter two electrode voltage clamp (TEVC) experiments or confocal and other experiments

were performed with oocytes<sup>216,217</sup>. Figure 2.2.3.3 depicts oocyte preparation, cRNA injection and subsequent procedure.

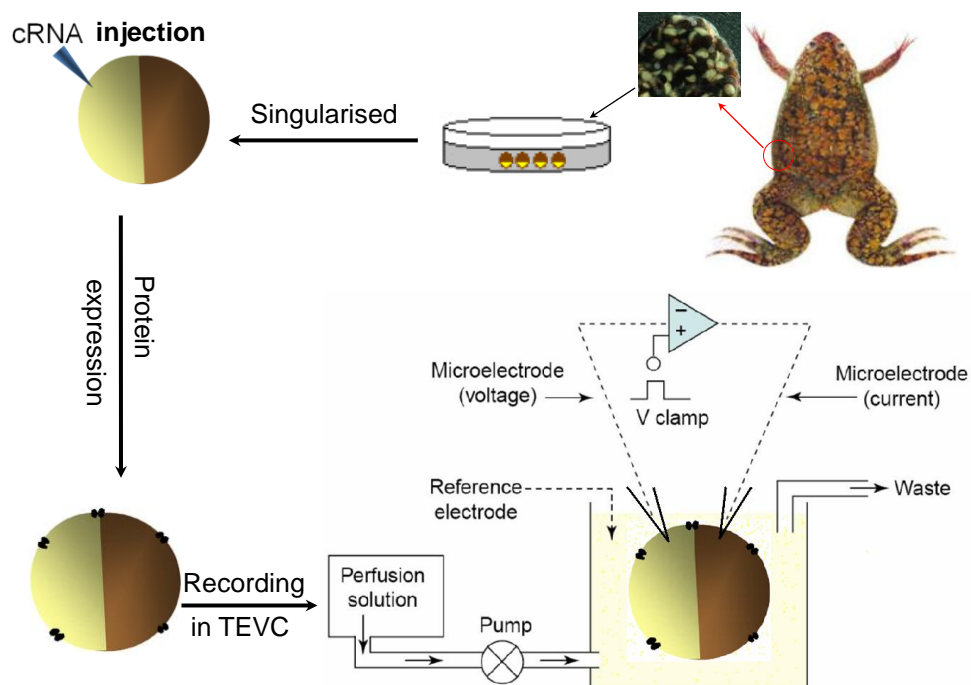


**Figure 2.2.3.3<sub>Method</sub>** An overview of oocytes preparation, cRNA injection, protein expression in oocytes, and TEVC measurement. Frog was operated and oocytes were taken from ovarian sacs, treated with collagenase to be singularized. After that treatment, oocytes were washed, sorted (stage V and VI), injected and then incubated for protein expression in ND 96 storage solution at 15°C. *X. laevis* oocytes expressing transporters were placed in a chamber and continuously perfused. Oocytes are pierced with two microelectrodes, one to maintain a constant voltage, the other to register changes in current and then were recorded.

#### 2.2.4 Protein expression in *Xenopus laevis* oocyte

Oocytes were injected with cRNA of AMP-activated protein kinase and/or SGLT1, EAAT1, EAAT2, EAAT3, EAAT4 and EAAT4-HA.

After expression time as detailed in Table 2.2.3.2.B, studies on the activity of the transporters, tracer uptake measurements were carried out. On the same day immunohistochemistry assay, chemiluminescence, western blots and confocal experiments were performed to study the plasma membrane abundance of the transporters.

### 2.2.5 Two-electrode-voltage clamp

TEVC technique is the most widely used electrophysiological technique for the measurement of whole cell currents through ion channels or electrogenic transporters expressed in *Xenopus* oocytes by allowing the scientists to control the membrane potential (clamping) and thus measuring currents flowing through ion channels, electrogenic transporters or pumps. Two glass microelectrodes are impaled into the oocyte (just under the cell membrane), a membrane potential recording electrode and a current-delivering electrode. The membrane voltage electrode connects to a feedback amplifier where the signal is compared to the voltage clamp command given by a generator. The highly amplified difference of these signals is applied as a current through the current-delivering electrode, across the membrane, and to the bath-grounding electrode. All electrogenic fluxes across the membrane are now measured as a deflection from the baseline current (Fig. 2.2.3.3.). The ground electrodes were made of 3 % Agar and 3 M KCl, whereas the microelectrodes were backfilled with 3 M KCl. With a Faraday cage the whole setup was carefully grounded and shielded against external currents. To reduce vibrations, which may otherwise damage the membrane around the site of electrode impalement, the whole setup is mounted on a pneumatic anti-vibration table<sup>216-218</sup>.

For the experiments glass capillaries were used with a thin filament (silver chloride coating on the Ag/AgCl<sub>2</sub> electrode) inserted into that glass capillary. Electrodes were backfilled with 3 M KCl and connected to the feedback amplifier. The electrode resistance varies between 0.3 (Mohms) and 3 MΩ. The flow rate of the superfusion was 20 ml/min and, in theory, a complete exchange of the bath solution was reached within about 10 s. However, due to unstirred layers the full exchange of fluid around the oocyte may be slower.<sup>216,218,219</sup>

The electrode offset, in the bath solution just before impaling the oocyte, was set to 0 mV. Using micromanipulators (Leitz, Wetzlar, Germany), under a low magnification stereomicroscope (5-20X), in the presence of light within the oocyte was impaled with the microelectrodes at opposite poles. After impalement of both electrodes the amplifier was turned to the voltage clamping mode at the voltage-clamp feedback gain 1. Currents were filtered at 10 Hz. Currents were measured with a Geneclamp 500 amplifier (Axon Instruments, Foster City, CA, USA) and recorded with a MacLab D/A converter (AD Instruments, Castle Hill, Australia) on a computer for data storage and subsequent analysis using chart or scope software.

Electrogenic transporters were measured at a fixed holding potential and varying application of different concentrations of substrate<sup>216,217,219</sup>.

### 2.2.6 Tracer flux measurements

The two Electrode Voltage Clamp (TEVC) setup was employed for electrophysiological recordings of transporters expressed in *X. laevis* oocytes. Functions of the sodium coupled transporters were demonstrated by means of tracer flux measurements. The transport assay was performed on the 3<sup>rd</sup> -5<sup>th</sup> day after respective cRNA injection. About 25 oocytes were incubated in app. 3 ml of ND96 storage (medium) solution.

For measuring SGLT1 activity as a superfusate was used ND-96 solution. Glucose was added to the solutions at a concentration of 10 mM unless otherwise stated. Where indicated, 1 mM ouabain was added to the control superfusate. The pump current generated by readdition of extracellular K<sup>+</sup> was determined by subsequent exposure of the oocytes for 5 hours to K<sup>+</sup>-free perfusate, for further 5 minutes to Ba<sup>2+</sup> (5 mM) containing K<sup>+</sup>-free perfusate and then to Ba<sup>2+</sup> containing K<sup>+</sup>-containing (5 mM) perfusate.

Same ND-96 solution was used as a superfusate to measure EAAT1-4 activity. Glutamate was added to the solutions at a concentration of 2 mM unless otherwise stated. Where indicated, Na<sup>+</sup> was replaced by Li<sup>+</sup> or NaCl by NaNO<sub>3</sub>.

**Table 2.2.6<sup>Method</sup>. Types of solutions used in two electrode voltage clamp experiments.**

<b>Solutions</b>	<b>ND-96</b>	<b>ND-96 storage solution</b>	<b>OR2</b>	<b>OR2 with collagenase</b>	<b>Li-based solution</b>	<b>NO<sub>3</sub>-based solution</b>	<b>K-free solution</b>	<b>Ba-solution</b>	<b>K-containing solution</b>	<b>Ouabain-containing solution</b>
Chemicals (mM)										
NaCl	96	96	82.5	82.5			96	96	96	96
KCl	2	2	2	2	2			5	5	5
CaCl <sub>2</sub>	1.8	1.8			1.8		1.8	1.8	1.8	1.8
MgCl <sub>2</sub>	1	1	1	1	1		1	1	1	1
HEPES	5	5	5	5	5	5	5	5	5	5
C <sub>3</sub> H <sub>3</sub> NaO <sub>3</sub>		5								
Theophylline		0.5								
Gentamycin		50								

		μg/ml								
Staurosporine		50								
		μg/ml								
Collagenase				2 mg/ml						
LiCl					96					
NaNO <sub>3</sub>						96				
KNO <sub>3</sub>						2				
CaNO <sub>3</sub>						1.8				
MgNO <sub>3</sub>						1				
Sucrose							25	10		
BaCl <sub>2</sub>								5	5	5
Ouabain										1
pH	7.4	7.4	7.4	7.4	7.4	7.4	7.4	7.4	7.4	7.4

## 2.2.7 Regulation of Na<sup>+</sup>-coupled glucose carrier SGLT1 by AMP-activated protein kinase

### 2.2.7.1 Constructs

For generation of cRNA, constructs were used encoding wild type human SGLT1 (SLC5A1)<sup>220</sup>, wild type AMPKα1-HA, AMPKβ1-flag, AMPKγ1-HA<sup>221</sup>, constitutively active <sup>γR70Q</sup>AMPKγ1-HA<sup>222</sup> and kinase dead mutant <sup>αK45R</sup>AMPKα.1-HA<sup>223</sup>. The cRNA was generated as described previously<sup>224</sup>.

### 2.2.7.2 Voltage clamp in *Xenopus oocytes*

*Xenopus oocytes* were prepared as previously described<sup>225</sup>. A total of 4.6 ng of each cRNA encoding AMPKα1-HA + AMPKβ1-flag + AMPKγ1-HA (<sup>WT</sup>AMPK), of AMPKα1-HA + AMPKβ1-flag + <sup>γR70Q</sup>AMPKγ1-HA (<sup>γR70Q</sup>AMPK) or of <sup>αK45R</sup>AMPKα1-HA + AMPKβ1-flag + AMPKγ1-HA (<sup>αK45R</sup>AMPK) were injected with or without 5 ng cRNA encoding SLC5A1 (SGLT1) on the day of preparation of the *Xenopus oocytes*. All experiments were performed at room temperature 3 days after injection. Two-electrode voltage-clamp recordings were performed at

a holding potential of -70 mV. The data were filtered at 10 Hz and recorded with a Digidata A/D-D/A converter and Clampex V.9 software for data acquisition and analysis (Axon Instruments). The control superfusate (ND96) contained 96 mM NaCl, 2 mM KCl, 1.8 mM CaCl<sub>2</sub>, 1 mM MgCl<sub>2</sub> and 5 mM HEPES, pH 7.4. Glucose was added to the solutions at a concentration of 10 mM unless otherwise stated. Where indicated, 1 mM ouabain (Sigma, Schnellendorf, Germany) was added to the control superfusate. The pump current generated by readdition of extracellular K<sup>+</sup> was determined by subsequent exposure of the oocytes for 5 hours to K<sup>+</sup>-free perfusate, for further 5 minutes to Ba<sup>2+</sup> (5 mM) containing K<sup>+</sup>-free perfusate and then to Ba<sup>2+</sup> containing K<sup>+</sup>-containing (5 mM) perfusate. The flow rate of the superfusion was approx. 20 ml/min, and a complete exchange of the bath solution was reached within about 10 s.

### **2.2.7.3 Immunofluorescence**

Caco2 cells (immortalized cell line of heterogeneous human epithelial colorectal adenocarcinoma cells) were cultured in DMEM medium containing 4.5 g/l glucose, 20% FBS, 1% L-glutamine, 1% non-essential amino acids and 1% penicillin/streptomycin. The cells were grown on 12-mm glass coverslips (neoLab Migge Laborbedarf-Vertriebs GmbH, Heidelberg, Germany) in 12-well plates (5×10<sup>4</sup> cells/well/coverslip). Two days after plating, the cells reached 80–90% confluence. Prior to immunohistochemistry, the cells were incubated in the absence or presence of 1 mM AMPK activator 5-aminoimidazole-4-carboxamide-1-beta-D-ribofuranoside (AICAR) (Calbiochem, Bad Soden, Germany), of 10 μM A-769662 (Tocris Biosciences) or of 1 mM phenformin hydrochloride (Sigma) for 6 h. The cells were then washed with PBS and fixed for 20 min in 4% paraformaldehyde in PBS/0.1% Triton. The cells were washed again and then blocked in 5% bovine serum albumin in PBS/0.1% Triton for 1 h at room temperature. The cells were incubated overnight at 4°C with goat anti-SGLT1 (1:300, Santa Cruz). After incubation, the cells were rinsed three times with PBS/0.1% Triton and incubated with the secondary FITC anti-goat antibody (1:500, Invitrogen) for 1 h at room temperature. After washing with PBS/0.1% Triton cells were incubated with rabbit anti-alpha tubulin (1:50, Cell Signalling Technology) antibody for 2 h at room temperature. The cells were again rinsed with PBS/0.1% Triton and incubated with Cy5 anti-rabbit (1:400, Jackson ImmunoResearch Laboratories) for 1 h at room temperature followed by washing with PBS/0.1% Triton. The nuclei were stained with DRAQ-5

dye (1:1000, Biostatus, Leicestershire, UK) for 5 min at 37°C. The slides were mounted with Prolong antifade reagent (Invitrogen). The images were taken on a Zeiss LSM 5 EXCITER Confocal Laser Scanning Microscope, equipped with a 405–633 nm laser (Carl Zeiss MicroImaging GmbH, Germany) using a water immersion Plan-Neofluar 63/1.3 NA DIC. Three independent experiments were performed.

#### **2.2.7.4 Biotinylation and Western blot analysis**

$10^9$  cells were biotinylated with EZ-link Sulfo-NHS-Biotin (Pierce protein research products, Thermo Scientific) for 30 min at room temperature. Then, the cells were washed 3 times. The cells were lysed with cell lysis buffer (20 mM Tris-HCl (pH 7.5), 150 mM NaCl, 1 mM Na<sub>2</sub>EDTA, 1 mM EGTA, 1% Triton, 2.5 mM sodium pyrophosphate, 1 mM beta-glycerophosphate, 1 mM Na<sub>3</sub>VO<sub>4</sub>, 1 µg/ml leupeptin and 1 mM PMSF, added immediately prior to use) followed by separation of the biotinylated proteins with NeutrAvidin Agarose Resin (Thermo Scientific) at 4°C. The NeutrAvidin Agarose Resin was washed three times with ice-cold PBS. The NeutrAvidin agarose-bound protein was separated by addition of 1:5 Laemmli buffer. The samples were boiled for 10 min. The biotinylated protein was subjected to 10% SDS-PAGE gel electrophoresis. Proteins were transferred to a nitrocellulose membrane (Millipore Corp.), and the membranes were then blocked for 2 h at room temperature with 5% non-fat dried milk in Tris-buffered saline (NFDN/TBS) containing 0.1% Tween 20. Incubation with the primary anti-SGLT1 antibody (1:1000, rabbit polyclonal antibody, Millipore) was carried out at 4°C overnight. Specific protein bands were visualized after subsequent incubation with a 1:5000 dilution of anti-rabbit IgG (Cell Signalling) conjugated to horseradish peroxidase and a Super Signal Chemiluminescence detection procedure (GE Healthcare, UK). Afterwards, the same membranes were stripped and reprobed with  $\alpha$ -actin antibody (1:1000, rabbit polyclonal antibody, Cell Signalling). The band intensity was determined by Quantity one software (Biorad gel doc system, Chemidoc XRS). Levels of SGLT1 were expressed as the ratio of signal intensity for the target protein relative to that of  $\alpha$ -actin.

### 2.2.7.5 Statistical analysis

Data are provided as means  $\pm$  SEM, n represents the number of oocytes investigated. All experiments were repeated with at least 3 batches of oocytes; in all repetitions qualitatively similar data were obtained. However, the absolute values of the currents may vary appreciably depending on the oocyte batch used (compare Fig. 3.2.2B and 3.2.2D). Data were tested for significance using ANOVA or t-test, as appropriate. Results with  $P < 0.05$  were considered statistically significant.

## 2.2.8 Downregulation of Na<sup>+</sup>-coupled glutamate transporter EAAT3 and EAAT4 by AMP-activated protein kinase

### 2.2.8.1 Constructs

For generation of cRNA, constructs were used encoding wild type human EAAT3<sup>226,227</sup>, wild type EAAT4<sup>218</sup>, wild type human EAAT1<sup>228</sup>, wild type human EAAT2<sup>229</sup>, wild type AMPK $\alpha$ 1-HA, AMPK $\beta$ 1-Flag, AMPK $\gamma$ 1-HA<sup>221</sup>, constitutively active R70Q AMPK $\gamma$ 1-HA<sup>222</sup> and kinase dead mutant K45R AMPK $\alpha$ 1-HA<sup>223</sup>. The cRNA was generated as described previously<sup>224</sup>. For the detection of EAAT4 surface expression, a rat EAAT4-HA construct, which contains an extracellular HA (hemagglutinin) epitope between aminoacids 374-375, was used.

### 2.2.8.2 Voltage clamp in *Xenopus* oocytes

*Xenopus* oocytes were prepared as previously described<sup>225</sup>. 4.6 ng of cRNA encoding either AMPK $\alpha$ 1-HA + AMPK $\beta$ 1-Flag + AMPK $\gamma$ 1-HA (WT AMPK), or AMPK $\alpha$ 1-HA + AMPK $\beta$ 1-Flag + R70Q AMPK $\gamma$ 1-HA ( $\gamma^{R70Q}$  AMPK) or K45R AMPK $\alpha$ 1KD-HA + AMPK $\beta$ 1-Flag + AMPK $\gamma$ 1-HA ( $\alpha^{K45R}$  AMPK) were injected with or without either 2 ng cRNA encoding EAAT1, 2 ng cRNA encoding EAAT2, 6 ng cRNA encoding EAAT3 or 6 ng cRNA encoding EAAT4 on the day of preparation of the *Xenopus* oocytes. All experiments were performed at room temperature 3 days (EAAT3), or 3-5 days (EAAT1, EAAT2, EAAT4) after injection. Two-electrode voltage-clamp recordings were performed at a holding potential of -60 mV or with step voltage increments of -20 mV from -120 mV to 80 mV. The data were filtered at 10 Hz and recorded with a Digidata A/D-D/A converter and Clampex V.9 software for data acquisition and analysis (Axon Instruments). The control superfusate (ND96) contained 96 mM NaCl, 2 mM KCl, 1.8 mM CaCl<sub>2</sub>, 1 mM MgCl<sub>2</sub> and 5



mM HEPES, pH 7.4. Glutamate was added to the solutions at a concentration of 2 mM unless otherwise stated. Where indicated, Na<sup>+</sup> was replaced by Li<sup>+</sup> or NaCl by NaNO<sub>3</sub>. The flow rate of the superfusion was app. 20 ml/min, and a complete exchange of the bath solution was reached within about 10 s.

### **2.2.8.3 Immunohistochemistry**

To quantify abundance of the transporters expressed on the plasma membrane of oocytes, immunohistochemistry assay was employed. After 4% paraformaldehyde fixation for at least 12 h, oocytes were cryoprotected in 30% sucrose, frozen in mounting medium, and placed on a cryostat<sup>230</sup>. Sections were collected at a thickness of 8 μm on coated slides and stored at -20°C. For immunostainings, sections were dehydrated at room temperature, fixated in acetone/methanol (1:1) for 15 min at RT, washed in PBS and pre-incubated for 1 h in 5% bovine serum albumin in PBS. The primary antibodies used were goat anti-EAAT3 antibody (for detection of EAAT3, diluted 1:2500, Millipore, Chemicon International, United States) or rat anti-HA antibody (for detection of EAAT4, diluted 1:100, clone 3 F10, Boehringer, Biberach, Germany). Incubation was performed in a moist chamber overnight at 4°C. In the case of EAAT3, binding of the primary antibody was visualised with a swine anti-goat conjugated FITC antibody (diluted 1:1000, Invitrogen, United States). For detection of EAAT4 a goat anti-rat conjugated Alexa488 antibody was used as secondary antibody (diluted 1:200, Invitrogen, United States). Then, oocytes were analyzed by a fluorescence laser scanning microscope (LSM 510, Carl Zeiss MicroImaging GmbH, Germany) with A-Plan 20x/0.48 Ph2 (fig. 2.2.8.3). Brightness and contrast settings were kept constant during imaging of all oocytes in each injection series. Due to autofluorescence of the oocyte yolk, unspecific immunofluorescence was observed inside the oocyte.

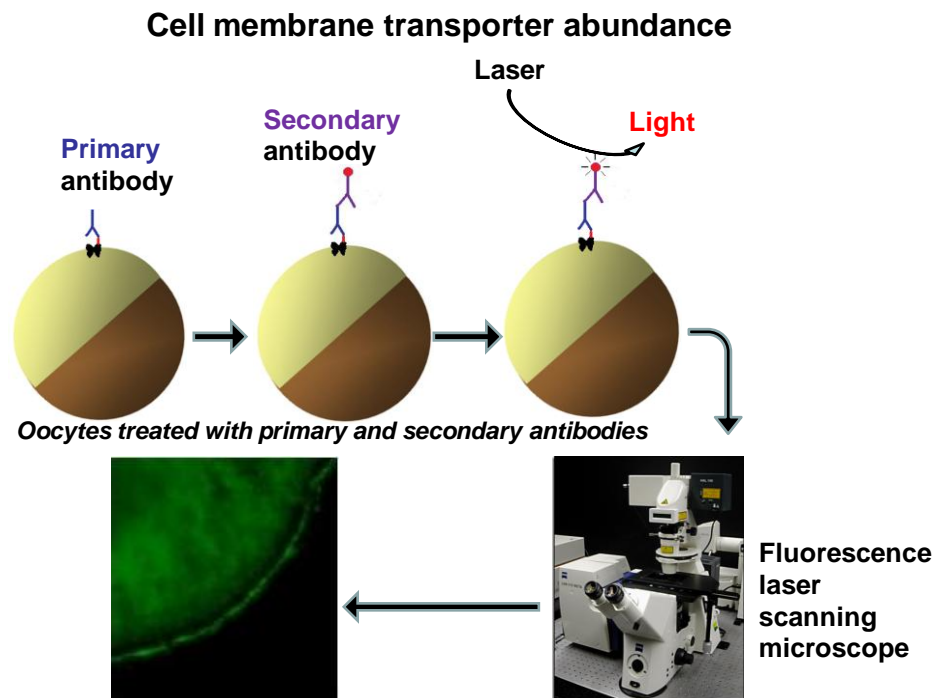


**Figure 2.2.8.3<sub>Method</sub>.** Overall view of an immunohistochemistry based cell membrane transporter abundance experiment.

#### **2.2.8.4 Detection of EAAT cell surface expression by chemiluminescence**

Defolliculated oocytes were incubated with 1  $\mu\text{g/ml}$  primary mouse monoclonal anti-EAAC1/EAAT3 antibody (in order to determine EAAT3 as shown in Fig. 3.3.3; Zymed Laboratories, Invitrogen, United States) or with 1  $\mu\text{g/ml}$  primary rat monoclonal anti-HA antibody (in order to determine HA-tagged EAAT4 as shown in Fig. 3.3.6; clone 3 F10, Boehringer, Biberach, Germany) and 2  $\mu\text{g/ml}$  secondary, peroxidase-conjugated sheep anti-mouse IgG antibody (for EAAT3; GE Healthcare, Amersham, United Kingdom) or with 2  $\mu\text{g/ml}$  secondary, peroxidase-conjugated affinity-purified F(ab')<sub>2</sub> goat anti-rat IgG antibody (for EAAT4; Jackson ImmunoResearch, West Grove, PA, USA). Individual oocytes were placed in 96 well plates with 20  $\mu\text{l}$  of SuperSignal ELISA Femto Maximum Sensitivity Substrate (Pierce, Rockford, IL, USA). Chemiluminescence of single oocytes was quantified in a luminometer (Walter Wallac 2 plate reader, Perkin Elmer, Juegesheim, Germany) by integrating the signal over a period of 1 s. Results display normalized arbitrary light units which are proportional to the detector voltage. For every oocyte preparation, the results were normalized by dividing each

value of a given oocyte by the mean value obtained from the oocytes injected with the respective glutamate transporter alone. Oocytes show autofluorescence due to yolk granules.

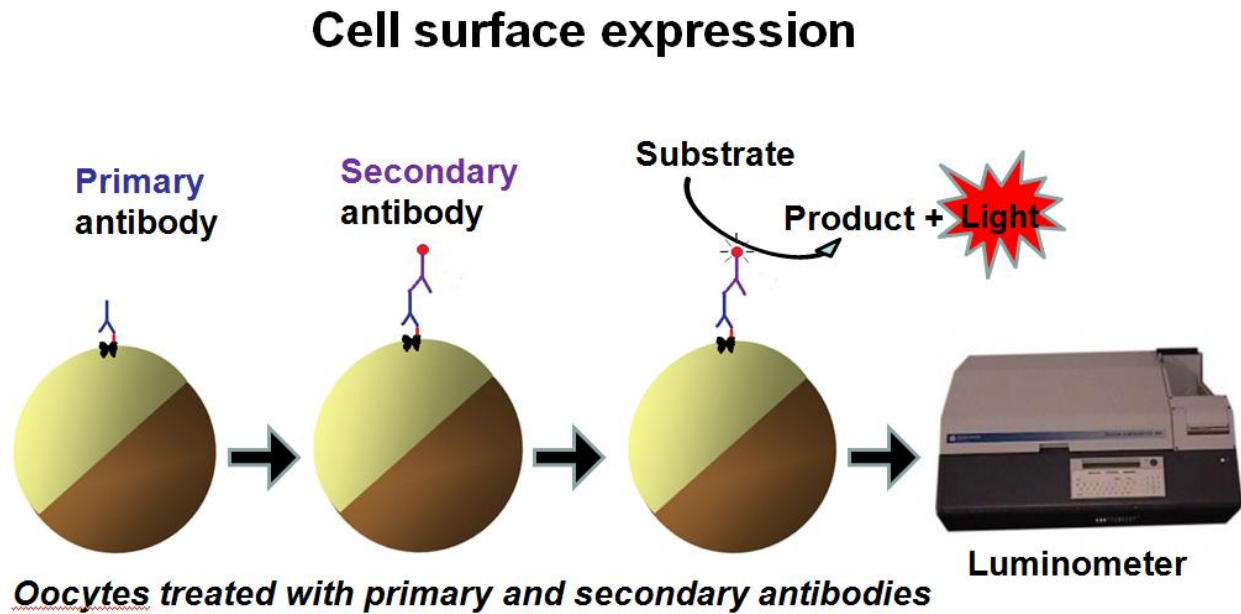


Figure 2.2.8.4<sub>Method</sub>. General view of a chemiluminescence-based cell surface experiment.

#### 2.2.8.5 Statistical analysis

Data are provided as means  $\pm$  SEM, n represents the number of oocytes investigated. All experiments were repeated with at least 4 batches of oocytes; in all repetitions qualitatively similar data were obtained. Data were tested for significance using ANOVA, and results with  $P < 0.05$  were considered statistically significant.

## 3 Results

### 3.1 AMP-activated protein kinase regulates erythrocyte survival

#### 3.1.1 Expression of AMP-activated protein kinase in erythrocytes

According to Western blotting, human erythrocytes express the AMPK $\alpha$  protein (Fig. 3.1.1A, left panel, left lane). Further experiments were performed to investigate the expression of AMPK $\alpha$  in murine erythrocytes. As shown in Fig. 3.1.1A (right), wild-type mouse erythrocytes (*ampk*<sup>+/+</sup>) expressed AMPK $\alpha$ , while no band was detectable in erythrocytes from a AMPK $\alpha$ 1-deficient mouse (*ampk*<sup>-/-</sup>). Confocal microscopy of human erythrocytes further confirmed the expression of AMPK $\alpha$  in human erythrocytes (Fig. 3.1.1B). Staining of human erythrocytes with the secondary FITC-conjugated antibody without the primary antibody did not result in detectable fluorescence (Fig. 3.1.1C).

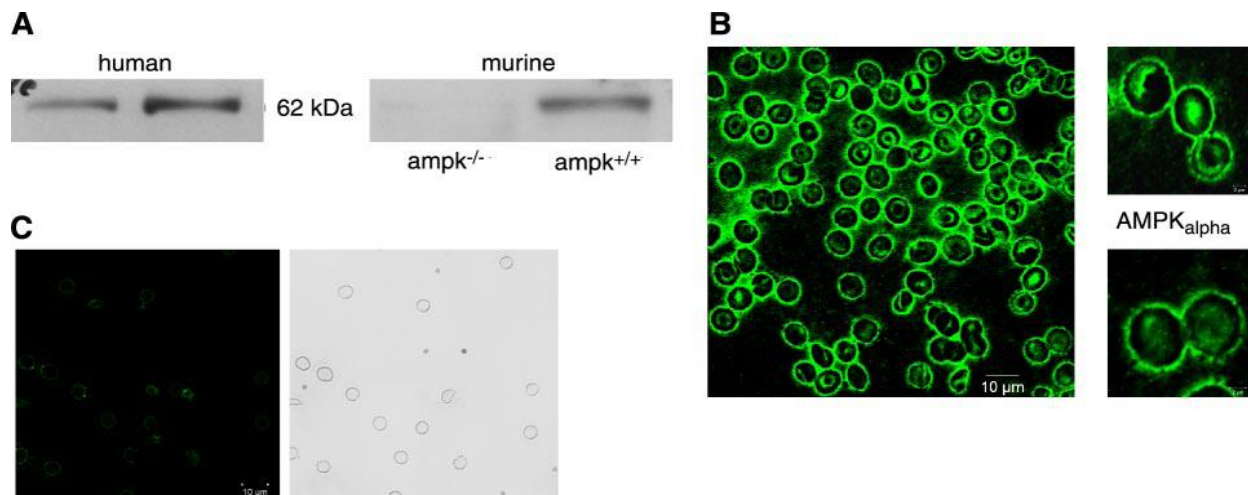


**Figure 3.1.1. Expression of AMPK in erythrocytes.**

**A.** Original Western blots demonstrating the expression of the AMPK $\alpha$  protein in two different membrane preparations of human erythrocytes (left) as well as in membrane preparations of erythrocytes from AMPK $\alpha$ 1-deficient mice (right, *ampk*<sup>-/-</sup>) and their wild-type littermates (right, *ampk*<sup>+/+</sup>).

**B.** Confocal microscopy of FITC-dependent fluorescence of human erythrocytes stained with a primary rabbit anti AMPK $\alpha$  and a secondary FITC-conjugated anti-rabbit antibody. Smaller top and bottom photos at right show two different regions of the large photo at left at higher magnification.

**C.** Left panel: FITC-dependent fluorescence of human erythrocytes stained only with a secondary FITC-conjugated anti-rabbit antibody as in B. Right panel: transmission light photograph representative for erythrocytes in B and C.

### 3.1.2 Compound C increased cytosolic Ca<sup>2+</sup> concentration and caused eryptosis in glucose depletion of RBCs

Energy depletion by withdrawal of glucose is known to increase the cytosolic Ca<sup>2+</sup> concentration<sup>231</sup>. Fluo3 fluorescence was used to determine whether energy depletion of human erythrocytes involves AMPK. To this end, the Ca<sup>2+</sup> concentration of human erythrocytes was determined in human erythrocytes after a 48 hours incubation in the presence or absence of glucose and either in the absence or presence of the AMPK inhibitor compound C (20 μM)<sup>232</sup>. As shown in Fig. 3.1.2A, B, energy depletion was followed by a significant increase in the erythrocyte Ca<sup>2+</sup> activity. Compound C did not significantly modify cytosolic Ca<sup>2+</sup> activity in the presence of glucose but led to a significant further increase in cytosolic Ca<sup>2+</sup> activity in the absence of glucose (Fig. 3.1.2A, B).

An increase in the cytosolic Ca<sup>2+</sup> activity leads to stimulation of Ca<sup>2+</sup>-sensitive K<sup>+</sup> channels, exit of K<sup>+</sup>, hyperpolarisation, Cl<sup>-</sup> exit, osmotic water loss and cell shrinkage<sup>89</sup>. Forward scatter was used to estimate alterations of cell volume. Glucose withdrawal was followed by the expected significant decrease of forward scatter. Again, compound C did not significantly affect the forward scatter in the presence of glucose but significantly augmented the decrease of forward scatter following glucose depletion (Fig. 3.1.2C, D).

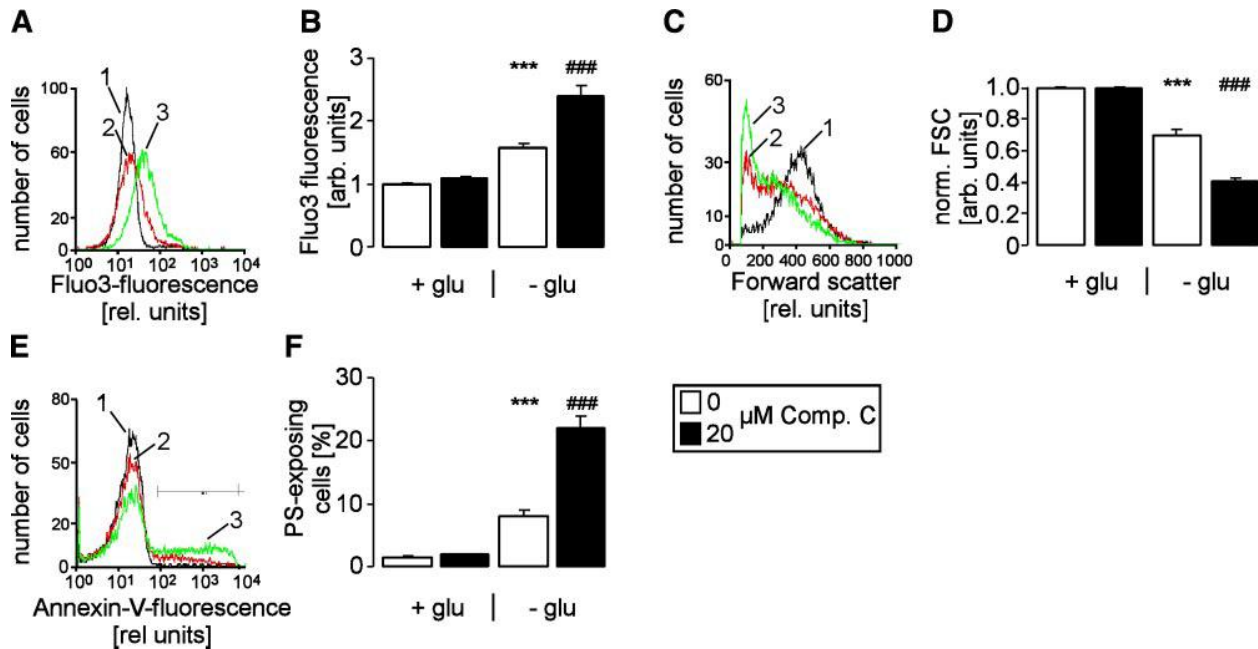


**Figure 3.1.2. Cytosolic  $\text{Ca}^{2+}$  concentration and eryptosis with or without glucose depletion in the presence and absence of compound C.**

**A.** Histogram of  $\text{Ca}^{2+}$ -dependent Fluo3 fluorescence in a representative experiment of erythrocytes exposed for 48 h to Ringer (1, black line), or glucose depleted Ringer in the absence (2, red line) or presence (3, green line) of AMPK inhibitor compound C (20  $\mu\text{M}$ ).

**B.** Arithmetic mean  $\pm$  SEM ( $n = 20$ ) of normalized Fluo3 fluorescence of erythrocytes exposed for 48 h to glucose-containing (+glu, left bars) or glucose-depleted (-glu, right bars) Ringer without (white bars) or with (black bars) compound C (20  $\mu\text{M}$ ). \*\*\* Significant ( $P < 0.001$ ) difference from glucose-containing Ringer, ### significant difference ( $P < 0.001$ ) from absence of compound C. (ANOVA).

**C.** Histogram of forward scatter as a measure of cell volume in a representative experiment of erythrocytes treated as in A.

**D.** Arithmetic mean  $\pm$  SEM ( $n = 27-28$ ) of normalized forward scatter of erythrocytes treated as in B.

**E.** Histogram of annexin V-binding reflecting phosphatidylserine exposure in a representative experiment of erythrocytes treated as in A.

**F.** Arithmetic mean  $\pm$  SEM ( $n = 24$ ) of the percentage of annexin V-binding erythrocytes treated as in B. \*\*\* $P < 0.001$  vs. glucose-containing Ringer, ###  $P < 0.001$  vs. absence of compound C; ANOVA.

An increase in cytosolic  $\text{Ca}^{2+}$  further triggers scrambling of the erythrocyte cell membrane resulting in exposure of phosphatidylserine at the erythrocyte surface<sup>91,99,162,163,233</sup>. Annexin V-binding was taken as evidence for phosphatidylserine at the erythrocyte surface. Glucose withdrawal was followed by the expected significant increase in annexin V-binding.

Again, the addition of compound C alone had little effect on annexin V binding in the presence of glucose. However, compound C led to a significant further increase in annexin V-binding of energy-depleted human erythrocytes (Fig. 3.1.2E, F).

### 3.1.3 AICAR decreased while compound C increased phosphatidylserine exposure in ionomycin treated erythrocytes

To test, whether AMPK modifies the eryptotic effect of increased cytosolic  $\text{Ca}^{2+}$  activity, the cytosolic  $\text{Ca}^{2+}$  concentration of human erythrocytes was increased by a 30 minute treatment with the  $\text{Ca}^{2+}$  ionophore ionomycin. The experiments were performed after a 6 hour pre-treatment with or without the AMPK activator AICAR<sup>232,234,235</sup> (1 mM) or with or without the AMPK inhibitor compound C. As shown in Fig. 3.1.3, exposure of human erythrocytes to ionomycin induced phosphatidylserine exposure. More importantly, activation of AMPK by AICAR significantly blunted (Fig. 3.1.3A, B), while inhibition of AMPK by compound C significantly enhanced (Fig. 3.1.3C, D) ionomycin-induced phosphatidylserine exposure of human erythrocytes.

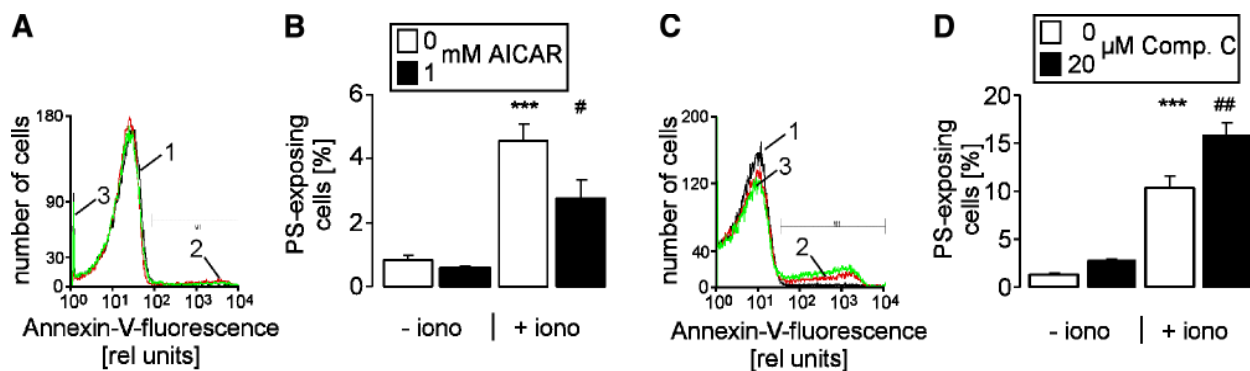


**Figure 3.1.3. Phosphatidylserine exposure of erythrocytes with or without ionomycin in the presence and absence of AICAR and compound C.**

**A.** Histogram of annexin V-binding reflecting phosphatidylserine exposure in a representative experiment of erythrocytes exposed for 6 h to Ringer and further 30 min in the absence (1, black line) or presence (2, red line) of 0.1  $\mu\text{M}$   $\text{Ca}^{2+}$  ionophore ionomycin or exposed for 6 h to Ringer containing AMPK activator AICAR (1 mM) and further 30 min to 0.1  $\mu\text{M}$  ionomycin (3, green line).

**B.** Arithmetic means  $\pm$  SEM ( $n = 12-16$ ) of the percentage of annexin V-binding erythrocytes exposed for 6 hours to Ringer in the absence (white bars) or presence (black bars) of 1 mM AICAR. In addition to this 6 hours incubation under both conditions, the erythrocytes were incubated for further 30 min in the absence (-iono, left bars) or presence of 0.1  $\mu\text{M}$  ionomycin (+iono, right bars). \*\*\* Significant difference from absence of ionomycin ( $P < 0.001$ ), # significant difference from absence of AICAR ( $P < 0.05$ ) (ANOVA).

**C.** Histogram of annexin V-binding reflecting phosphatidylserine exposure in a representative experiment of erythrocytes exposed for 6 h to Ringer and further 30 min in the absence (1, black line) or presence (2, red line) of 0.1  $\mu\text{M}$   $\text{Ca}^{2+}$  ionophore ionomycin or exposed for 6 h to Ringer containing AMPK inhibitor compound C (20  $\mu\text{M}$ ) and further 30 minutes to 0.1  $\mu\text{M}$  ionomycin (3, green line).

**D.** Arithmetic means  $\pm$  SEM ( $n = 8-16$ ) of the percentage of annexin V-binding erythrocytes exposed for 6 hours to Ringer in the absence (white bars) or presence (black bars) of 20  $\mu\text{M}$  compound C. In addition to 6 hours incubation under both conditions, erythrocytes were incubated for further 30 min in the

absence (-iono, left bars) or presence of 0.1  $\mu$ M ionomycin (+ iono, right bars). \*\*\* $P < 0.001$  vs. absence of ionomycin, # $P < 0.05$  vs. absence of AICAR, ## $P < 0.01$  vs. absence of compound C; ANOVA.

### 3.1.4 AMPK-deficient mice exhibit anemia

To investigate the *in vivo* significance of AMPK for erythrocytic survival, further experiments were performed in *ampk*<sup>-/-</sup> and *ampk*<sup>+/+</sup> mice. As shown in Fig. 3.1.4A, AMPK $\alpha$ 1-deficient mice had three times as many reticulocytes as their wild type littermates, a finding pointing to dramatically enhanced turnover of erythrocytes. The reticulocytosis of AMPK $\alpha$ 1-deficient mice could have been due to enhanced stimulation of erythropoiesis by erythropoietin.

As illustrated in Fig. 3.1.4B, the plasma concentration of erythropoietin was indeed significantly increased in AMPK $\alpha$ 1-deficient mice. The analysis of peripheral blood revealed a normocytic anemia in AMPK $\alpha$ -deficient mice as evident from a decreased red blood cell count (RBC), hematocrit (HCT), and hemoglobin (HGB) concentration and an increased red cell distribution width (RDW) whereas MCV, MCHC, and MCH were not significantly different between *ampk*<sup>-/-</sup> and *ampk*<sup>+/+</sup> mice (Fig. 3.1.4C). The plasma concentrations of vitamin B<sub>12</sub> (*ampk*<sup>+/+</sup>: 4.3  $\mu$ g/dl  $\pm$  0.1; *ampk*<sup>-/-</sup>: 4.0  $\pm$  0.1  $\mu$ g/dl; n=5) and folate (*ampk*<sup>+/+</sup>: 36.9  $\pm$  4.2  $\mu$ g/dl; *ampk*<sup>-/-</sup>: 28.2  $\pm$  4.5  $\mu$ g/dl; n=5) were not significantly different between the genotypes.



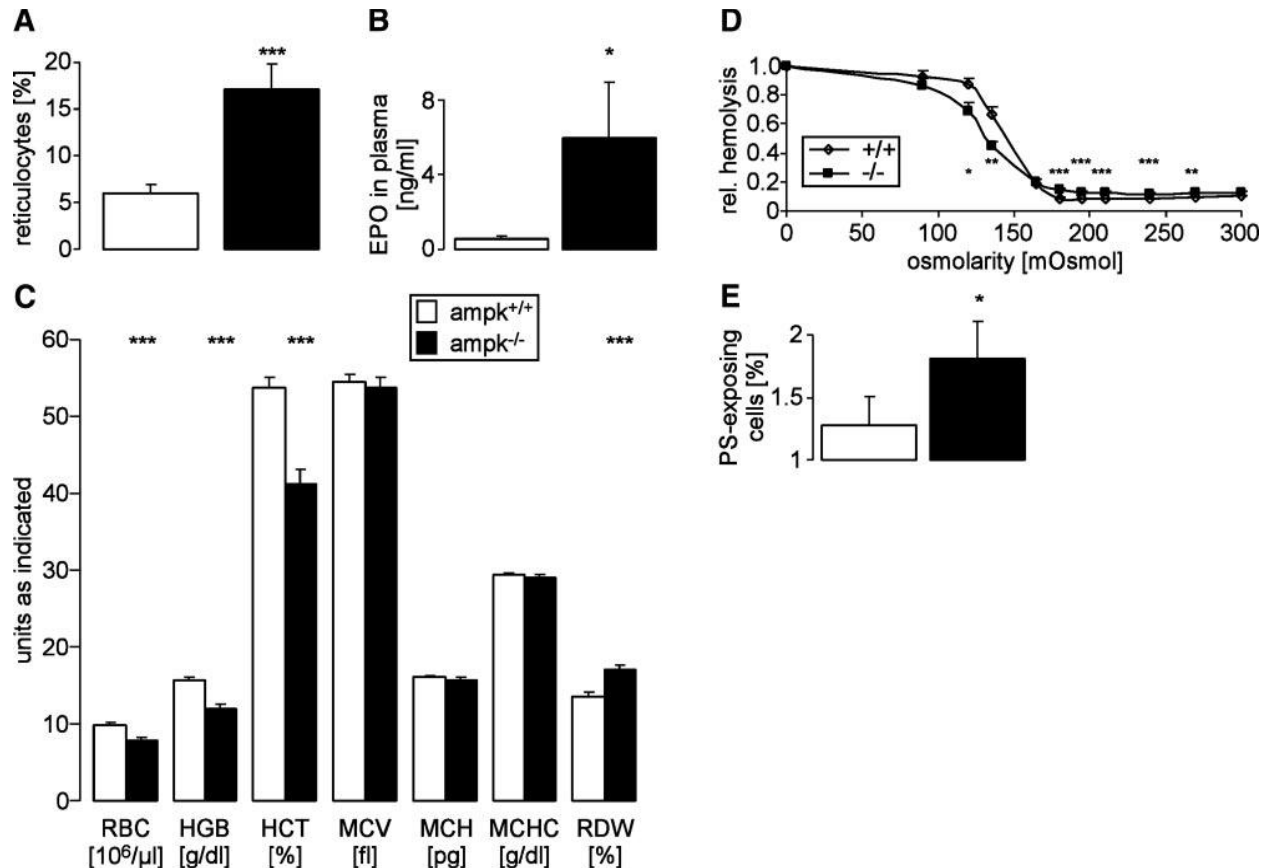


**Figure 3.1.4. Anemia in AMPK $\alpha$ 1-deficient mice.**

**A.** Arithmetic mean  $\pm$  SEM of reticulocyte number ( $n = 19$ ) of *ampk<sup>-/-</sup>* (black bar) and *ampk<sup>+/+</sup>* (white bar) mice. \*\*\* $P < 0.001$ ;  $t$  test.

**B.** Arithmetic mean  $\pm$  SEM of the plasma erythropoietin concentration ( $n=8$ ) of *ampk<sup>-/-</sup>* (black bar) and *ampk<sup>+/+</sup>* (white bar) mice. \* $P < 0.05$ ;  $U$  test.

**C.** Arithmetic mean  $\pm$  SEM ( $n = 13$ ) of erythrocyte count (RBC), hemoglobin concentration (HGB), hematocrit (HCT), mean corpuscular volume (MCV), mean corpuscular hemoglobin (MCH), mean corpuscular hemoglobin concentration (MCHC), and red cell distribution width (RDW) of *ampk<sup>-/-</sup>* (black bars) and *ampk<sup>+/+</sup>* (white bars) mice.

**D.** Osmotic resistance of erythrocytes from *ampk<sup>-/-</sup>* (solid symbols) and *ampk<sup>+/+</sup>* (open symbols) mice.

**E.** Arithmetic mean  $\pm$  SEM ( $n = 14$ ) of percentage of annexin V-binding erythrocytes from *ampk<sup>-/-</sup>* (black bar) and *ampk<sup>+/+</sup>* (white bar) mice immediately stained after retrieval. \* $P < 0.05$ , \*\* $P < 0.01$ , \*\*\* $P < 0.001$ ;  $t$  test (C–E).

To investigate whether mechanical instability accounts for anemia of AMPK $\alpha$ 1-deficient mice, the osmotic resistance of erythrocytes from *ampk<sup>-/-</sup>* and *ampk<sup>+/+</sup>* mice was determined. As shown in Fig. 3.1.4D, AMPK $\alpha$ 1-deficient erythrocytes were significantly more resistant against osmotic lysis while the basal hemolysis of AMPK $\alpha$ -deficient erythrocytes at higher osmolarity was slightly but significantly increased.

Since phosphatidylserine-exposing erythrocytes are rapidly engulfed and degraded by macrophages<sup>84</sup>, enhanced phosphatidylserine exposure of erythrocytes may result in anemia. To

assess, whether this mechanism may account for the observed anemia of AMPK $\alpha$ 1-deficient mice, annexin V-binding of erythrocytes from *ampk*<sup>-/-</sup> and *ampk*<sup>+/+</sup> mice was determined immediately on retrieval. As shown in Fig. 3.1.4E, phosphatidylserine of freshly drawn erythrocytes was indeed significantly more pronounced in *ampk*<sup>-/-</sup> than in *ampk*<sup>+/+</sup> mice.

### 3.1.5 AMPK $\alpha$ 1-deficient mice enhanced suicidal erythrocyte death

Further experiments were performed to investigate whether AMPK $\alpha$ 1-deficient erythrocytes are also more susceptible to suicidal cell death (eryptosis) due to energy depletion *in vitro*. According to Fluo3 fluorescence, the increase in cytosolic Ca<sup>2+</sup> concentration after 16 hours glucose depletion was significantly stronger in *ampk*<sup>-/-</sup> erythrocytes than in *ampk*<sup>+/+</sup> erythrocytes (3.1.5A, B). Similarly to what has been observed in human erythrocytes, energy-depletion resulted in shrinkage of *ampk*<sup>-/-</sup> and *ampk*<sup>+/+</sup> erythrocytes, an effect, significantly more pronounced in *ampk*<sup>+/+</sup> erythrocytes (Fig. 3.1.5C, D).

Most importantly, glucose depletion was followed by an increase in phosphatidylserine exposure, an effect significantly more pronounced in *ampk*<sup>-/-</sup> than in *ampk*<sup>+/+</sup> erythrocytes (Fig. 3.1.5E, F).

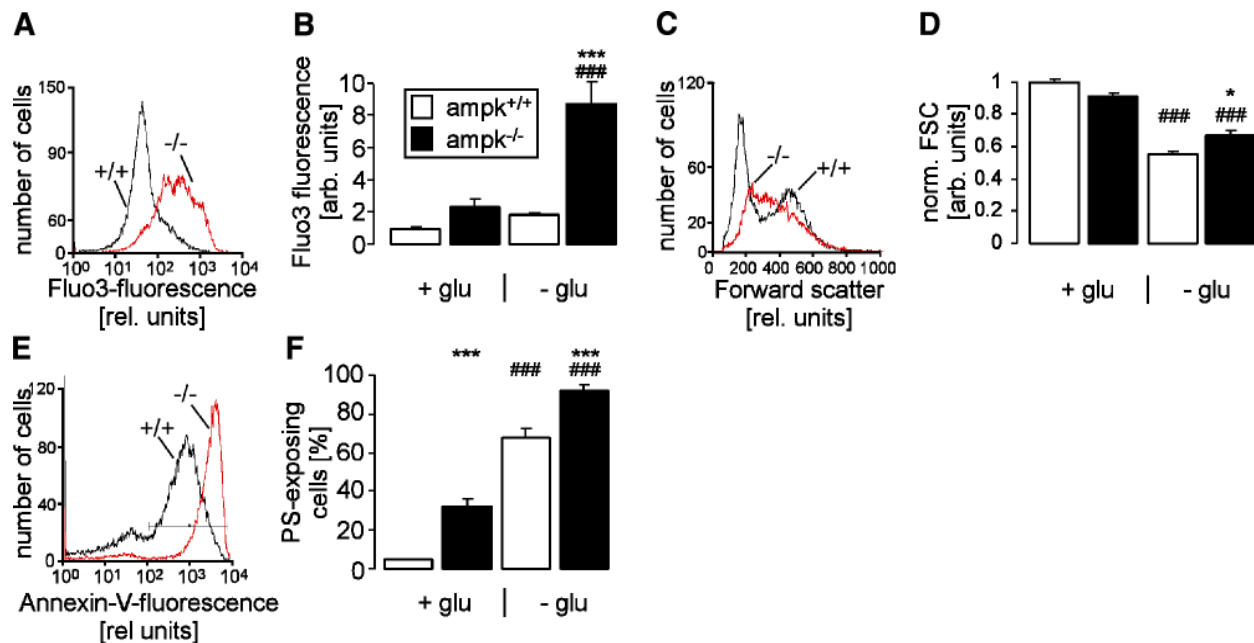


**Figure 3.1.5. Enhanced eryptosis of erythrocytes from AMPK $\alpha$ 1-deficient mice.**

A. Histogram of Ca<sup>2+</sup>-dependent Fluo3 fluorescence of erythrocytes from *ampk*<sup>-/-</sup> and *ampk*<sup>+/+</sup> mice exposed for 16 h to glucose-depleted Ringer.

- B.** Arithmetic mean  $\pm$  SEM ( $n = 5$ ) of normalized Fluo3 fluorescence in erythrocytes from *ampk*<sup>-/-</sup> (black bars) and *ampk*<sup>+/+</sup> (white bars) mice exposed for 16 h to glucose-containing (left bars) or glucose-depleted Ringer (right bars).
- C.** Histogram of forward scatter as a measure of cell volume in a representative experiment of erythrocytes from *ampk*<sup>-/-</sup> and *ampk*<sup>+/+</sup> mice exposed for 16 h to glucose-depleted Ringer.
- D.** Arithmetic mean  $\pm$  SEM ( $n = 5$ ) of normalized forward scatter of erythrocytes from *ampk*<sup>-/-</sup> (black bars) and *ampk*<sup>+/+</sup> (white bars) mice exposed for 16 h to glucose-containing (left bars) or glucose-depleted Ringer (right bars).
- E.** Histogram of annexin V-binding reflecting phosphatidylserine exposure in a representative experiment of erythrocytes from *ampk*<sup>-/-</sup> and *ampk*<sup>+/+</sup> mice exposed for 16 h to glucose-depleted Ringer.
- F.** Arithmetic mean  $\pm$  SEM ( $n = 5$ ) of percentage of annexin V-binding erythrocytes from *ampk*<sup>-/-</sup> (black bars) and *ampk*<sup>+/+</sup> (white bars) mice exposed for 16 h to glucose-containing (left bars) or glucose-depleted Ringer (right bars). \* $P < 0.05$ , \*\*\* $P < 0.001$  vs. wild-type; ANOVA. ### $P < 0.001$  vs. glucose-containing Ringer; ANOVA.

### 3.1.6 Accelerated erythrocyte clearance in AMPK $\alpha$ 1-deficient mice

The increased percentage of circulating phosphatidylserine-exposing erythrocytes in *ampk*<sup>-/-</sup> mice (Fig. 3.1.4E) and the enhanced *in vitro* eryptosis of *ampk*<sup>-/-</sup> erythrocytes under energy-repleted and-depleted conditions (Fig. 3.1.5E, F) suggest that the anemia of AMPK $\alpha$ 1-deficient mice is due to enhanced susceptibility of *ampk*<sup>-/-</sup> erythrocytes to eryptosis.

To elucidate whether AMPK $\alpha$ 1 deficiency indeed influenced the *in vivo* life span of erythrocytes, erythrocytes were isolated from *ampk*<sup>-/-</sup> and *ampk*<sup>+/+</sup> mice, labeled with the fluorescent dye CFSE, and subsequently injected into the tail vein of same mice. The clearance of CFSE-labeled erythrocytes from the circulation was determined on the three consecutive days after reinjection. As illustrated in Fig. 3.1.6, the CFSE-labeled erythrocytes disappeared significantly faster from the circulating blood of *ampk*<sup>-/-</sup> than of *ampk*<sup>+/+</sup> mice.

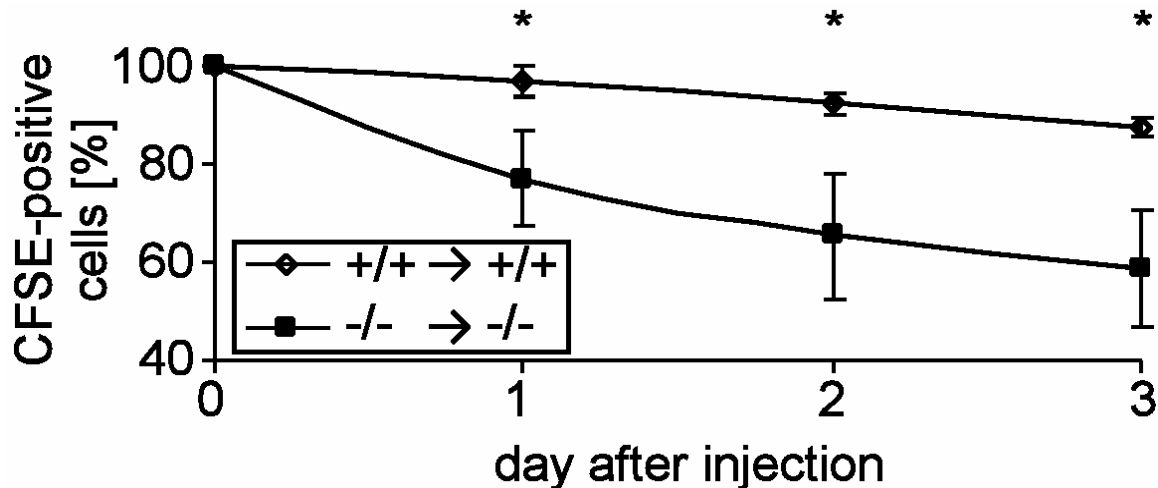


**Figure 3.1.6. Accelerated erythrocyte clearance of erythrocytes in AMPK $\alpha$ 1-deficient mice.**

Time-dependent decay of CFSE-labeled circulating erythrocytes drawn from AMPK $\alpha$ 1-deficient mice (solid symbols) and their wild-type littermates (open symbols) injected into either *ampk*<sup>-/-</sup> or *ampk*<sup>+/+</sup> mice, respectively. Percentage of CFSE-labeled circulating cells is plotted against time after injection. Values are normalized arithmetic mean  $\pm$  SE ( $n = 4$ ) of percentages of CFSE-labeled erythrocytes. \* $P < 0.05$ ;  $t$  test.

### 3.1.7 Splenomegaly in AMPK $\alpha$ 1-deficient mice

Cleared erythrocytes are mostly retained in the spleen where they are degraded by macrophages. Therefore, the spleens of *ampk*<sup>-/-</sup> and of *ampk*<sup>+/+</sup> mice were analysed. As a result, the spleens of *ampk*<sup>-/-</sup> mice were dramatically enlarged (Fig. 3.1.7A, B).

CSFE-labeled erythrocytes trapped in the spleens one day after injection into the tail vein were subsequently identified by confocal microscopy. As shown in Fig. 3.1.7C (lower panels) and 3.1.7D, appreciable amounts of CFSE-labeled, annexin V-binding erythrocytes were found in spleens from *ampk*<sup>-/-</sup> mice but not from *ampk*<sup>+/+</sup> mice. Integration of the CFSE-dependent fluorescence intensity resulted in a mean intensity of 25.2 in spleens from *ampk*<sup>-/-</sup> mice and in a mean intensity of 8.3 in *ampk*<sup>+/+</sup> mice.

A similar integration of the annexin V-dependent fluorescence yielded a mean intensity of 16.4 in spleens from *ampk*<sup>-/-</sup> mice and a mean intensity of 5.9 in spleens from *ampk*<sup>+/+</sup> mice.

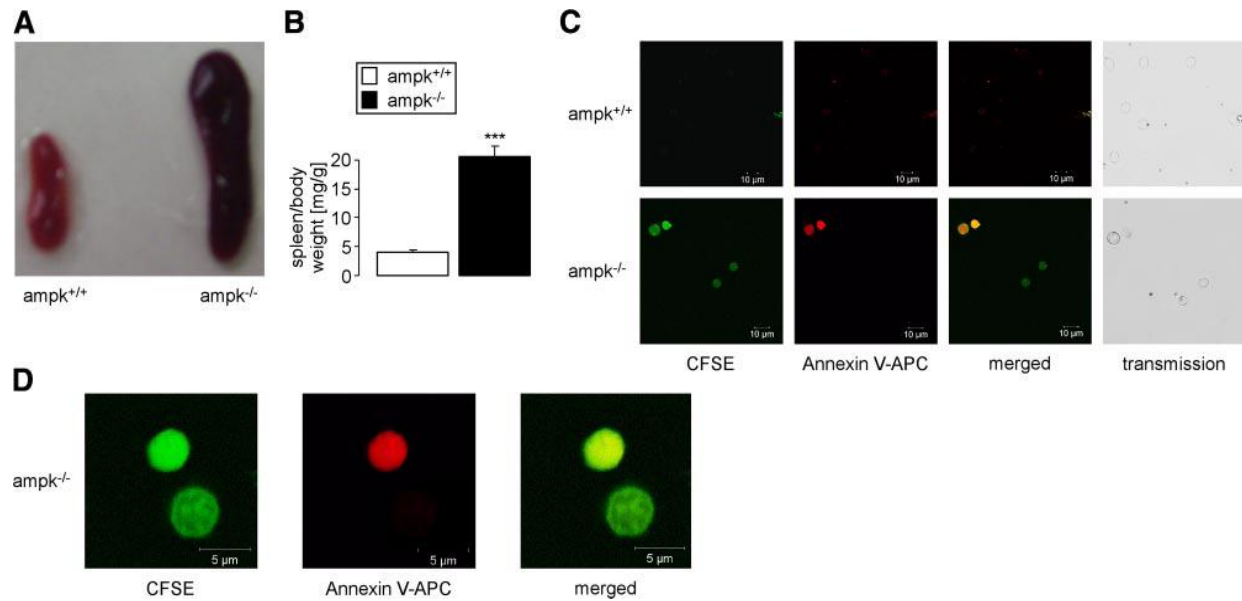


**Figure 3.1.7. Splenomegaly associated with increased erythroid cell mass in AMPK $\alpha$ 1-deficient mice.**

**A.** Photograph and

**B.** Arithmetic mean  $\pm$  SEM ( $n = 4$ ) of spleen/body weight ratios of 12-week-old *ampk*<sup>-/-</sup> (black bar) and *ampk*<sup>+/+</sup> (white bar) mice. \*\*\* Significant differences between genotypes ( $P < 0.001$ ;  $t$  test).

**C.** Confocal microscopy of CFSE-dependent (left), annexin V-APC-dependent (middle), and merged fluorescence (right) of erythrocytes from the spleens of *ampk*<sup>-/-</sup> (bottom) and *ampk*<sup>+/+</sup> (top) mice. For comparison, rightmost panels depict photographs of transmission light microscopy of the studied erythrocytes.

**D.** Confocal microscopy of erythrocytes from spleens of *ampk*<sup>-/-</sup> mice as in C at higher magnification.

Taken together, the *in vitro* and *in vivo* data suggest that the anemia of AMPK $\alpha$ -deficient mice is secondary to accelerated erythrocyte death.

## 3.2 AMP activated protein kinase regulate Na<sup>+</sup>-coupled glucose carrier SGLT1

### 3.2.1 Constitutively active AMPK stimulates SGLT1-mediated electrogenic glucose transport

Electrogenic glucose transport was minimal in noninjected or water-injected *Xenopus* oocytes (Fig. 3.2.1). In *Xenopus* oocytes expressing SGLT1 (SLC5A1), however, glucose (10 mM) induced an inward current ( $I_g$ ) reflecting electrogenic entry of Na<sup>+</sup> and glucose.  $I_g$  was significantly enhanced by additional expression of the constitutively active mutant AMP-activated protein kinase  $\gamma^{R70Q}$ AMPK (AMPK $\alpha$ 1 + AMPK $\beta$ 1 +  $\gamma^{R70Q}$ AMPK $\gamma$ 1). Expression of  $\gamma^{R70Q}$ AMPK alone did not lead to appreciable  $I_g$ . Thus,  $\gamma^{R70Q}$ AMPK stimulated SGLT1 activity. Wild type AMPK (AMPK $\alpha$ 1+AMPK $\beta$ 1+AMPK $\gamma$ 1) failed to stimulate SGLT1.

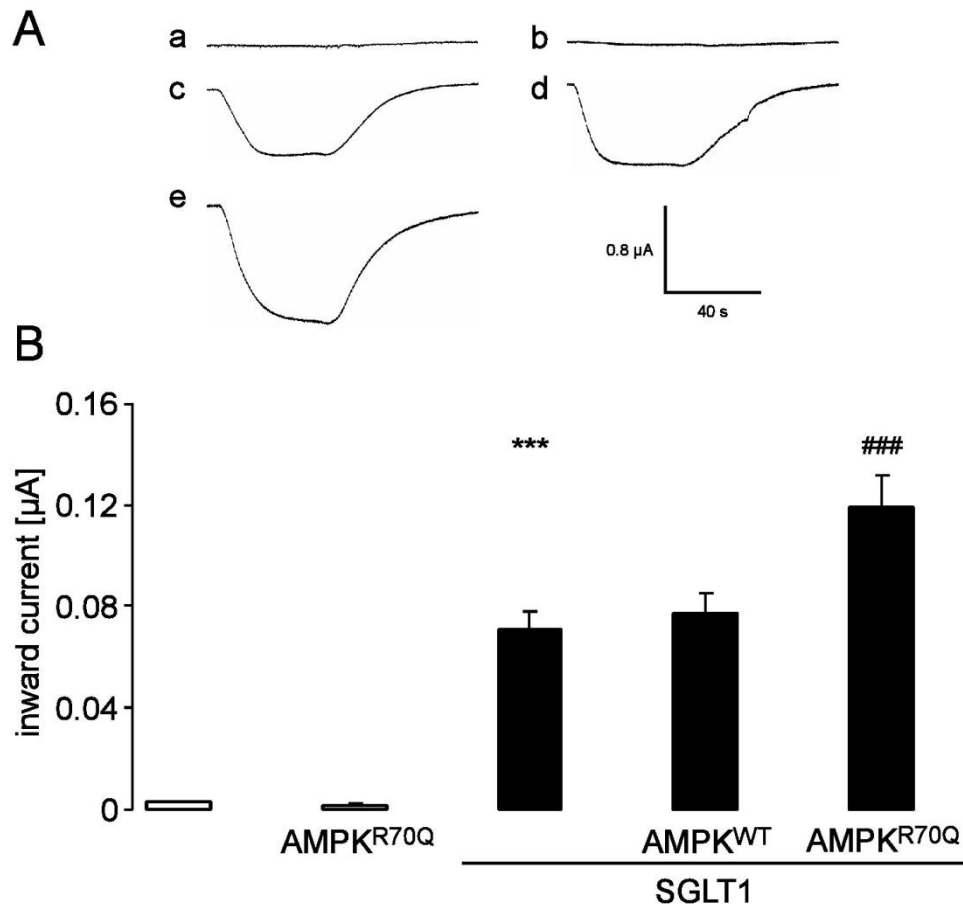


**Figure 3.2.1. Coexpression of  $\gamma^{R70Q}$ AMPK stimulated electrogenic glucose transport in SGLT1-expressing *Xenopus* oocyte.**

**A.** Representative original tracings showing glucose (10 mM)-induced current ( $I_g$ ) in *Xenopus* oocytes injected with water (a), expressing SGLT1 without (c) or with (d) additional coexpression of wild type

AMPK (AMPK $\alpha$ 1+AMPK $\beta$ 1+AMPK $\gamma$ 1) or with constitutively-active  $\gamma^{R70Q}$ AMPK (e), or expressing  $\gamma^{R70Q}$ AMPK alone (b).

**B.** Arithmetic means  $\pm$  SEM (n = 6-33) of glucose (10 mM)-induced current ( $I_g$ ) in *Xenopus* oocytes injected with water (1<sup>st</sup> bar), expressing SGLT1 without (3<sup>rd</sup> bar) or with (4<sup>th</sup> bar) additional coexpression of wild type AMPK (AMPK $\alpha$ 1+AMPK $\beta$ 1+AMPK $\gamma$ 1) or with constitutively-active  $\gamma^{R70Q}$ AMPK (5<sup>th</sup> bar; AMPK $\alpha$ 1+AMPK $\beta$ 1+ $\gamma^{R70Q}$ AMPK $\gamma$ 1), or expressing  $\gamma^{R70Q}$ AMPK alone (2<sup>nd</sup> bar). \*\*\* ( $P < 0.001$ ) indicates statistically significant difference from the absence of SGLT1. ### ( $P < 0.001$ ) indicates statistically significant difference from the absence of  $\gamma^{R70Q}$ AMPK.

Since SGLT1-mediated glucose transport depends on Na<sup>+</sup>/K<sup>+</sup> ATPase, further experiments addressed a possible participation of the Na<sup>+</sup>/K<sup>+</sup> ATPase in the AMPK-dependent stimulation of SGLT1 activity. To this end, SGLT1-dependent currents were determined in the presence and absence of the Na<sup>+</sup>/K<sup>+</sup> ATPase inhibitor ouabain (1 mM). The current was  $23.6 \pm 1.5$  nA (n = 12) in oocytes injected with SGLT1 cRNA in the absence and  $26.2 \pm 1.9$  nA (n = 11) in the presence of 1 mM ouabain. Expression of SGLT1 together with  $\gamma^{R70Q}$ AMPK increased the glucose-dependent current to  $36.2 \pm 1.9$  nA (n = 12) in the absence and to  $38.3 \pm 1.7$  nA (n = 12) in the presence of 1 mM ouabain. Additional experiments were performed elucidating the effect of AMPK expression on the pump current. The current was  $2.5 \pm 0.3$  nA (n = 5) in AMPK-expressing oocytes and  $2.6 \pm 0.15$  nA (n = 5) in water-injected oocytes. Thus, in oocytes AMPK did not appreciably modify the Na<sup>+</sup>/K<sup>+</sup> ATPase activity and the Na<sup>+</sup>/K<sup>+</sup> ATPase was not required for the AMPK-dependent stimulation of SGLT1-mediated currents.

### 3.2.2 The dead mutant $K^{45R}$ AMPK did not stimulate SGLT1 and blunted the stimulating effect of AMPK

As shown in Fig. 3.2.2A, B, electrogenic glucose transport was not significantly modified by the coexpression of inactive  $\alpha^{K45R}$ AMPK ( $\alpha^{K45R}$ AMPK $\alpha$ 1+AMPK $\beta$ 1+AMPK $\gamma$ 1). Coexpression of SGLT1 with  $\alpha^{K45R}$ AMPK in addition to constitutively active  $\gamma^{R70Q}$ AMPK $\alpha$ 1 (AMPK $\alpha$ 1+AMPK $\alpha$ 1+AMPK $\beta$ 1+ $\gamma^{R70Q}$ AMPK $\gamma$ 1) yielded glucose-induced currents, which were significantly smaller than the currents observed with  $\gamma^{R70Q}$ AMPK alone. Thus,  $\alpha^{K45R}$ AMPK exerted a dominant-negative action on AMPK (Fig. 3.2.2C, D).

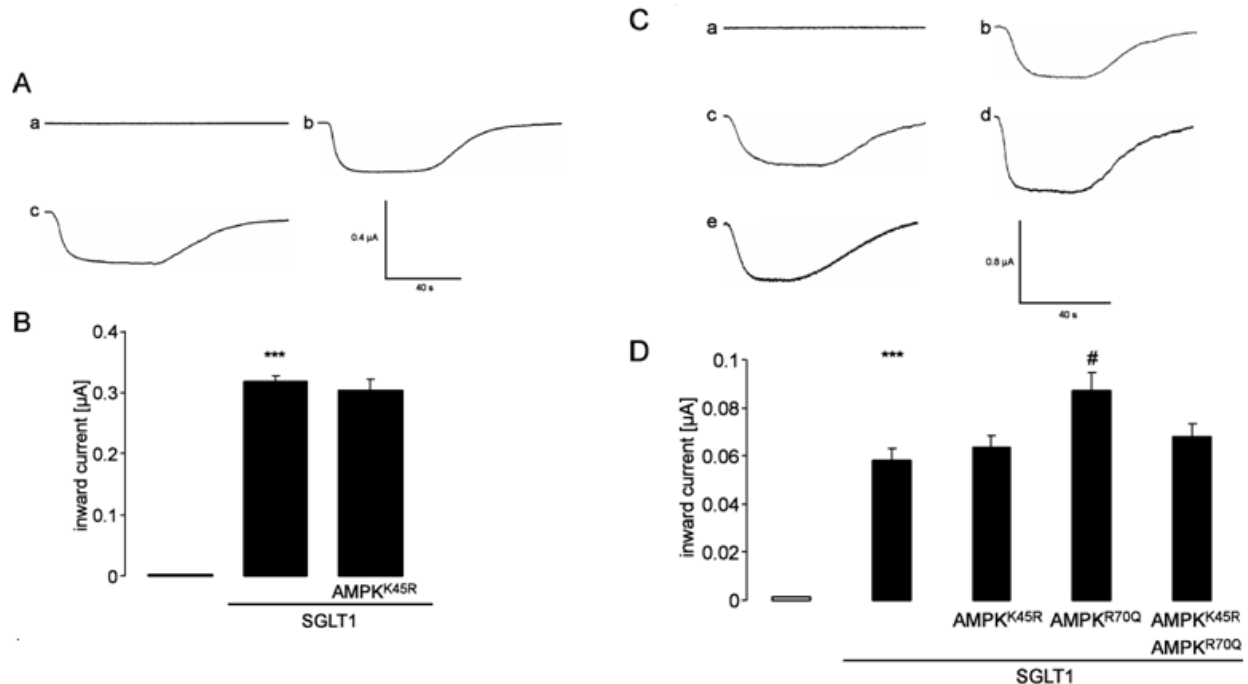


**Figure 3.2.2. The catalytically inactive mutant <sup>K45R</sup>AMPK did not stimulate SGLT1.**

**A.** Representative original tracings showing glucose (10 mM)-induced current ( $I_g$ ) in *Xenopus* oocytes injected with water alone (a) or expressing SGLT1 without (b) and with (c) inactive <sup>K45R</sup>AMPK.

**B.** Arithmetic means  $\pm$  SEM (n = 10-15) of glucose (10 mM)-induced current ( $I_g$ ) in *Xenopus* oocytes injected with water alone (1<sup>st</sup> bar) or expressing SGLT1 without (2<sup>nd</sup> bar) and with (3<sup>rd</sup> bar) inactive <sup>K45R</sup>AMPK (<sup>K45R</sup>AMPK $\alpha$ 1+AMPK $\beta$ 1+AMPK $\gamma$ 1). \*\*\* ( $P < 0.001$ ) indicates statistically significant difference from the absence of SGLT1.

**C.** Representative original tracings showing glucose (10 mM)-induced current ( $I_g$ ) in *Xenopus* oocytes injected with water alone (a) or expressing SGLT1 without (b) and with (c) inactive <sup>K45R</sup>AMPK or with constitutively-active <sup>R70Q</sup>AMPK (d) or with both, <sup>K45R</sup>AMPK and <sup>R70Q</sup>AMPK (e).

**D.** Arithmetic means  $\pm$  SEM (n = 9-15) of glucose (10 mM)-induced current ( $I_g$ ) in *Xenopus* oocytes injected with water alone (1<sup>st</sup> bar) or expressing SGLT1 without (2<sup>nd</sup> bar) and with (3<sup>rd</sup> bar) inactive <sup>K45R</sup>AMPK (<sup>K45R</sup>AMPK $\alpha$ 1+AMPK $\beta$ 1+AMPK $\gamma$ 1) or with constitutively-active <sup>R70Q</sup>AMPK (4<sup>th</sup> bar; AMPK $\alpha$ 1+AMPK $\beta$ 1+<sup>R70Q</sup>AMPK $\gamma$ 1) or with both, <sup>K45R</sup>AMPK and <sup>R70Q</sup>AMPK (5<sup>th</sup> bar). \*\*\* ( $P < 0.001$ ) indicates statistically significant difference from the absence of SGLT1. # ( $P < 0.05$ ) indicates statistically significant difference from the absence of <sup>R70Q</sup>AMPK.

### 3.2.3 AMPK enhanced the maximal current

Kinetics of glucose-induced currents in SGLT1-expressing *Xenopus* oocytes (Fig. 3.2.3) yielded a maximal current of  $0.098 \pm 0.001 \mu\text{A}$ . The data was fitted to a hyperbola. The glucose concentration needed for halfmaximal current ( $K_M$ ) was  $650 \pm 28 \mu\text{M}$ . The coexpression of constitutively-active <sup>R70Q</sup>AMPK did not significantly modify  $K_M$  ( $581 \pm 29 \mu\text{M}$ ), but significantly increased the maximal current (to  $0.160 \pm 0.002 \mu\text{A}$ ).



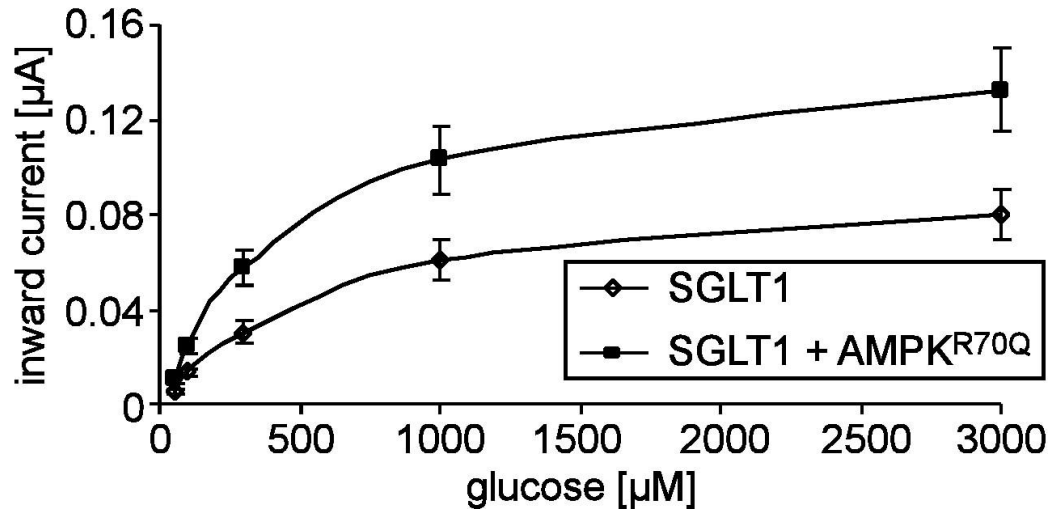


**Figure 3.2.3. AMPK enhanced the maximal current without appreciably affecting affinity.**

Arithmetic means  $\pm$  SEM ( $n = 16-22$ ) of  $I_g$  as a function of glucose concentration in *Xenopus* oocytes expressing SGLT1 without (open diamonds) and with (closed squares) constitutively-active  $\gamma^{R70Q}$ AMPK (AMPK $\alpha 1$ +AMPK $\beta 1$ + $\gamma^{R70Q}$ AMPK $\gamma 1$ ). The difference from the absence of  $\gamma^{R70Q}$ AMPK is significant ( $P < 0.05$ ) at every glucose concentration applied.

### 3.2.4 SGLT1 protein abundance is enhanced by activation of AMPK

The enhanced SGLT1 activity could result from increased carrier protein abundance in the plasma membrane. To test for that possibility, immunohistochemistry and confocal microscopy were performed. As illustrated in Fig. 3.2.4A a 6 h treatment of Caco2 cells with the AMPK activator AICAR-5'-Phosphate (1 mM) was followed by a significant increase in the SGLT1 protein abundance. The results were confirmed by biotinylation of the surface proteins and subsequent Western Blotting (Fig. 3.2.4B).

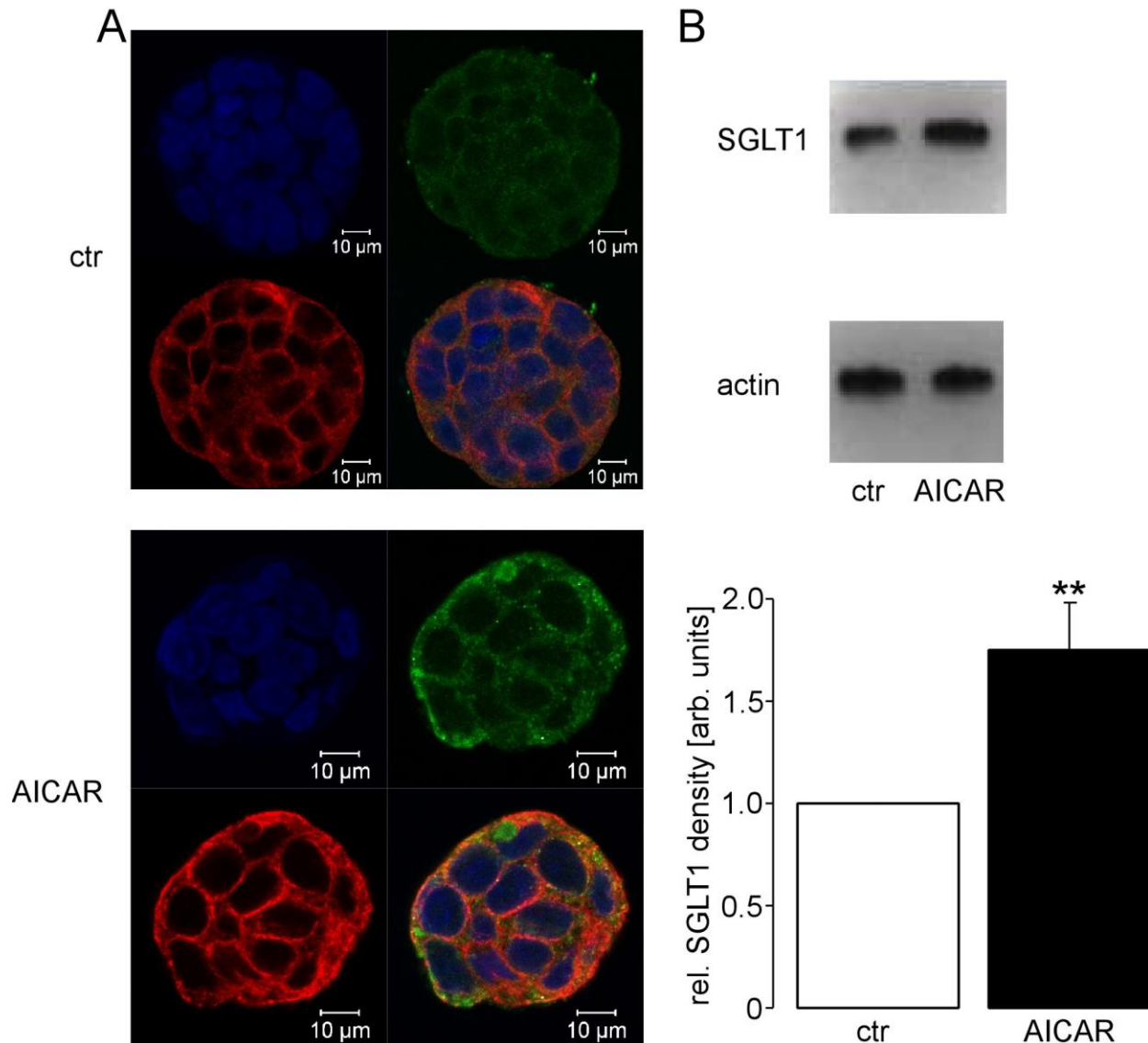


**Figure 3.2.4. Cell surface SGLT1 protein abundance in Caco2 cells was upregulated by the AMPK activator AICAR.**

**A.** Confocal microscopy of Caco2 cells incubated for 6 h in medium without (upper panel) or with (lower panel) AMPK activator AICAR (1 mM). The Caco2 cells were subjected to immunofluorescent staining using FITC-conjugated anti-SGLT1 (green), Cy5-conjugated anti-alpha tubulin (red) and DRAQ-5 dye (blue) for nuclear staining. The images are representative for three independent experiments.

**B.** Original Western blot of SGLT1 protein abundance in Caco2 cells (upper panel) treated as in A. Caco2 surface proteins were biotinylated and subsequently subjected to Western Blotting. Expression of actin served as loading control (middle panel). The lower panel depicts the arithmetic means  $\pm$  SEM ( $n = 12$ ) of the SGLT1 density of AICAR (1 mM)-treated Caco2 cells relative to the non-treated Caco2 cells. The SGLT1 density of non-treated Caco2 cells was set to 1. \*\* ( $P < 0.01$ ) indicates statistically significant difference from the absence of AICAR ( $t$  test).

Similarly, activation of AMPK by 1 mM phenformin or 10  $\mu$ M A-769662 increased the SGLT1 membrane abundance (Fig. 3.2.5).

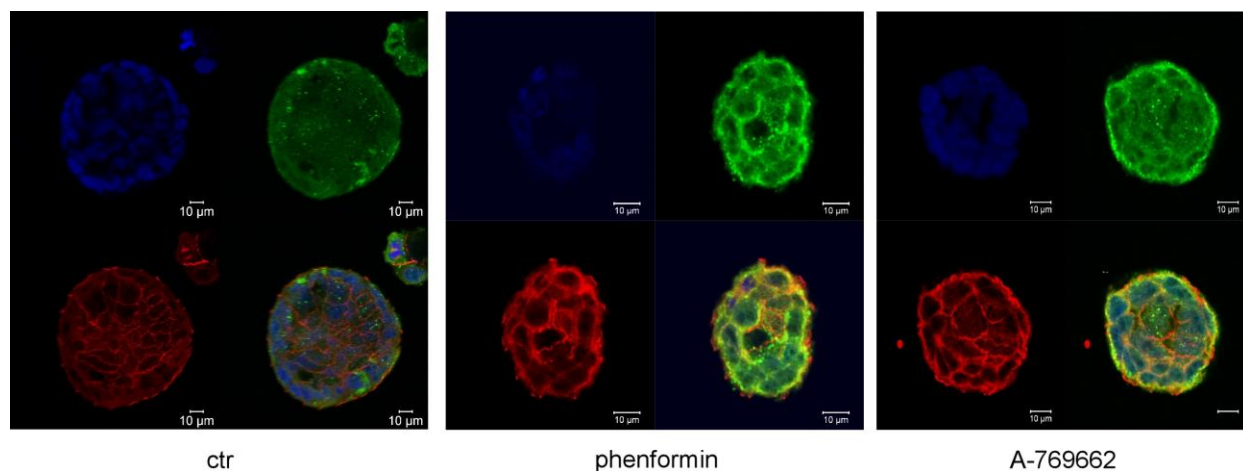


**Figure 3.2.5. Cell surface SGLT1 protein abundance in Caco2 cells was similarly upregulated by phenformin and A-769662.**

Confocal microscopy of Caco2 cells incubated for 6 h in medium without (left panel) or with (middle panel) AMPK activator phenformin (1 mM) or with (left panel) AMPK activator A-769662 (10 μM). The Caco2 cells were subjected to immunofluorescent staining using FITC-conjugated anti-SGLT1 (green) and Cy5-conjugated anti-alpha tubulin antibody (red) and DRAQ-5 dye (blue) for nuclear staining.

### 3.3 AMPK downregulates Na<sup>+</sup>-coupled glutamate transporter EAAT3 and EAAT4

#### 3.3.1 Constitutively active AMPK downregulated EAAT3-mediated electrogenic glutamate transport

Electrogenic glutamate transport was minimal in noninjected or water-injected *Xenopus* oocytes (Fig. 3.3.1A, B). In *Xenopus* oocytes expressing EAAT3 (SLC1A1), however, glutamate (2 mM) induced an inward current ( $I_g$ ) reflecting electrogenic entry of Na<sup>+</sup> and glutamate.  $I_g$  was significantly decreased by additional expression of the constitutively active mutant AMP-activated protein kinase  $\gamma^{R70Q}$ AMPK (AMPK $\alpha$ 1 + AMPK $\beta$ 1 +  $\gamma^{R70Q}$ AMPK $\gamma$ 1). Expression of  $\gamma^{R70Q}$ AMPK alone did not lead to appreciable  $I_g$ . Wild type AMPK (AMPK $\alpha$ 1+AMPK $\beta$ 1+AMPK $\gamma$ 1) also decreased the glutamate-induced current in EAAT3-expressing oocytes but appeared to be less effective than constitutively active  $\gamma^{R70Q}$ AMPK. Since EAAT3 also mediates anion currents, further experiments were performed to discriminate between electrogenic glutamate transport and EAAT3-mediated anion currents. To this end, in the bath solution Na<sup>+</sup> was replaced by Li<sup>+</sup>, which suppresses anion currents, to measure electrogenic glutamate transport. As shown in Fig. 3.3.1C, constitutively active  $\gamma^{R70Q}$ AMPK decreased EAAT3-mediated currents also under those conditions. To investigate whether EAAT3-dependent anion currents are also affected by AMPK, in the bath solution Cl<sup>-</sup> was replaced by NO<sub>3</sub><sup>-</sup> and anion currents were measured at positive potentials<sup>236</sup>. As shown in Fig. 3.3.1D, constitutively active  $\gamma^{R70Q}$ AMPK also decreased EAAT3-dependent anion currents.

Additional series of experiments were performed on AMPK-dependent regulation of EAAT1. In water-injected oocytes, the current approached  $5.6 \pm 0.4$  nA (n = 4), The expression of EAAT1 resulted in an increase in the current to  $1015 \pm 94$  nA (n = 9), the additional expression of  $\gamma^{R70Q}$ AMPK did not significantly alter the current ( $1099 \pm 37$  nA (n = 6). Similarly, EAAT2 was not significantly modified by AMPK. The respective currents were  $7.1$  nA  $\pm$   $0.9$  (n = 6) in water-injected oocytes,  $1006 \pm 65$  nA (n = 10) in EAAT2-injected oocytes and  $912 \pm 63$  nA (n = 5) in oocytes expressing both, EAAT2 and  $\gamma^{R70Q}$ AMPK.

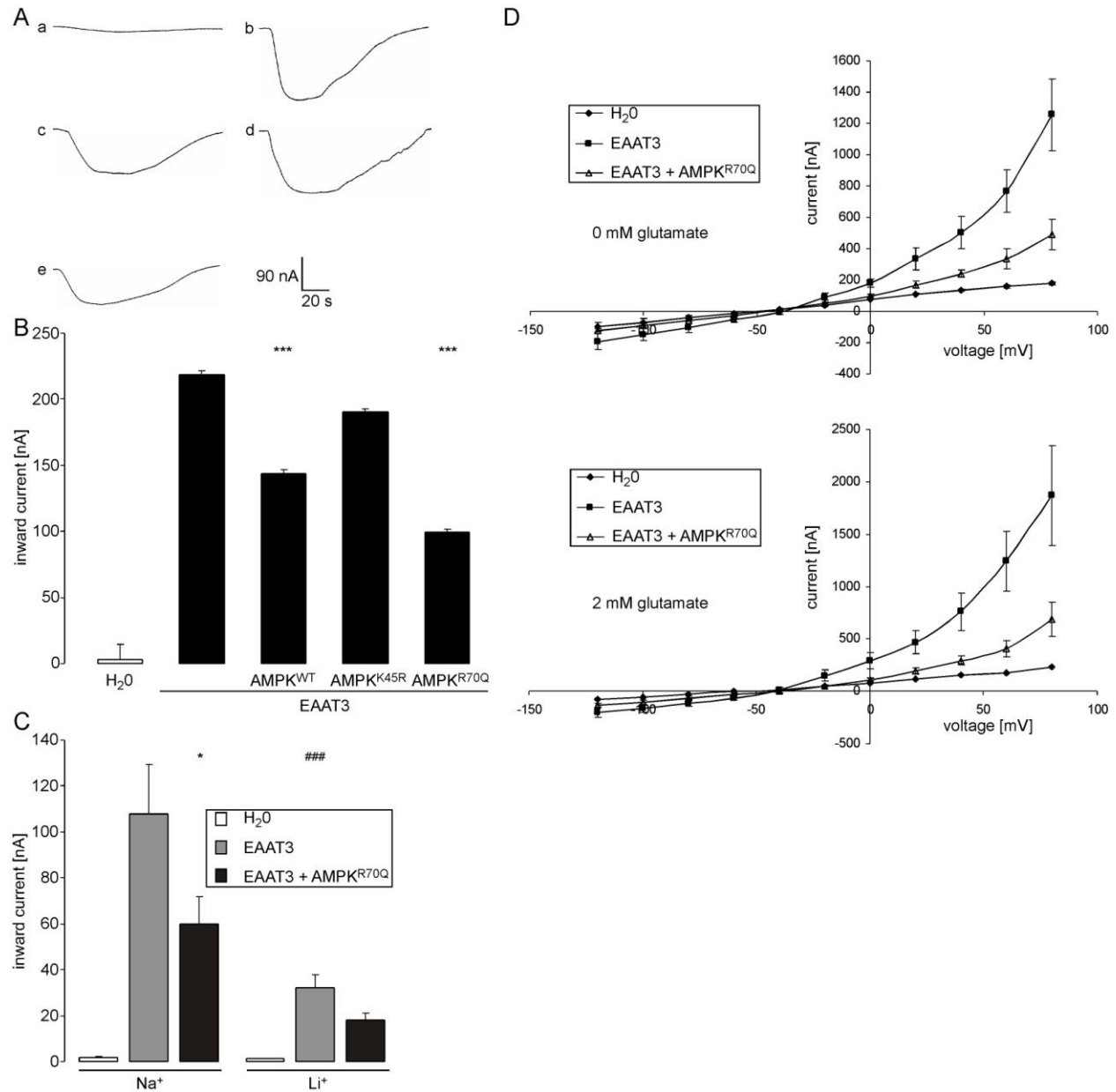


**Figure 3.3.1. Coexpression of <sup>R70Q</sup>AMPK decreased electrogenic glutamate transport in EAAT3-expressing *Xenopus* oocytes.**

**A.** Representative original tracings of glutamate-induced current in *Xenopus* oocytes injected with water (a), expressing EAAT3 without (b) or with (c) additional coexpression of wild type AMPK, of kinase dead mutant <sup>K45R</sup>AMPK (d) or of constitutively-active <sup>R70Q</sup>AMPK (e).

**B.** Arithmetic means  $\pm$  SEM (n = 14-20) of glutamate (2 mM)-induced current ( $I_g$ ) in *Xenopus* oocytes injected with water (1<sup>st</sup> bar), expressing EAAT3 without (2<sup>nd</sup> bar) or with (3<sup>rd</sup> bar) additional coexpression of wild type AMPK, of kinase dead mutant <sup>K45R</sup>AMPK (4<sup>th</sup> bar) or of constitutively-active <sup>R70Q</sup>AMPK (5<sup>th</sup> bar). \*\*\* ( $P < 0.001$ ) indicates statistically significant difference from the absence of <sup>R70Q</sup>AMPK.

**C.** Arithmetic means  $\pm$  SEM (n = 12-23) of glutamate (2 mM)-induced current ( $I_g$ ) in *Xenopus* oocytes injected with water (1<sup>st</sup>, 4<sup>th</sup> bar) or expressing EAAT3 without (2<sup>nd</sup>, 5<sup>th</sup> bar) or with (3<sup>rd</sup>, 6<sup>th</sup> bar) additional coexpression of constitutively-active <sup>R70Q</sup>AMPK (5<sup>th</sup> bar) in Na<sup>+</sup>-based (left bars) or Li<sup>+</sup>-based bath solution. \* ( $P < 0.05$ ) indicates statistically significant difference from the absence of <sup>R70Q</sup>AMPK. ### ( $P < 0.001$ ) indicates statistically significant difference from presence of Na<sup>+</sup>.

**D.** Arithmetic means  $\pm$  SEM ( $n = 6-10$ ) of the current-voltage relationship determined in *Xenopus* oocytes injected with water or expressing EAAT3 without or with additional coexpression of constitutively-active  $\gamma^{R70Q}$ AMPK in bath solution without (upper panel) or with 2 mM glutamate (lower panel).

### 3.3.2 AMPK decreased the maximal glutamate-induced current in EAAT3-expressing oocytes

Exposure of EAAT3-expressing *Xenopus* oocytes to glutamate concentrations ranging from 0 mM to 2 mM (Fig. 3.3.2) yielded concentration-dependent currents which resulted in a maximal current of  $247 \pm 4$  nA ( $n = 12-18$ ). The glutamate concentration needed for halfmaximal current ( $K_M$ ) was  $74 \pm 6$   $\mu$ M ( $n = 12-18$ ). The coexpression of constitutively-active  $\gamma^{R70Q}$ AMPK did not significantly modify  $K_M$  ( $60 \pm 3$   $\mu$ M;  $n = 7-16$ ), but significantly decreased the maximal current (to  $164 \pm 1$  nA;  $n = 7-16$ ).

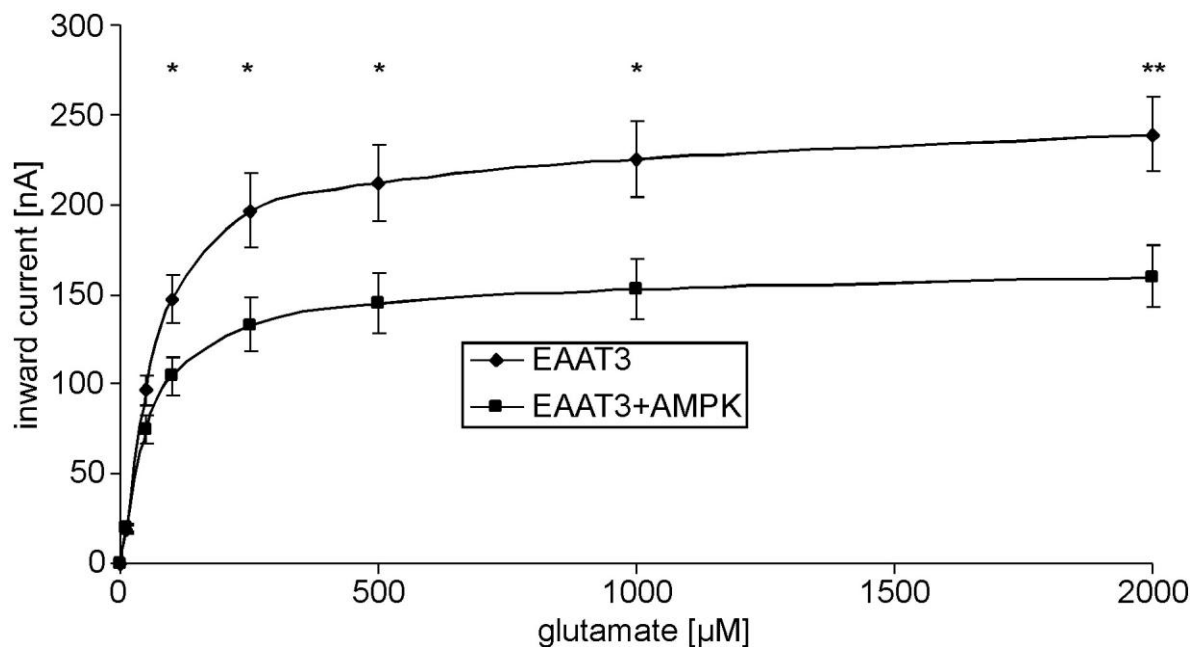


**Figure 3.3.2. AMPK decreased the EAAT3 maximal current without appreciably affecting affinity.** Arithmetic means  $\pm$  SEM ( $n = 7-18$ ) of  $I_g$  as a function of glutamate concentration in *Xenopus* oocytes expressing EAAT3 without and with constitutively-active  $\gamma^{R70Q}$ AMPK. \*, \*\* indicate significant difference ( $P < 0.05$ ,  $P < 0.01$ ) from the absence of  $\gamma^{R70Q}$ AMPK.

### 3.3.3 AMPK decreased the EAAT3 cell plasma membrane protein abundance

The decrease of maximal EAAT3-induced current following coexpression of constitutively-active  $\gamma^{R70Q}$ AMPK could have resulted from decreased carrier protein abundance in the plasma membrane. Immunohistochemistry and confocal microscopy were thus utilized to

visualize the EAAT3 protein abundance in the cell membrane. As shown in Fig. 3.3.3A, coexpression of  $\gamma^{R70Q}$ AMPK or of wild type AMPK indeed decreased the abundance of EAAT3 in the plasma membrane. To quantify EAAT3 surface expression, a chemiluminescence-based assay was used. As shown in Fig. 3.3.3B, coexpression of  $\gamma^{R70Q}$ AMPK indeed significantly reduced EAAT3 surface expression by  $59 \pm 6\%$  ( $n=75$ ).

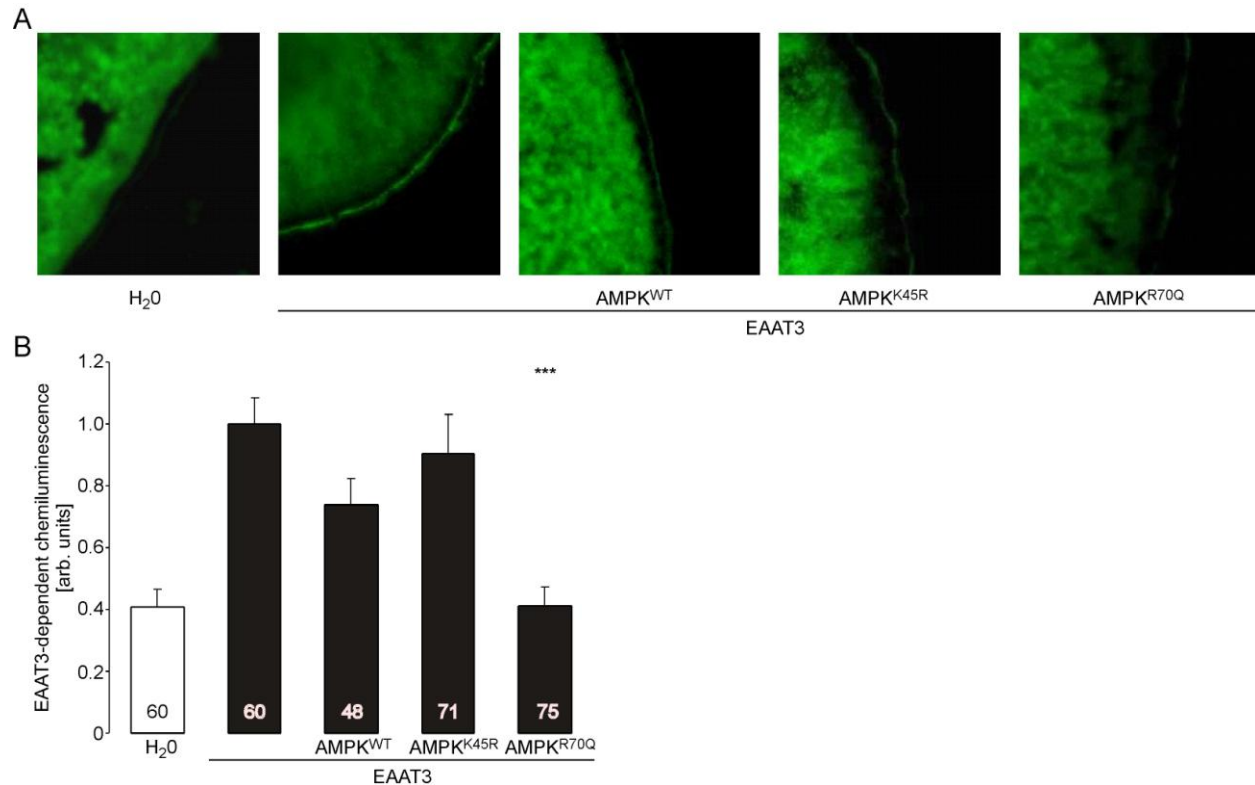


**Figure 3.3.3. Coexpression of  $\gamma^{R70Q}$ AMPK decreased cell surface EAAT3 protein abundance.**

**A.** Confocal microscopy of *Xenopus* oocytes in *Xenopus* oocytes injected with water (1<sup>st</sup> panel), expressing EAAT3 without (2<sup>nd</sup> panel) or with (3<sup>rd</sup> panel) additional coexpression of wild type AMPK, of kinase dead mutant  $\alpha^{K45R}$ AMPK (4<sup>th</sup> panel) or of constitutively-active  $\gamma^{R70Q}$ AMPK (5<sup>th</sup> panel). The cells were subjected to immunofluorescent staining using FITC-conjugated antibody (green). The images are representative for two independent experiments.

**B.** Chemiluminescence assay of EAAT3 protein abundance. Arithmetic means  $\pm$  SEM ( $n = 48-71$ ) of the EAAT3-dependent chemiluminescence in *Xenopus* oocytes injected with water (1<sup>st</sup> bar), expressing EAAT3 without (2<sup>nd</sup> bar) or with (3<sup>rd</sup> bar) additional coexpression of wild type AMPK, of kinase dead mutant  $\alpha^{K45R}$ AMPK (4<sup>th</sup> bar) or of constitutively-active  $\gamma^{R70Q}$ AMPK (5<sup>th</sup> bar). \*\*\* ( $P < 0.001$ ) indicates statistically significant difference from the absence of  $\gamma^{R70Q}$ AMPK.

### 3.3.4 Constitutively active AMPK downregulated EAAT4-mediated electrogenic glutamate transport

As shown in Fig. 3.3.4A, B, glutamate (2 mM) triggered an inward current ( $I_g$ ) in *Xenopus* oocytes expressing EAAT4 (SLC1A6). Similar to what was observed in EAAT3-expressing

*Xenopus* oocytes, the glutamate-induced current in EAAT4-expressing oocytes was significantly decreased by the additional expression of the constitutively active mutant AMP-activated protein kinase  $\gamma^{R70Q}$ AMPK. Thus,  $\gamma^{R70Q}$ AMPK decreased the EAAT4 activity. Again, wild type AMPK significantly reduced the inward current in EAAT4-expressing oocytes. The wild type AMPK was, however, significantly less effective than the constitutively active  $\gamma^{R70Q}$ AMPK. Similar to EAAT3, EAAT4 also mediates anion currents. As shown in Fig. 3.3.4C, constitutively active  $\gamma^{R70Q}$ AMPK also decreased EAAT4-mediated currents when  $\text{Na}^+$  had been replaced by  $\text{Li}^+$  in the bath solution to suppress anion currents. Similar to EAAT3, constitutively active  $\gamma^{R70Q}$ AMPK decreased EAAT4-dependent anion currents measured at positive potentials using a bath solution in which  $\text{Cl}^-$  had been replaced by  $\text{NO}_3^-$  (Fig. 3.3.4D; <sup>237</sup>).



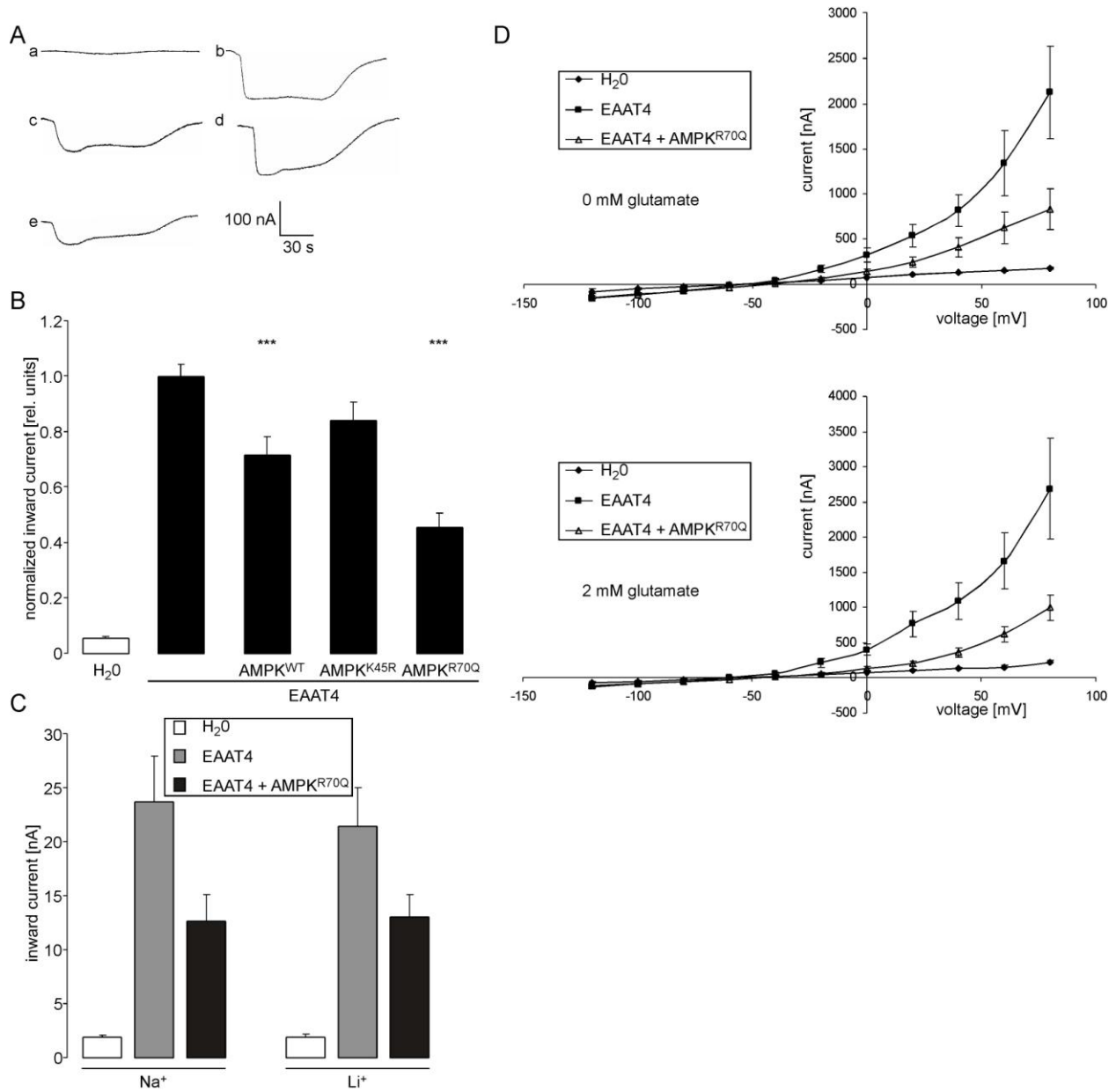


**Figure 3.3.4. Coexpression of  $\gamma^{R70Q}$  AMPK decreased electrogenic glutamate transport in EAAT4-expressing *Xenopus* oocytes.**

**A.** Representative original tracings of glutamate (2 mM)-induced current ( $I_g$ ) in *Xenopus* oocytes injected with water (a), expressing EAAT4 without (b) or with (c) additional coexpression of wild type AMPK, of kinase dead mutant  $\alpha^{K45R}$  AMPK (d) or of constitutively-active  $\gamma^{R70Q}$  AMPK (e).

**B.** Arithmetic means  $\pm$  SEM ( $n = 13$ -25) of glutamate (2 mM)-induced current ( $I_g$ ) in *Xenopus* oocytes injected with water (1<sup>st</sup> bar), expressing EAAT4 without (2<sup>nd</sup> bar) or with (3<sup>rd</sup> bar) additional coexpression of wild type AMPK, of kinase dead mutant  $\alpha^{K45R}$  AMPK (4<sup>th</sup> bar) or of constitutively-active  $\gamma^{R70Q}$  AMPK (5<sup>th</sup> bar). \*\*\* ( $P < 0.001$ ) indicates statistically significant difference from the absence of  $\gamma^{R70Q}$  AMPK.

**C.** Arithmetic means  $\pm$  SEM ( $n = 15$ -25) of glutamate (2 mM)-induced current ( $I_g$ ) in *Xenopus* oocytes injected with water (1<sup>st</sup>, 4<sup>th</sup> bar) or expressing EAAT4 without (2<sup>nd</sup>, 5<sup>th</sup> bar) or with (3<sup>rd</sup>, 6<sup>th</sup> bar) additional coexpression of constitutively-active  $\gamma^{R70Q}$  AMPK (5<sup>th</sup> bar) in Na<sup>+</sup>-based (left bars) or Li<sup>+</sup>-based bath solution.

D. Arithmetic means  $\pm$  SEM (n = 5-15) of the current-voltage relationship determined in *Xenopus* oocytes injected with water or expressing EAAT4 without or with additional coexpression of constitutively-active  $\gamma^{R70Q}$ AMPK in bath solution without (upper panel) or with 2 mM glutamate (lower panel).

### 3.3.5 AMPK decreased the maximal glutamate-induced current in EAAT4-expressing oocytes

A kinetic analysis of glutamate-induced currents in EAAT4-expressing *Xenopus* oocytes (Fig. 3.3.5) yielded a maximal current of  $22.6 \pm 0.3$  nA (n = 13). The glutamate concentration needed for halfmaximal current ( $K_M$ ) in EAAT4-expressing *Xenopus* oocytes was  $3.9 \pm 0.3$   $\mu$ M (n = 13). Similar to what was observed in EAAT3-expressing *Xenopus* oocytes, the coexpression of constitutively-active  $\gamma^{R70Q}$ AMPK did not significantly modify  $K_M$  ( $3.5 \pm 0.8$   $\mu$ M; n = 10), but significantly decreased the maximal current (to  $11.6 \pm 0.5$  nA; n = 10).

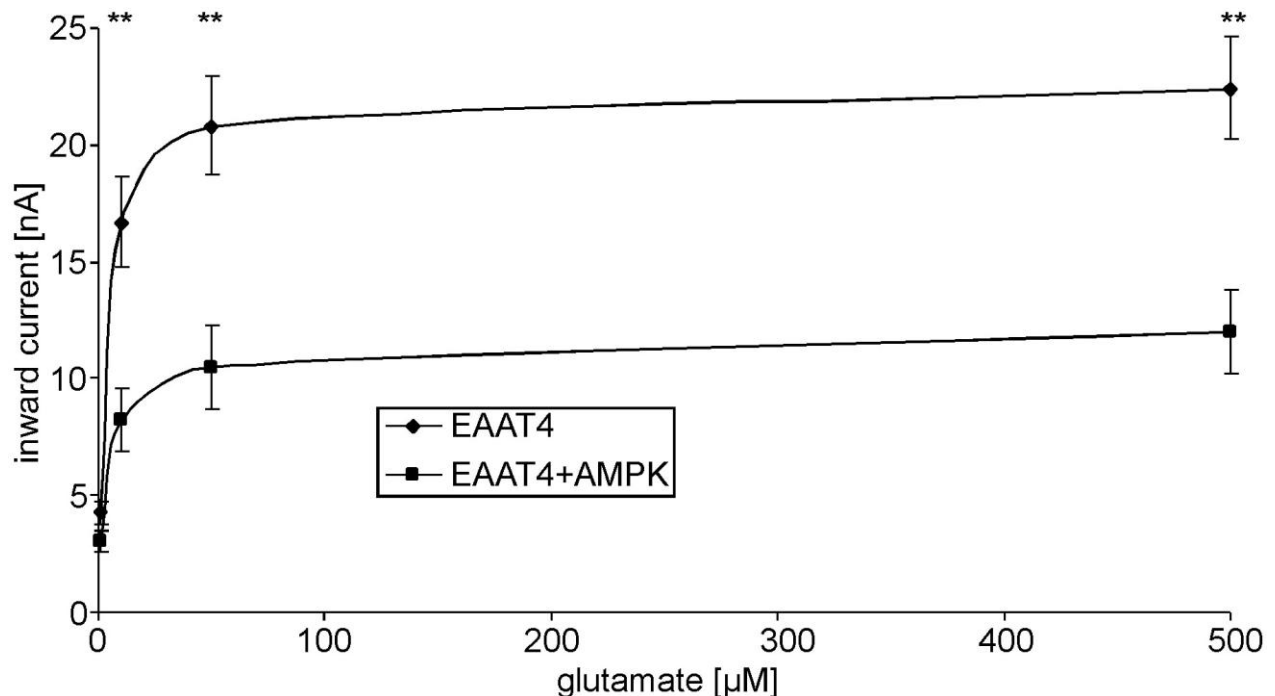


**Figure 3.3.5. AMPK decreased the EAAT4 maximal current without appreciably affecting affinity.** Arithmetic means  $\pm$  SEM (n = 10-13) of  $I_g$  as a function of glutamate concentration in *Xenopus* oocytes expressing EAAT4 without and with constitutively-active  $\gamma^{R70Q}$ AMPK. \*\* indicates significant difference ( $P < 0.01$ ) from the absence of  $\gamma^{R70Q}$ AMPK. Three different preparations of oocytes were analyzed.

### 3.3.6 AMPK decreased the EAAT4 cell plasma membrane protein abundance

Immunohistochemistry and confocal microscopy were utilized to visualize the EAAT4 protein abundance in the cell membrane. As shown in Fig. 3.3.6A, coexpression of  $\gamma^{R70Q}$ AMPK or

of wild type AMPK indeed decreased the abundance of EAAT4 in the plasma membrane. Quantification by a chemiluminescence assay confirmed that coexpression of wild type AMPK or of  $R^{70Q}$ AMPK indeed significantly reduced EAAT4 surface expression (wild type AMPK by  $42 \pm 9\%$  (n=49) and  $R^{70Q}$ AMPK by  $85 \pm 3\%$  (n=57; Fig. 3.3.6B).

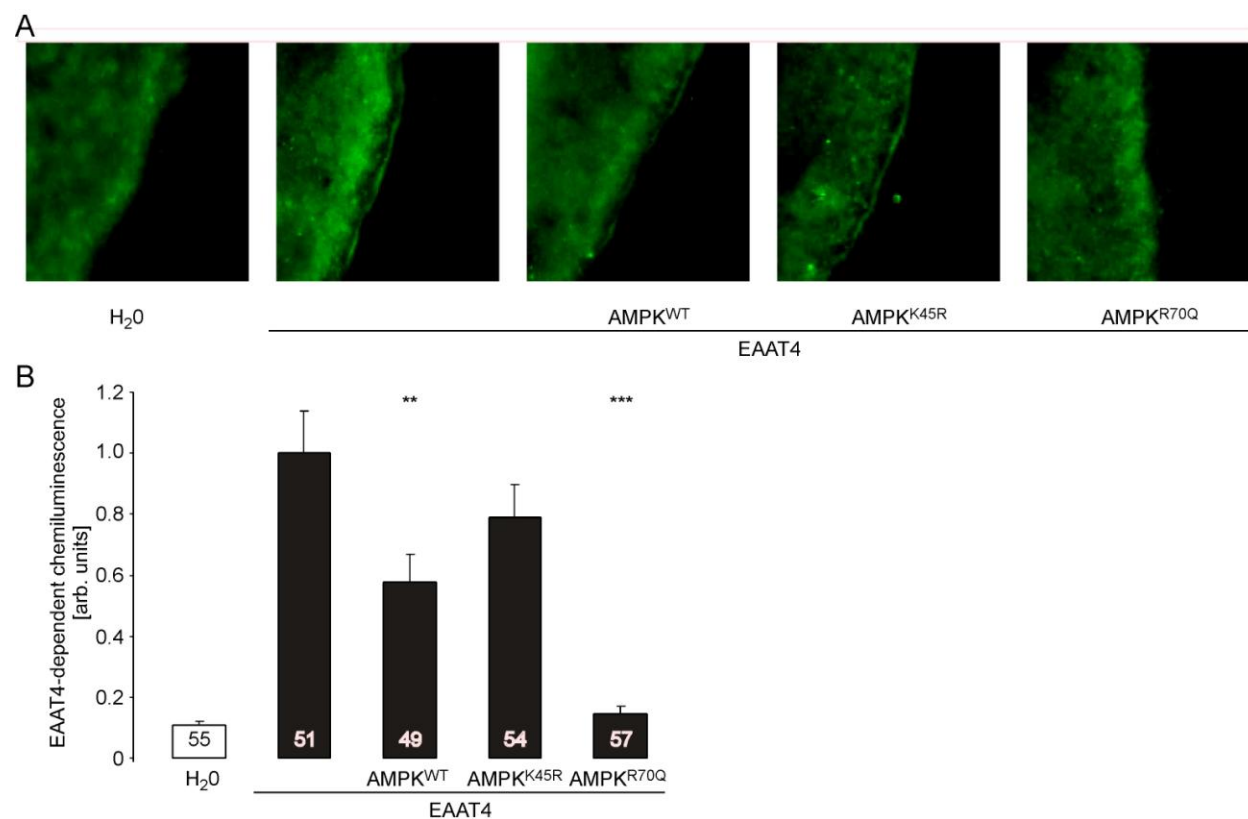


**Fig. 3.3.6. Coexpression of  $R^{70Q}$ AMPK decreased cell surface EAAT4 protein abundance.**

**A.** Confocal microscopy of *Xenopus* oocytes injected with water (1<sup>st</sup> panel), expressing EAAT4 without (2<sup>nd</sup> panel) or with (3<sup>rd</sup> panel) additional coexpression of wild type AMPK, of kinase dead mutant  $\alpha^{K45R}$ AMPK (4<sup>th</sup> panel) or of constitutively-active  $\gamma^{R70Q}$ AMPK (5<sup>th</sup> panel). Two different preparations of oocytes were analyzed.

**B.** Chemiluminescence assay of EAAT4 protein abundance. Arithmetic means  $\pm$  SEM (n = 49-57; the exact number is provided in the respective column) of the EAAT4-dependent chemiluminescence in *Xenopus* oocytes injected with water (1<sup>st</sup> bar), expressing EAAT4 without (2<sup>nd</sup> bar) or with (3<sup>rd</sup> bar) additional coexpression of wild type AMPK, of kinase dead mutant  $K^{45R}$ AMPK (4<sup>th</sup> bar) or of constitutively-active  $R^{70Q}$ AMPK (5<sup>th</sup> bar). \*\*, \*\*\* ( $P < 0.01$ ,  $P < 0.001$ ) indicate statistically significant difference from the absence of  $\gamma^{R70Q}$ AMPK. Three different preparations of oocytes were analyzed.

## 4 Discussion

### 4.1 Regulation of erythrocyte survival by AMP-activated protein kinase

The present study demonstrates for the first time expression of the AMP-dependent kinase in erythrocytes. Moreover, the present study discloses a functional role of AMPK in the regulation of suicidal erythrocyte death during energy depletion and increase in cytosolic  $\text{Ca}^{2+}$  activity. At first glance, it may appear surprising that AMPK plays a decisive role in erythrocyte survival, as metabolic activity of erythrocytes is low and not highly variable. However, the marked increase in erythrocyte turnover in  $\alpha 1$ -AMPK-deficient mice (*ampk*<sup>-/-</sup>) highlights the functional significance of AMPK in those cells.

As already shown previously<sup>231</sup>, energy depletion of erythrocytes by withdrawal of glucose increases cytosolic  $\text{Ca}^{2+}$  activity, which in turn triggers scrambling of the cell membrane with subsequent phosphatidylserine exposure at the erythrocyte surface<sup>91,99,162,163,233</sup>. Glucose depletion further decreases cell volume, a further consequence of increased cytosolic  $\text{Ca}^{2+}$  activity.  $\text{Ca}^{2+}$  activates  $\text{Ca}^{2+}$ -sensitive  $\text{K}^+$  channels<sup>32,111</sup> leading to  $\text{K}^+$  exit, hyperpolarization of the cell membrane,  $\text{Cl}^-$  exit and cellular loss of  $\text{K}^+$ ,  $\text{Cl}^-$ , and osmotically obliged water. Increase in cytosolic  $\text{Ca}^{2+}$  activity, cell membrane scrambling, and cell shrinkage are hallmarks of eryptosis, the suicidal death of erythrocytes<sup>161</sup>.

In other cell types, AMPK may be protective by stimulation of cellular glucose uptake, glycolysis, fatty acid oxidation, and expression of enzymes required for ATP production<sup>155,156</sup>. However, those mechanisms cannot be operative in glucose-depleted erythrocytes. Instead, in those erythrocytes AMPK is at least partially effective by blunting the increase in cytosolic  $\text{Ca}^{2+}$  activity. In other cell types, AMPK has been shown to enhance cytosolic  $\text{Ca}^{2+}$  activity<sup>212</sup>.

In several cell types, AMPK has been shown to be activated by an increase in cytosolic  $\text{Ca}^{2+}$  activity<sup>149</sup>. Accordingly, the eryptotic effect of the  $\text{Ca}^{2+}$  ionophore ionomycin is blunted by the AMPK agonist AICAR<sup>232,234,235</sup> and potentiated by the AMPK inhibitor compound C<sup>232</sup>. Apparently, the increase in cytosolic  $\text{Ca}^{2+}$  stimulates AMPK in erythrocytes. The kinase then counteracts the eryptotic effects of  $\text{Ca}^{2+}$ . Ionomycin has been added in the presence of glucose,

and the protective effect of AMPK under those conditions may be related to enhanced energy supply.

In carotid body type 1 cells, AMPK also senses O<sub>2</sub> levels<sup>238</sup>. Thus, at least in theory, AMPK may sense the oxygenation of erythrocyte hemoglobin. Hemoglobin deoxygenation has previously been shown to stimulate glycolysis due to the binding of deoxygenated hemoglobin to band 3<sup>239</sup>. It is tempting to speculate that AMPK is involved in the regulation of glycolysis by oxygenation of hemoglobin. Deoxygenation of hemoglobin further fosters the formation of peroxynitrate, which in turn is known to enhance glycolysis<sup>240</sup>.

It is noteworthy that AMPK could be activated by nitric oxide<sup>232</sup>, which has previously been shown to counteract Ca<sup>2+</sup>-induced cell membrane scrambling of erythrocytes<sup>241</sup>. The effect of nitric oxide is, however, presumably due to nitrosylation rather than activation of AMPK<sup>241</sup>.

As shown in this study, AMPK-sensitive survival is relevant for the life span of circulating erythrocytes. Phosphatidylserine-exposing erythrocytes bind to phosphatidylserine receptors on macrophages<sup>100</sup>, which engulf phosphatidylserine-exposing cells<sup>84</sup>. Phosphatidylserine-exposing erythrocytes are thus cleared from circulating blood<sup>83</sup>. The clearance of eryptotic erythrocytes is mostly due to trapping in the spleen. Accordingly, CFSE-labeled erythrocytes are identified 1 day after reinjection in the spleens of *ampk*<sup>-/-</sup> mice but not of *ampk*<sup>+/+</sup> mice. The enhanced trapping of circulating erythrocytes contributes to or even accounts for the severe splenomegaly of *ampk*<sup>-/-</sup> mice, which has been observed earlier<sup>150</sup>. The splenomegaly may in turn contribute to the enhanced clearance of erythrocytes. As a matter of fact, the decline of CFSE-labeled *ampk*<sup>+/+</sup> erythrocytes tended to be faster in *ampk*<sup>-/-</sup> than in *ampk*<sup>+/+</sup> mice (data not shown). However, the clearance of CFSE labeled *ampk*<sup>-/-</sup> erythrocytes was significantly enhanced not only in *ampk*<sup>-/-</sup> mice (Fig. 3.1.6), but as well in *ampk*<sup>+/+</sup> mice (data not shown), indicating that the reduced life span of circulating erythrocytes in *ampk*<sup>-/-</sup> mice is at least partially a property of the erythrocytes.

Besides its effect on erythrocyte survival, eryptosis may affect the microcirculation. Phosphatidylserine exposing erythrocytes may bind to receptors on the vascular wall<sup>242-246</sup>. Moreover, phosphatidylserine exposure fosters the assembly of prothrombinase and tenase and thus contributes to the generation of thrombin and clotting<sup>120,242,247</sup>. The trapping of eryptotic erythrocytes has previously been observed in renal medulla after ischemia of the mouse

kidney<sup>248</sup>. Suicidal erythrocytes have thus been proposed to participate in vascular injury of metabolic syndrome<sup>240</sup>.

## 4.2 Upregulation of Na<sup>+</sup>-coupled glucose carrier SGLT1 by AMPK

The sodium glucose cotransporter SGLT1 is a high affinity glucose transporter that is expressed predominantly in the brush border of the small intestine and the proximal tubule within the kidney. The uphill reabsorption of glucose is coupled to Na<sup>+</sup> down its electrochemical potential gradient across the plasma membrane. The regulation of the activity has been demonstrated to be responsive to phosphorylation by kinases including protein kinase A (PKA) and protein kinase C (PKC)<sup>249,250</sup>.

The present study demonstrates that the metabolic sensing kinase AMP-dependent kinase stimulates the electrogenic glucose transporter SGLT1 (SLC5A1). A catalytically inactive AMPK ( $\alpha$ K45R mutation) and the constitutively active AMPK  $\gamma$ R70Q mutation were expressed with the SGLT1 transporter in the heterologous oocyte expression system. Expression of constitutively active AMPK resulted in an increase in the maximal current generated by the electrogenic Na<sup>+</sup> transport coupled to glucose through the SGLT1 transporter, reflecting a 61% increase in membrane transport. The kinetics demonstrated that this was not due to an increased affinity for glucose but rather the result of an increased maximal transport, while  $K_M$  was not significantly altered by AMPK coexpression. Interestingly, the catalytically inactive- and the wild type AMPK had no effect on activity suggesting that the change in membrane transport is indeed due to AMPK activity.

Regulation of SGLT1 activity has previously been shown to be mediated via altering the expression of the co-transporter within the plasma membrane. Activation of PKC is able to decrease membrane SGLT1 through both direct and indirect means leading to decreased glucose uptake whereas PKA activates SGLT-dependent currents<sup>249,250</sup>. To determine whether AMPK-mediated regulation of SGLT1 activity was due to altered membrane trafficking, the colorectal adenocarcinoma cell line Caco-2 was stimulated with the AMPK agonists AICAR, phenformin and A-769662, and an increased membrane staining of SGLT1 was observed. These data therefore suggest that alterations in activity are probably due to membrane insertion.

The ability of AMPK to stimulate cellular glucose uptake has been shown before<sup>155,156</sup>. However, glucose uptake was considered to be due to activation of the GLUT family of facilitative glucose carriers, predominantly mediated by its effects on GLUT1 and GLUT4<sup>171-182</sup>.

During energy depletion, during which AMPK activity is maximal, glucose uptake through those passive carriers appears, at first glance, to be more appropriate than the Na<sup>+</sup>-coupled secondary glucose uptake, which requires ATP-consuming extrusion of Na<sup>+</sup> by the Na<sup>+</sup>/K<sup>+</sup> ATPase if cellular K<sup>+</sup> loss and subsequent depolarisation and cell swelling are to be avoided<sup>251</sup>. The events in energy-depleted cells are difficult to assess, as several mechanisms may compromise Na<sup>+</sup>-coupled and/or facilitative glucose transport. ATP depletion may decrease the hexokinase reaction, which otherwise generates a glucose gradient by trapping cellular glucose. In the alveolar epithelium, activation of AMPK may reduce Na<sup>+</sup>,K<sup>+</sup> ATPase activity<sup>183-185</sup>, which would decline the electrochemical gradient for Na<sup>+</sup>-coupled glucose uptake. In any case, decreasing extracellular glucose concentrations, which parallel the lack of oxygen during ischemia, are expected to affect the glucose uptake through the facilitative glucose carriers more severely than Na<sup>+</sup>-coupled glucose uptake. Even at partially dissipated Na<sup>+</sup> gradients SGLT1 is more prone to accumulate glucose in the cell even at minimal extracellular glucose concentration than facilitative glucose carriers. As the Na<sup>+</sup>, K<sup>+</sup> ATPase extrudes 3 Na<sup>+</sup> ions for one ATP; the energy needed for subsequent extrusion of the cotransported Na<sup>+</sup> is only a fraction of the energy gained, even if glucose is utilized for ATP generation by glycolysis only.

### **4.3 Downregulation of Na<sup>+</sup>-coupled glutamate transporter EAAT3 and EAAT4 by AMP-activated protein kinase**

AMPK is a kinase which is expressed ubiquitously<sup>252</sup> including neurons<sup>253</sup> and glial cells<sup>254</sup>. The present observations reveal that AMPK downregulates the transport rate of both EAAT3 and EAAT4, and is thus expected to compromise cellular glutamate uptake by those two carriers. The decrease of transport is at least partially due to a decrease of the protein abundance in the cell membrane. Accordingly, AMPK decreases the maximal transport rate but does not modify the affinity of the carrier. Earlier, AMPK has been shown to regulate glucose transport in neurons and thus to protect those cells against glutamate-induced toxicity<sup>253</sup>. To our knowledge, we do show for the first time that AMPK modifies the transport of neurotransmitters.

The decreased surface expression of Na<sup>+</sup>-coupled secondary glutamate uptake may serve to reduce energy expenditure. Na<sup>+</sup>-coupled transport leads to entry of Na<sup>+</sup>, which must be extruded by the ATP-consuming Na<sup>+</sup>/K<sup>+</sup> ATPase, if cellular K<sup>+</sup> loss with subsequent depolarisation and cell swelling are to be avoided<sup>251</sup>.

In contrast to the regulation of EAAT3 and EAAT4, the uptake of glucose is stimulated by AMPK, an effect at least partially due to activation of the GLUT family of facilitative glucose transporters<sup>171-182</sup>. AMPK stimulates the cellular glucose uptake to provide the cell with the substrate of glycolysis and glycogen storage and NB  $\gamma$  mutants lead to elevated glycogen levels<sup>155,156</sup>. AMPK further stimulates glycolysis depending on the phosphofructose 2 kinase isoform expression, fatty acid oxidation and expression of enzymes required for ATP production<sup>155,156</sup>.

The decreased energy consumption following the AMPK-induced reduction of the EAAT3 and EAAT4 surface expression may provide some protection due to decreased energy expenditure by Na<sup>+</sup>-coupled transport. By the same token, however, the impaired cellular uptake of glutamate during ischemia and subsequent extracellular accumulation of glutamate may result in neuroexcitotoxicity<sup>186,187</sup>. It appears, however, that AMPK does not decrease the activity of EAAT1 and EAAT2, which thus may accomplish clearance of extracellular glutamate during energy depletion.

Besides an increase in the AMP/ATP ratio, an increase in the cytosolic Ca<sup>2+</sup> activity<sup>149</sup> and a decrease of the O<sub>2</sub> levels<sup>238</sup> may trigger the activation of AMPK. AMP kinase may further be activated by nitric oxide<sup>232</sup>. AMPK-dependent regulation of glutamate transporters may thus be triggered by alterations of cytosolic Ca<sup>2+</sup> activity, oxygen pressure and nitric oxide formation. The AMPK-dependent downregulation of EAAT3 and EAAT4 could thus mediate some of the effects of excessive cytosolic Ca<sup>2+</sup>, lack of O<sub>2</sub> and release of NO.



## 5 Conclusions

The results conclude as follows:

- 1) Erythrocytes express AMPK, which in turn participates in the regulation of eryptosis, the suicidal death of erythrocytes. AMPK-dependent survival influences the life span of circulating erythrocytes, and deranged AMP-dependent signaling may contribute to the development of anemia.
- 2) AMP-dependent kinase is a powerful regulator of the Na<sup>+</sup>-coupled glucose transporter SGLT1 and thus does not only stimulate passive but secondary-active cellular uptake of glucose.
- 3) AMPK is a powerful regulator of the Na<sup>+</sup>-coupled glutamate transporter EAAT3 and EAAT4 and thus participates in the downregulation of extracellular glutamate concentration.

## 6 Summary

AMP-activated protein kinase (AMPK), an energy-sensing enzyme, counteracts energy depletion by stimulation of energy production and limitation of energy utilization. On energy depletion, erythrocytes undergo suicidal death or eryptosis, triggered by an increase in cytosolic  $\text{Ca}^{2+}$  activity ( $[\text{Ca}^{2+}]_i$ ) and characterized by cell shrinkage and phosphatidylserine (PS) exposure at the erythrocyte surface. The present study explored whether AMPK participates in the regulation of eryptosis. Western blotting and confocal microscopy disclosed AMPK expression in erythrocytes.  $[\text{Ca}^{2+}]_i$  (Fluo3 fluorescence), cell volume (forward scatter), and PS exposure (annexin V binding) were determined by fluorescence-activated cell sorting (FACS) analysis. Glucose removal increased  $[\text{Ca}^{2+}]_i$ , decreased cell volume, and increased PS exposure. The AMPK-inhibitor compound C (20  $\mu\text{M}$ ) did not significantly modify eryptosis under glucose-replete conditions but significantly augmented the eryptotic effect of glucose withdrawal. An increase in  $[\text{Ca}^{2+}]_i$  by  $\text{Ca}^{2+}$  ionophore ionomycin triggered eryptosis, an effect blunted by the AMPK activator 5-aminoimidazole-4-carboxamide-1- $\beta$ -D-ribofuranoside (AICAR; 1 mM). As compared with erythrocytes from wild-type littermates (*ampk*<sup>+/+</sup>), erythrocytes from AMPK $\alpha$ 1-deficient mice (*ampk*<sup>-/-</sup>) were significantly more susceptible to the eryptotic effect of energy depletion. The *ampk*<sup>-/-</sup> mice were anemic despite excessive reticulocytosis, and they suffered from severe splenomegaly, again pointing to enhanced erythrocyte turnover. The observations disclose a critical role of AMPK in the survival of circulating erythrocytes.

AMP-activated protein kinase, a serine/threonine kinase activated upon energy depletion, stimulates energy production and limits energy utilisation. It has previously been shown to enhance cellular glucose uptake through the GLUT family of facilitative glucose transporters. The present study explored the possibility that AMPK may regulate  $\text{Na}^+$ -coupled glucose transport through SGLT1 (SLC5A1). To this end, SGLT1 was expressed in *Xenopus* oocytes with and without AMPK and electrogenic glucose transport determined by dual electrode voltage clamping experiments. In SGLT1-expressing oocytes but not in oocytes injected with water or expressing constitutively active  $\gamma^{\text{R70Q}}$ AMPK ( $\alpha$ 1 $\beta$ 1 $\gamma$ 1 (R70Q)) alone, the addition of glucose to the extracellular bath generated a current ( $I_g$ ), which was halfmaximal ( $K_M$ ) at  $\approx 650$   $\mu\text{M}$  glucose concentration. Coexpression of  $\gamma^{\text{R70Q}}$ AMPK did not affect  $K_M$  but significantly enhanced the maximal current ( $\approx$

1.7 fold). Coexpression of wild type AMPK or the kinase dead  $\alpha^{K45R}$ AMPK mutant ( $\alpha 1$  (K45R)  $\beta 1\gamma 1$ ) did not appreciably affect  $I_g$ . According to confocal microscopy and Western Blotting, AICAR (1 mM), phenformin (1 mM) and A-769662 (10  $\mu$ M) enhanced the SGLT1 protein abundance in the cell membrane of Caco-2 cells suggesting that AMPK activity may increase membrane translocation of SGLT1. These observations support a role for AMPK in the regulation of  $\text{Na}^+$ -coupled glucose transport.

The glutamate transporters EAAT3 and EAAT4 are expressed in neurons. They contribute to the cellular uptake of glutamate and aspartate and thus to the clearance of the excitatory transmitters from the extracellular space. During ischemia, extracellular accumulation of glutamate may trigger excitotoxicity. Energy depletion leads to activation of the AMP-activated protein kinase, a kinase enhancing energy production and limiting energy expenditure. The present study thus explored the possibility that AMPK regulates EAAT3 and/or EAAT4. To this end, EAAT3 or EAAT4 were expressed in *Xenopus* oocytes with or without AMPK and electrogenic glutamate transport determined by dual electrode voltage clamp. In EAAT3- and in EAAT4- expressing oocytes glutamate generated a current ( $I_g$ ), which was half maximal ( $K_M$ ) at 74  $\mu$ M (EAAT3) or at 4  $\mu$ M (EAAT4) glutamate. Coexpression of constitutively active  $\gamma^{R70Q}$ AMPK or of wild type AMPK did not affect  $K_M$  but significantly decreased the maximal  $I_g$  in both EAAT3-(by 34%) and EAAT4-(by 49%) expressing oocytes. Coexpression of the inactive mutant  $\alpha^{K45R}$ AMPK ( $\alpha 1$  (K45R)  $\beta 1\gamma 1$ ) did not appreciably affect  $I_g$ . According to confocal microscopy and chemiluminescence coexpression of  $\gamma^{R70Q}$ AMPK or of wild type AMPK reduced the membrane abundance of EAAT3 and EAAT4. The observations show that AMPK downregulates  $\text{Na}^+$ -coupled glutamate transport.

## 7 Zusammenfassung

Die AMP-aktivierte Proteinkinase (AMPK) ist ein Enzym, das den Energiehaushalt der Zelle reguliert: AMPK erhöht die intrazelluläre ATP Konzentration, indem es energieverbrauchende Prozesse bremst und energieproduzierende fördert. Im Falle erschöpfter Energiereserven starten Erythrozyten ihr Apoptose-Programm, auch Eryptose genannt. Initiiert durch eine Zunahme der zytosolischen  $\text{Ca}^{2+}$ -Konzentration ( $[\text{Ca}^{2+}]_i$ ) kommt es zu Zellschrumpfung und der Exposition von Phosphatidylserin (PS) auf der Außenseite der Erythrozytenmembran. Die vorliegende Studie untersuchte, welche Rolle die AMPK in der Regulation der Eryptosis spielt. Die Expression von AMPK in den Erythrocyten wurde mittels der Western Blot Methode und Konfokalmikroskopie nachgewiesen. Die intrazelluläre  $\text{Ca}^{2+}$ -Konzentration ( $[\text{Ca}^{2+}]_i$ ), das Zellvolumen der Erythrozyten sowie Phosphatidylserin auf der Außenseite der Membran wurden mittels Durchflusszytometrie (FACS) ermittelt. Glukosemangel im Extrazellulärmedium führte zu einer Erhöhung von  $[\text{Ca}^{2+}]_i$ , verkleinerte das Zellvolumen und erhöhte den Anteil von PS in der äußeren Membran. Versuchsreihen mit dem AMPK-Inhibitor Compound C (20  $\mu\text{M}$ ) ergaben, dass bei Anwesenheit von Glukose keine signifikante Veränderung der Eryptoserate eintritt. Hingegen verstärkte Compound C bei Glucoseentzug die Eryptose deutlich. Das  $\text{Ca}^{2+}$ -Ionophor Ionomycin führt zu einer Erhöhung von  $[\text{Ca}^{2+}]_i$ , welche wiederum die Eryptose auslöst. Dieser Effekt wurde durch den AMPK-Aktivator 5-Aminoimidazol-4-carboxamid-1- $\beta$ -D-ribofuranosid (AICAR; 1 mM) abgeschwächt. Verglichen mit Erythrozyten des Wild-Typs (*ampk*<sup>+/+</sup>), waren Erythrozyten von AMPK $\alpha$ 1-defizienten Mäusen (*ampk*<sup>-/-</sup>) signifikant anfälliger für Energiemangel bedingte Eryptose. Die *ampk*<sup>-/-</sup>-Mäuse hatten trotz exzessiver Retikulozytose eine Anämie und litten unter schwerer Splenomegalie, was auf einen erhöhten Erythrozytenumsatz hinweist. Diese Beobachtungen zeigen, dass AMPK die Lebensdauer von zirkulierenden Erythrozyten beeinflusst.

AMP-aktivierte Protein Kinase, eine Serin/Threonin-Kinase, wird durch Energiemangel aktiviert. Sie stimuliert die Energieproduktion und hemmt den Energieverbrauch. Dieser Effekt der AMPK wurde insofern für die GLUT-Familie der erleichterten Glucosetransporter nachgewiesen, als die Aktivierung der AMPK zu einem erhöhten Glukoseeinstrom durch GLUT-Transporter führt. Die vorliegende Studie untersuchte die Möglichkeit, ob die AMPK eventuell den  $\text{Na}^+$  gekoppelten Glukosetransport durch SGLT1 (SLC5A1) reguliert. Dazu wurde die cRNA von SGLT1 in

*Xenopus laevis*-Oozyten mit und ohne AMPK exprimiert. Der elektrogene Symport von Na<sup>+</sup>/Glucose wurde mithilfe der Zwei-Elektroden-Spannungsklemme (DEVC) gemessen. In SGLT1-exprimierenden Oozyten konnte durch die Zugabe von Glukose zum extrazellulären Bad ein Strom ( $I_g$ ) generiert werden. Dieser erreichte seine halbmaximale Stärke bei einer Konzentration von ( $K_M$ )  $\approx 650 \mu\text{M}$  Glucose. Bei Oozyten, in die lediglich Wasser oder die konstitutiv aktive  $\gamma^{R70Q}$ AMPK ( $\alpha 1\beta 1\gamma 1(R70Q)$ ) injiziert wurde, ließ sich dieser Strom durch Glukosezugabe nicht erzeugen. Die Koexpression von  $\gamma^{R70Q}$ AMPK hatte keinen Einfluss auf  $K_M$ , erhöhte aber signifikant den maximalen Strom  $I_{g \text{ max}}$  ( $\approx 1.7$  fach). Die Koexpression des AMPK-Wildtyps oder der inaktivierten  $\alpha^{K45R}$ AMPK Mutante ( $\alpha 1(K45R)\beta 1\gamma 1$ ) wirkte sich auf  $I_g$  nicht messbar aus. AICAR (1 mM), Phenformin (1 mM) und A-769662 (10  $\mu\text{M}$ ) erhöhten die SGLT1-Expression in der Zellmembran von Caco-2 Zellen, wie durch Konfokalmikroskopie und Western Blotting gezeigt werden konnte. Dies legt nahe, dass die AMPK-Aktivität die Membrantranslokation von SGLT1 erhöhen könnte. Diese Beobachtungen deuten auf eine Rolle der AMPK für die Regulation des Na<sup>+</sup>-gekoppelten Glukosetransports.

Die Glutamattransporter EAAT3 und EAAT4 werden in Neuronen exprimiert. Durch die Aufnahme von Glutamat und Aspartat in die Neuronen dienen die beiden Transporter der Entfernung anregender Transmitter aus dem Extrazellulärraum. In einer Sauerstoffmangelsituation sammelt sich Glutamat im Extrazellulärraum an und kann damit exzitotoxisch wirken. Diese Studie erforschte die Möglichkeit der Regulation von EAAT3 und/oder EAAT4 durch die AMPK. Hierzu wurde die cRNA von EAAT3 oder EAAT4 sowohl mit als auch ohne cRNA der AMPK in *Xenopus* Oozyten exprimiert. Der elektrogene Na<sup>+</sup>/Glutamat Kotransport wurde elektrophysiologisch gemessen. In EAAT3- und in EAAT4-exprimierenden Oozyten generierte Glutamat einen Strom ( $I_g$ ), welcher seine halbmaximale Stärke bei Glutamatkonzentrationen von ( $K_{M \text{ EAAT3}}$ )  $\approx 74\mu\text{M}$  (EAAT3) beziehungsweise ( $K_{M \text{ EAAT4}}$ )  $\approx 4\mu\text{M}$  (EAAT4) erreichte. Die Koexpression der konstitutiv aktiven  $\gamma^{R70Q}$ AMPK oder der Wildtyp-AMPK hatte keinen Einfluss auf  $K_M$ , aber reduzierte den maximalen Strom  $I_g$ : in Oozyten mit EAAT3 um 34% und Oozyten mit EAAT4 um 49%. Die Koexpression der inaktiven Mutante  $\alpha^{K45R}$ AMPK ( $\alpha 1(K45R)\beta 1\gamma 1$ ) hatte keinen erkennbaren Einfluss auf  $I_g$ . Unter dem Einfluss von  $\gamma^{R70Q}$ AMPK oder des Wildtyps der AMPK wurden deutlich weniger EAAT3- und EAAT4-Transporter in die Membran eingebaut. Dies wurde mit Konfokalmikroskopie und Chemilumineszenz nachgewiesen. Die Untersuchungen zeigten, dass die AMPK den Na<sup>+</sup>-gekoppelten Glutamat Transport reduziert.

## 8 References

1. Lew, V.L. & Bookchin, R.M. Ion transport pathology in the mechanism of sickle cell dehydration. *Physiol Rev.* **85**, 179-200 (2005).
2. Mohandas, N. & Gallagher, P.G. Red cell membrane: past, present, and future. *Blood* **112**, 3939-3948 (2008).
3. Bossi, D. & Giardina, B. Red cell physiology. *Mol. Aspects Med.* **17**, 117-128 (1996).
4. Alberts, B. *et al.* Molecular biology of the cell., pp. 1283-1295 (Garland Science, New York, 2002).
5. Charles Janeway, P.T.M.W.M.S. **Immunobiology**. Garland science: New York and London (2004).
6. Lang, F., Lang, K.S., Lang, P.A., Huber, S.M. & Wieder, T. Mechanisms and significance of eryptosis. *Antioxid. Redox. Signal.* **8**, 1183-1192 (2006).
7. Blaque Belair AMDF & Fourestier M. Dictionnaire des constantes biologiques et physiques en medicine: Applications cliniques et pratiques. (1991).
8. Harris JW, K.R., pp. 281-333 (1970).
9. Dean, J. & Schechter, A.N. Sickle-cell anemia: molecular and cellular bases of therapeutic approaches (second of three parts). *N. Engl. J. Med.* **299**, 804-811 (1978).
10. Paoli, M., Liddington, R., Tame, J., Wilkinson, A. & Dodson, G. Crystal structure of T state haemoglobin with oxygen bound at all four haems. *J. Mol. Biol.* **256**, 775-792 (1996).
11. Maher, A.D. & Kuchel, P.W. The Gardos channel: a review of the Ca<sup>2+</sup>-activated K<sup>+</sup> channel in human erythrocytes. *Int. J. Biochem. Cell Biol.* **35**, 1182-1197 (2003).
12. HOFFMAN, J.F. & Laris, P.C. Membrane electrical parameters of normal human red blood cells. *Soc. Gen. Physiol Ser.* **38**, 287-293 (1984).
13. Lauf, P.K. *et al.* Physiology and biophysics of chloride and cation cotransport across cell membranes. *Fed. Proc.* **46**, 2377-2394 (1987).
14. Kaestner, L., Bollensdorff, C. & Bernhardt, I. Non-selective voltage-activated cation channel in the human red blood cell membrane. *Biochim. Biophys Acta* **1417**, 9-15 (1999).
15. Bennekou, P. The voltage-gated non-selective cation channel from human red cells is sensitive to acetylcholine. *Biochim. Biophys Acta* **1147**, 165-167 (1993).

16. Christophersen,P. & Bennekou,P. Evidence for a voltage-gated, non-selective cation channel in the human red cell membrane. *Biochim. Biophys Acta* **1065**, 103-106 (1991).
17. Rodighiero,S., De Simoni,A. & Formenti,A. The voltage-dependent nonselective cation current in human red blood cells studied by means of whole-cell and nystatin-perforated patch-clamp techniques. *Biochim. Biophys. Acta* **1660**, 164-170 (2004).
18. Kaestner,L. & Bernhardt,I. Ion channels in the human red blood cell membrane: their further investigation and physiological relevance. *Bioelectrochemistry*. **55**, 71-74 (2002).
19. Foller,M. *et al.* TRPC6 contributes to the Ca(2+) leak of human erythrocytes. *Cell Physiol Biochem*. **21**, 183-192 (2008).
20. Sluyter,R., Shemon,A.N. & Wiley,J.S. P2X(7) receptor activation causes phosphatidylserine exposure in human erythrocytes. *Biochem. Biophys. Res. Commun.* **355**, 169-173 (2007).
21. Lang,F. *et al.* Eryptosis, a window to systemic disease. *Cell Physiol Biochem*. **22**, 373-380 (2008).
22. Duranton,C., Huber,S.M. & Lang,F. Oxidation induces a Cl(-)-dependent cation conductance in human red blood cells. *J. Physiol* **539**, 847-855 (2002).
23. Bosia,A. *et al.* Kinetic characterization of Na<sup>+</sup>/H<sup>+</sup> antiport of Plasmodium falciparum membrane. *J. Cell Physiol* **154**, 527-534 (1993).
24. David-Dufilho,M., Montenay-Garestier,T. & Devynck,M.A. Fluorescence measurements of free Ca<sup>2+</sup> concentration in human erythrocytes using the Ca<sup>2+</sup>-indicator fura-2. *Cell Calcium* **9**, 167-179 (1988).
25. Tiffert,T. & Lew,V.L. Cytoplasmic calcium buffers in intact human red cells. *J. Physiol* **500** ( Pt 1), 139-154 (1997).
26. Schatzmann,H.J. The red cell calcium pump. *Annu. Rev. Physiol* **45**, 303-312 (1983).
27. Lew,V.L., Tsien,R.Y., Miner,C. & Bookchin,R.M. Physiological [Ca<sup>2+</sup>]<sub>i</sub> level and pump-leak turnover in intact red cells measured using an incorporated Ca chelator. *Nature* **298**, 478-481 (1982).
28. Lew,V.L. & Hockaday,A.R. The effects of transport perturbations on the homeostasis of erythrocytes. *Novartis. Found. Symp.* **226**, 37-50 (1999).
29. Petersen,O.H. & Maruyama,Y. Calcium-activated potassium channels and their role in secretion. *Nature* **307**, 693-696 (1984).
30. Gillen,C.M., Brill,S., Payne,J.A. & Forbush,B., III. Molecular cloning and functional expression of the K-Cl cotransporter from rabbit, rat, and human. A new member of the cation-chloride cotransporter family. *J. Biol. Chem.* **271**, 16237-16244 (1996).

31. Skou, J.C. & Esmann, M. The Na,K-ATPase. *J. Bioenerg. Biomembr.* **24**, 249-261 (1992).
32. Brugnara, C., de Franceschi, L. & Alper, S.L. Inhibition of Ca(2+)-dependent K<sup>+</sup> transport and cell dehydration in sickle erythrocytes by clotrimazole and other imidazole derivatives. *J. Clin. Invest* **92**, 520-526 (1993).
33. GARDOS, G. The function of calcium in the potassium permeability of human erythrocytes. *Biochim. Biophys. Acta* **30**, 653-654 (1958).
34. Lew, V.L., Muallem, S. & Seymour, C.A. Properties of the Ca<sup>2+</sup>-activated K<sup>+</sup> channel in one-step inside-out vesicles from human red cell membranes. *Nature* **296**, 742-744 (1982).
35. Pellegrino, M. & Pellegrini, M. Modulation of Ca<sup>2+</sup>-activated K<sup>+</sup> channels of human erythrocytes by endogenous cAMP-dependent protein kinase. *Pflugers Arch.* **436**, 749-756 (1998).
36. Del Carlo, B., Pellegrini, M. & Pellegrino, M. Calmodulin antagonists do not inhibit IK(Ca) channels of human erythrocytes. *Biochim. Biophys. Acta* **1558**, 133-141 (2002).
37. Romero, P.J. & Rojas, L. The effect of ATP on Ca(2+)-dependent K<sup>+</sup> channels of human red cells. *Acta Cient. Venez.* **43**, 19-25 (1992).
38. Lang, F. *et al.* Cation channels, cell volume and the death of an erythrocyte. *Pflugers Arch.* **447**, 121-125 (2003).
39. Zidek, W., Losse, H., Lange-Asschenfeldt, H. & Vetter, H. Intracellular chloride in essential hypertension. *Clin. Sci. (Lond)* **68**, 45-47 (1985).
40. Cheng, K., Haspel, H.C., Vallano, M.L., Osotimehin, B. & Sonenberg, M. Measurement of membrane potentials (psi) of erythrocytes and white adipocytes by the accumulation of triphenylmethylphosphonium cation. *Journal of Membrane Biology* **56**, 191-201 (1980).
41. Grygorczyk, R. & Schwarz, W. Properties of the CA<sup>2+</sup>-activated K<sup>+</sup> conductance of human red cells as revealed by the patch-clamp technique. *Cell Calcium* **4**, 499-510 (1983).
42. Leinders, T., van Kleef, R.G. & Vijverberg, H.P. Single Ca(2+)-activated K<sup>+</sup> channels in human erythrocytes: Ca<sup>2+</sup> dependence of opening frequency but not of open lifetimes. *Biochim. Biophys. Acta* **1112**, 67-74 (1992).
43. Tiffert, T., Spivak, J.L. & Lew, V.L. Magnitude of calcium influx required to induce dehydration of normal human red cells. *Biochim. Biophys. Acta* **943**, 157-165 (1988).
44. Grygorczyk, R., Schwarz, W. & Passow, H. Ca<sup>2+</sup>-activated K<sup>+</sup> channels in human red cells. Comparison of single-channel currents with ion fluxes. *Biophys. J.* **45**, 693-698 (1984).



45. Birka,C. *et al.* Enhanced susceptibility to erythrocyte "apoptosis" following phosphate depletion. *Pflugers Arch* **448**, 471-477 (2004).
46. Lang,K.S. *et al.* Cation channels trigger apoptotic death of erythrocytes. *Cell. Death. Differ.* **10**, 249-256 (2003).
47. Jennings,M.L. & Adame,M.F. Direct estimate of 1:1 stoichiometry of K(+)-Cl(-) cotransport in rabbit erythrocytes. *Am. J. Physiol Cell Physiol* **281**, C825-C832 (2001).
48. Gibson,J.S., Speake,P.F. & Ellory,J.C. Differential oxygen sensitivity of the K+-Cl- cotransporter in normal and sickle human red blood cells. *J. Physiol* **511** ( Pt 1), 225-234 (1998).
49. Jennings,M.L. Volume-sensitive K(+)/Cl(-) cotransport in rabbit erythrocytes. Analysis of the rate-limiting activation and inactivation events. *J. Gen. Physiol* **114**, 743-758 (1999).
50. Lauf,P.K. *et al.* Erythrocyte K-Cl cotransport: properties and regulation. *Am. J. Physiol* **263**, C917-C932 (1992).
51. Jennings,M.L. & Schulz,R.K. Okadaic acid inhibition of KCl cotransport. Evidence that protein dephosphorylation is necessary for activation of transport by either cell swelling or N-ethylmaleimide. *J. Gen. Physiol* **97**, 799-817 (1991).
52. Bize,I., Taher,S. & Brugnara,C. Regulation of K-Cl cotransport during reticulocyte maturation and erythrocyte aging in normal and sickle erythrocytes. *Am. J. Physiol Cell Physiol* **285**, C31-C38 (2003).
53. Bookchin,R.M., Ortiz,O.E. & Lew,V.L. Evidence for a direct reticulocyte origin of dense red cells in sickle cell anemia. *J. Clin. Invest* **87**, 113-124 (1991).
54. Freeman,C.J., Bookchin,R.M., Ortiz,O.E. & Lew,V.L. K-permeabilized human red cells lose an alkaline, hypertonic fluid containing excess K over diffusible anions. *J. Membr. Biol.* **96**, 235-241 (1987).
55. Jacobs,W.A. & Craig,L.C. THE ERGOT ALKALOIDS. SYNTHESIS OF 4-CARBOLINE CARBONIC ACIDS. *Science* **82**, 421-422 (1935).
56. Post,R.L., Albright,C.D. & Dayani,K. Resolution of pump and leak components of sodium and potassium ion transport in human erythrocytes. *J. Gen. Physiol* **50**, 1201-1220 (1967).
57. TOSTESON,D.C. & HOFFMAN,J.F. Regulation of cell volume by active cation transport in high and low potassium sheep red cells. *J. Gen. Physiol* **44**, 169-194 (1960).
58. Joiner,C.H., Platt,O.S. & Lux,S.E. Cation depletion by the sodium pump in red cells with pathologic cation leaks. Sick cells and xerocytes. *J. Clin. Invest* **78**, 1487-1496 (1986).

59. Deal, J.E., Shah, V., Goodenough, G. & Dillon, M.J. Red cell membrane sodium transport: possible genetic role and use in identifying patients at risk of essential hypertension. *Arch. Dis. Child* **65**, 1154-1157 (1990).
60. Girardin, E. & Paunier, L. Relationship between magnesium, potassium and sodium concentrations in lymphocytes and erythrocytes from normal subjects. *Magnesium* **4**, 188-192 (1985).
61. Kaji, D.M., Thakkar, U. & Kahn, T. Glucocorticoid-induced alterations in the sodium potassium pump of the human erythrocyte. *J. Clin. Invest* **68**, 422-430 (1981).
62. Korff, J.M., Siebens, A.W. & Gill, J.R., Jr. Correction of hypokalemia corrects the abnormalities in erythrocyte sodium transport in Bartter's syndrome. *J. Clin. Invest* **74**, 1724-1729 (1984).
63. Hotchkiss, R.S., Strasser, A., McDunn, J.E. & Swanson, P.E. Cell death. *N. Engl. J. Med.* **361**, 1570-1583 (2009).
64. Kroemer, G. *et al.* Classification of cell death: recommendations of the Nomenclature Committee on Cell Death 2009. *Cell Death. Differ.* **16**, 3-11 (2009).
65. Melino, G. The Sirens' song. *Nature* **412**, 23 (2001).
66. Fillon, S., Lang, F. & Jendrossek, V. Pseudomonas aeruginosa triggered apoptosis of human epithelial cells depends on the temperature during infection. *Cell Physiol Biochem.* **12**, 207-214 (2002).
67. Pozzi, S., Malferrari, G., Biunno, I. & Samaja, M. Low-flow ischemia and hypoxia stimulate apoptosis in perfused hearts independently of reperfusion. *Cell Physiol Biochem.* **12**, 39-46 (2002).
68. Bortner, C.D. & Cidlowski, J.A. A necessary role for cell shrinkage in apoptosis. *Biochem Pharmacol* **56**, 1549-59 (1998).
69. Rosette, C. & Karin, M. Ultraviolet light and osmotic stress: activation of the JNK cascade through multiple growth factor and cytokine receptors. *Science* **274**, 1194-1197 (1996).
70. Cariers, A., Reinehr, R., Fischer, R., Warskulat, U. & Haussinger, D. c-Jun-N-terminal kinase dependent membrane targeting of CD95 in rat hepatic stellate cells. *Cell Physiol Biochem.* **12**, 179-186 (2002).
71. Wieder, T. *et al.* Piceatannol, a hydroxylated analog of the chemopreventive agent resveratrol, is a potent inducer of apoptosis in the lymphoma cell line BJAB and in primary, leukemic lymphoblasts. *Leukemia* **15**, 1735-1742 (2001).
72. Bosman, G.J., Willekens, F.L. & Werre, J.M. Erythrocyte aging: a more than superficial resemblance to apoptosis? *Cell Physiol Biochem* **16**, 1-8 (2005).

73. Bosman,G.J. Erythrocyte aging in sickle cell disease. *Cell Mol. Biol. (Noisy. -le-grand)* **50**, 81-86 (2004).
74. Bratosin,D. *et al.* Flow cytofluorimetric analysis of young and senescent human erythrocytes probed with lectins. Evidence that sialic acids control their life span. *Glycoconj. J.* **12**, 258-267 (1995).
75. Crespo,L.M., Novak,T.S. & Freedman,J.C. Calcium, cell shrinkage, and prolytic state of human red blood cells. *Am J Physiol* **252**, C138-C152 (1987).
76. Kuypers,F.A. & de Jong,K. The role of phosphatidylserine in recognition and removal of erythrocytes. *Cell Mol. Biol. (Noisy. -le-grand)* **50**, 147-158 (2004).
77. Lang,K.S. *et al.* Mechanisms of Suicidal Erythrocyte Death. *Cell Physiol Biochem* **15**, 195-202 (2005).
78. Schlegel,R.A. & Williamson,P. Phosphatidylserine, a death knell. *Cell Death. Differ.* **8**, 551-563 (2001).
79. Allan,D. & Thomas,P. Ca<sup>2+</sup>-induced biochemical changes in human erythrocytes and their relation to microvesiculation. *Biochem. J* **198**, 433-440 (1981).
80. Allen,T.M., Williamson,P. & Schlegel,R.A. Phosphatidylserine as a determinant of reticuloendothelial recognition of liposome models of the erythrocyte surface. *Proc. Natl. Acad. Sci. U. S. A* **85**, 8067-8071 (1988).
81. Connor,J., Pak,C.C. & Schroit,A.J. Exposure of phosphatidylserine in the outer leaflet of human red blood cells. Relationship to cell density, cell age, and clearance by mononuclear cells. *J Biol. Chem.* **269**, 2399-2404 (1994).
82. Schroit,A.J., Madsen,J.W. & Tanaka,Y. In vivo recognition and clearance of red blood cells containing phosphatidylserine in their plasma membranes. *J Biol. Chem.* **260**, 5131-5138 (1985).
83. Kempe,D.S. *et al.* Enhanced programmed cell death of iron-deficient erythrocytes. *FASEB J* **20**, 368-370 (2006).
84. Boas,F.E., Forman,L. & Beutler,E. Phosphatidylserine exposure and red cell viability in red cell aging and in hemolytic anemia. *Proc. Natl. Acad. Sci. U. S. A* **95**, 3077-3081 (1998).
85. Daugas,E., Cande,C. & Kroemer,G. Erythrocytes: death of a mummy. *Cell Death. Differ.* **8**, 1131-1133 (2001).
86. Lang,K.S. *et al.* Inhibition of erythrocyte cation channels and apoptosis by ethylisopropylamiloride. *Naunyn Schmiedebergs Arch. Pharmacol.* **367**, 391-396 (2003).

87. Lang,P.A. *et al.* Inhibition of erythrocyte "apoptosis" by catecholamines. *Naunyn Schmiedebergs Arch. Pharmacol.* **372**, 228-235 (2005).
88. Myssina,S. *et al.* Cl<sup>-</sup> channel blockers NPPB and niflumic acid blunt Ca<sup>(2+)</sup>-induced erythrocyte 'apoptosis'. *Cell Physiol Biochem* **14**, 241-248 (2004).
89. Lang,P.A. *et al.* Role of Ca<sup>2+</sup>-activated K<sup>+</sup> channels in human erythrocyte apoptosis. *Am J Physiol Cell Physiol* **285**, C1553-C1560 (2003).
90. Lorand,L., Siefiring,G.E., Jr. & Lowe-Krentz,L. Enzymatic basis of membrane stiffening in human erythrocytes. *Semin. Hematol.* **16**, 65-74 (1979).
91. Berg,C.P. *et al.* Human mature red blood cells express caspase-3 and caspase-8, but are devoid of mitochondrial regulators of apoptosis. *Cell Death. Differ.* **8**, 1197-1206 (2001).
92. Zwaal,R.F. *et al.* Loss of membrane phospholipid asymmetry during activation of blood platelets and sickled red cells; mechanisms and physiological significance. *Mol. Cell Biochem.* **91**, 23-31 (1989).
93. Lang,P.A. *et al.* PGE<sub>2</sub> in the regulation of programmed erythrocyte death. *Cell Death Differ* **12**, 415-428 (2005).
94. Lang,P.A. *et al.* Stimulation of erythrocyte phosphatidylserine exposure by paclitaxel. *Cell Physiol Biochem.* **18**, 151-164 (2006).
95. Weed,R.I., LaCelle,P.L. & Merrill,E.W. Metabolic dependence of red cell deformability. *J. Clin. Invest* **48**, 795-809 (1969).
96. Woon,L.A., Holland,J.W., Kable,E.P. & Roufogalis,B.D. Ca<sup>2+</sup> sensitivity of phospholipid scrambling in human red cell ghosts. *Cell Calcium* **25**, 313-320 (1999).
97. Aiken,N.R., Satterlee,J.D. & Galey,W.R. Measurement of intracellular Ca<sup>2+</sup> in young and old human erythrocytes using <sup>19</sup>F-NMR spectroscopy. *Biochim. Biophys. Acta* **1136**, 155-160 (1992).
98. Romero,P.J. & Romero,E.A. The role of calcium metabolism in human red blood cell ageing: a proposal. *Blood Cells Mol. Dis.* **25**, 9-19 (1999).
99. Bratosin,D. *et al.* Programmed cell death in mature erythrocytes: a model for investigating death effector pathways operating in the absence of mitochondria. *Cell Death. Differ.* **8**, 1143-1156 (2001).
100. Fadok,V.A. *et al.* A receptor for phosphatidylserine-specific clearance of apoptotic cells. *Nature* **405**, 85-90 (2000).
101. Henson,P.M., Bratton,D.L. & Fadok,V.A. The phosphatidylserine receptor: a crucial molecular switch? *Nat. Rev. Mol. Cell Biol.* **2**, 627-633 (2001).

102. Messmer,U.K. & Pfeilschifter,J. New insights into the mechanism for clearance of apoptotic cells. *Bioessays* **22**, 878-881 (2000).
103. Eda,S. & Sherman,I.W. Cytoadherence of malaria-infected red blood cells involves exposure of phosphatidylserine. *Cell Physiol Biochem.* **12**, 373-384 (2002).
104. Fadok,V.A., Bratton,D.L., Frasch,S.C., Warner,M.L. & Henson,P.M. The role of phosphatidylserine in recognition of apoptotic cells by phagocytes. *Cell Death. Differ.* **5**, 551-562 (1998).
105. Zwaal,R.F. & Schroit,A.J. Pathophysiologic implications of membrane phospholipid asymmetry in blood cells. *Blood* **89**, 1121-1132 (1997).
106. Dumaswala,U.J., Zhuo,L., Jacobsen,D.W., Jain,S.K. & Sukalski,K.A. Protein and lipid oxidation of banked human erythrocytes: role of glutathione. *Free Radic. Biol. Med.* **27**, 1041-1049 (1999).
107. Gomez-Angelats,M., Bortner,C.D. & Cidlowski,J.A. Cell volume regulation in immune cell apoptosis. *Cell Tissue Res.* **301**, 33-42 (2000).
108. Gomez-Angelats,M. & Cidlowski,J.A. Cell volume control and signal transduction in apoptosis. *Toxicol. Pathol.* **30**, 541-551 (2002).
109. Green,D.R. & Reed,J.C. Mitochondria and apoptosis. *Science* **281**, 1309-1312 (1998).
110. Lang,K.S. *et al.* Involvement of ceramide in hyperosmotic shock-induced death of erythrocytes. *Cell Death Differ* **11**, 231-243 (2004).
111. Bookchin,R.M., Ortiz,O.E. & Lew,V.L. Activation of calcium-dependent potassium channels in deoxygenated sickled red cells. *Prog. Clin. Biol. Res.* **240**, 193-200 (1987).
112. Duranton,C. *et al.* Electrophysiological properties of the Plasmodium Falciparum-induced cation conductance of human erythrocytes. *Cell Physiol Biochem* **13**, 189-198 (2003).
113. Huber,S.M., Gamper,N. & Lang,F. Chloride conductance and volume-regulatory nonselective cation conductance in human red blood cell ghosts. *Pflugers Arch.* **441**, 551-558 (2001).
114. Barvitenko,N.N., Adragna,N.C. & Weber,R.E. Erythrocyte signal transduction pathways, their oxygenation dependence and functional significance. *Cell Physiol Biochem* **15**, 1-18 (2005).
115. Schwarzer,E., Kühn,H., Valente,E. & Arese,P. Band 3/COMPLEMENT-mediated Recognition and Removal of Normally Senescent and Pathological Human Erythrocytes. *Cell Physiol Biochem* **16**, 133-146 (2005).

116. Rice, L. & Alfrey, C.P. The negative regulation of red cell mass by neocytolysis: physiologic and pathophysiologic manifestations. *Cell Physiol Biochem* **15**, 245-250 (2005).
117. Op den Kamp, J.A. Lipid asymmetry in membranes. *Annu. Rev. Biochem.* **48**, 47-71 (1979).
118. Rothman, J.E. & Lenard, J. Membrane asymmetry. *Science* **195**, 743-753 (1977).
119. Bratosin, D. *et al.* Molecular mechanisms of erythrophagocytosis. Characterization of the senescent erythrocytes that are phagocytized by macrophages. *C. R. Acad. Sci. III* **320**, 811-818 (1997).
120. Zwaal, R.F., Comfurius, P. & Bevers, E.M. Surface exposure of phosphatidylserine in pathological cells. *Cell Mol Life Sci* **62**, 971-988 (2005).
121. Colleau, M., Herve, P., Fellmann, P. & Devaux, P.F. Transmembrane diffusion of fluorescent phospholipids in human erythrocytes. *Chem. Phys. Lipids* **57**, 29-37 (1991).
122. Morrot, G., Herve, P., Zachowski, A., Fellmann, P. & Devaux, P.F. Aminophospholipid translocase of human erythrocytes: phospholipid substrate specificity and effect of cholesterol. *Biochemistry* **28**, 3456-3462 (1989).
123. Smeets, E.F., Comfurius, P., Bevers, E.M. & Zwaal, R.F. Calcium-induced transbilayer scrambling of fluorescent phospholipid analogs in platelets and erythrocytes. *Biochim. Biophys. Acta* **1195**, 281-286 (1994).
124. Gaffet, P., Bettache, N. & Bienvenue, A. Phosphatidylserine exposure on the platelet plasma membrane during A23187-induced activation is independent of cytoskeleton reorganization. *Eur. J. Cell Biol.* **67**, 336-345 (1995).
125. Zwaal, R.F., Comfurius, P. & Bevers, E.M. Mechanism and function of changes in membrane-phospholipid asymmetry in platelets and erythrocytes. *Biochem. Soc. Trans.* **21**, 248-253 (1993).
126. Sulpice, J.C., Zachowski, A., Devaux, P.F. & Giraud, F. Requirement for phosphatidylinositol 4,5-bisphosphate in the Ca<sup>2+</sup>-induced phospholipid redistribution in the human erythrocyte membrane. *J. Biol. Chem.* **269**, 6347-6354 (1994).
127. Zhou, Q., Zhao, J., Wiedmer, T. & Sims, P.J. Normal hemostasis but defective hematopoietic response to growth factors in mice deficient in phospholipid scramblase 1. *Blood* **99**, 4030-4038 (2002).
128. Dekkers, D.W., Comfurius, P., Bevers, E.M. & Zwaal, R.F. Comparison between Ca<sup>2+</sup>-induced scrambling of various fluorescently labelled lipid analogues in red blood cells. *Biochem. J.* **362**, 741-747 (2002).

129. Bevers,E.M., Comfurius,P. & Zwaal,R.F. Changes in membrane phospholipid distribution during platelet activation. *Biochim. Biophys. Acta* **736**, 57-66 (1983).
130. Comfurius,P. *et al.* Loss of membrane phospholipid asymmetry in platelets and red cells may be associated with calcium-induced shedding of plasma membrane and inhibition of aminophospholipid translocase. *Biochim. Biophys. Acta* **1026**, 153-160 (1990).
131. Fadok,V.A. *et al.* Exposure of phosphatidylserine on the surface of apoptotic lymphocytes triggers specific recognition and removal by macrophages. *J. Immunol.* **148**, 2207-2216 (1992).
132. Wright,E.M., Hirayama,B.A. & Loo,D.F. Active sugar transport in health and disease. *J. Intern. Med.* **261**, 32-43 (2007).
133. Uldry,M. & Thorens,B. The SLC2 family of facilitated hexose and polyol transporters. *Pflugers Arch.* **447**, 480-489 (2004).
134. Wright,E.M. & Turk,E. The sodium/glucose cotransport family SLC5. *Pflugers Arch.* **447**, 510-518 (2004).
135. Nieoullon,A. *et al.* The neuronal excitatory amino acid transporter EAAC1/EAAT3: does it represent a major actor at the brain excitatory synapse? *J Neurochem* **98**, 1007-1018 (2006).
136. Danbolt,N.C. Glutamate uptake. *Prog. Neurobiol.* **65**, 1-105 (2001).
137. Dingledine,R., Borges,K., Bowie,D. & Traynelis,S.F. The glutamate receptor ion channels. *Pharmacol. Rev.* **51**, 7-61 (1999).
138. O'Kane,R.L., Martinez-Lopez,I., DeJoseph,M.R., Vina,J.R. & Hawkins,R.A. Na(+)-dependent glutamate transporters (EAAT1, EAAT2, and EAAT3) of the blood-brain barrier. A mechanism for glutamate removal. *J Biol Chem.* **274**, 31891-31895 (1999).
139. Miralles,V.J. *et al.* Na<sup>+</sup> dependent glutamate transporters (EAAT1, EAAT2, and EAAT3) in primary astrocyte cultures: effect of oxidative stress. *Brain Res.* **922**, 21-29 (2001).
140. Hamberger,A. & Nystrom,B. Extra- and intracellular amino acids in the hippocampus during development of hepatic encephalopathy. *Neurochem. Res.* **9**, 1181-1192 (1984).
141. Kanai,Y. & Hediger,M.A. The glutamate/neutral amino acid transporter family SLC1: molecular, physiological and pharmacological aspects. *Pflugers Arch.* **447**, 469-479 (2004).
142. Deng,X. *et al.* Association study of polymorphisms in the glutamate transporter genes SLC1A1, SLC1A3, and SLC1A6 with schizophrenia. *Am J Med Genet. B Neuropsychiatr. Genet.* **144B**, 271-278 (2007).

143. Fairman,W.A., Vandenberg,R.J., Arriza,J.L., Kavanaugh,M.P. & Amara,S.G. An excitatory amino-acid transporter with properties of a ligand-gated chloride channel. *Nature* **375**, 599-603 (1995).
144. Kugler,P. & Schmitt,A. Glutamate transporter EAAC1 is expressed in neurons and glial cells in the rat nervous system. *Glia* **27**, 129-142 (1999).
145. Verrey,F. *et al.* Novel renal amino acid transporters. *Annu. Rev. Physiol* **67**, 557-572 (2005).
146. Huang,Y.H., Dykes-Hoberg,M., Tanaka,K., Rothstein,J.D. & Bergles,D.E. Climbing fiber activation of EAAT4 transporters and kainate receptors in cerebellar Purkinje cells. *J Neurosci.* **24**, 103-111 (2004).
147. Furuta,A., Martin,L.J., Lin,C.L., Dykes-Hoberg,M. & Rothstein,J.D. Cellular and synaptic localization of the neuronal glutamate transporters excitatory amino acid transporter 3 and 4. *Neuroscience* **81**, 1031-1042 (1997).
148. Hardie,D.G. AMPK: a key regulator of energy balance in the single cell and the whole organism. *Int. J. Obes. (Lond)* **32 Suppl 4**, S7-12 (2008).
149. Towler,M.C. & Hardie,D.G. AMP-activated protein kinase in metabolic control and insulin signaling. *Circ. Res* **100**, 328-341 (2007).
150. Mayer,A., Denanglaire,S., Viollet,B., Leo,O. & Andris,F. AMP-activated protein kinase regulates lymphocyte responses to metabolic stress but is largely dispensable for immune cell development and function. *Eur J Immunol* **38**, 948-956 (2008).
151. Long,Y.C. & Zierath,J.R. AMP-activated protein kinase signaling in metabolic regulation. *J. Clin. Invest* **116**, 1776-1783 (2006).
152. Scott,J.W. *et al.* CBS domains form energy-sensing modules whose binding of adenosine ligands is disrupted by disease mutations. *J. Clin. Invest* **113**, 274-284 (2004).
153. Rutter,G.A., da,S., X & Leclerc,I. Roles of 5'-AMP-activated protein kinase (AMPK) in mammalian glucose homeostasis. *Biochem. J.* **375**, 1-16 (2003).
154. Witczak,C.A., Sharoff,C.G. & Goodyear,L.J. AMP-activated protein kinase in skeletal muscle: from structure and localization to its role as a master regulator of cellular metabolism. *Cell Mol. Life Sci.* **65**, 3737-3755 (2008).
155. Winder,W.W. & Thomson,D.M. Cellular energy sensing and signaling by AMP-activated protein kinase. *Cell Biochem Biophys* **47**, 332-347 (2007).
156. Carling,D. The role of the AMP-activated protein kinase in the regulation of energy homeostasis. *Novartis. Found. Symp.* **286**, 72-81 (2007).



157. Horie, T. *et al.* Oxidative stress induces GLUT4 translocation by activation of PI3-K/Akt and dual AMPK kinase in cardiac myocytes. *J Cell Physiol* **215**, 733-742 (2008).
158. Jensen, T.E., Rose, A.J., Hellsten, Y., Wojtaszewski, J.F. & Richter, E.A. Caffeine-induced Ca(2+) release increases AMPK-dependent glucose uptake in rodent soleus muscle. *Am J Physiol Endocrinol. Metab* **293**, E286-E292 (2007).
159. McGee, S.L. & Hargreaves, M. AMPK and transcriptional regulation. *Front Biosci.* **13**, 3022-3033 (2008).
160. Hardie, D.G. The AMP-activated protein kinase pathway--new players upstream and downstream. *J Cell Sci.* **117**, 5479-5487 (2004).
161. Lang, K.S. *et al.* Mechanisms of suicidal erythrocyte death. *Cell Physiol Biochem* **15**, 195-202 (2005).
162. Brand, V.B. *et al.* Dependence of Plasmodium falciparum in vitro growth on the cation permeability of the human host erythrocyte. *Cell Physiol Biochem* **13**, 347-356 (2003).
163. Lang, P.A. *et al.* Blunted apoptosis of erythrocytes from taurine transporter deficient mice. *Cell Physiol Biochem* **13**, 337-346 (2003).
164. Kaestner, L., Tabellion, W., Lipp, P. & Bernhardt, I. Prostaglandin E2 activates channel-mediated calcium entry in human erythrocytes: an indication for a blood clot formation supporting process. *Thromb. Haemost.* **92**, 1269-1272 (2004).
165. Schneider, J., Nicolay, J.P., Foller, M., Wieder, T. & Lang, F. Suicidal erythrocyte death following cellular K+ loss. *Cell Physiol Biochem.* **20**, 35-44 (2007).
166. Gulbins, E. Regulation of death receptor signaling and apoptosis by ceramide. *Pharmacol Res* **47**, 393-399 (2003).
167. Nicolay, J.P. *et al.* Stimulation of suicidal erythrocyte death by methylglyoxal. *Cell Physiol Biochem.* **18**, 223-232 (2006).
168. Nicolay, J.P., Gatz, S., Liebig, G., Gulbins, E. & Lang, F. Amyloid induced suicidal erythrocyte death. *Cell Physiol Biochem.* **19**, 175-184 (2007).
169. Steinberg, G.R. & Kemp, B.E. AMPK in Health and Disease. *Physiol Rev.* **89**, 1025-1078 (2009).
170. Foller, M. *et al.* Regulation of erythrocyte survival by AMP-activated protein kinase. *FASEB J* **23**, 1072-1080 (2009).
171. Guan, F. *et al.* Chemical hypoxia-induced glucose transporter-4 translocation in neonatal rat cardiomyocytes. *Arch Med Res* **39**, 52-60 (2008).

172. Jessen, N. *et al.* Effects of AICAR and exercise on insulin-stimulated glucose uptake, signaling, and GLUT-4 content in rat muscles. *J Appl Physiol* **94**, 1373-1379 (2003).
173. Luiken, J.J. *et al.* Regulation of cardiac long-chain fatty acid and glucose uptake by translocation of substrate transporters. *Pflugers Arch* **448**, 1-15 (2004).
174. Winder, W.W. *et al.* Activation of AMP-activated protein kinase increases mitochondrial enzymes in skeletal muscle. *J Appl Physiol* **88**, 2219-2226 (2000).
175. Zheng, D. *et al.* Regulation of muscle GLUT-4 transcription by AMP-activated protein kinase. *J Appl Physiol* **91**, 1073-1083 (2001).
176. Li, J. *et al.* Role of the nitric oxide pathway in AMPK-mediated glucose uptake and GLUT4 translocation in heart muscle. *Am J Physiol Endocrinol. Metab* **287**, E834-E841 (2004).
177. MacLean, P.S., Zheng, D., Jones, J.P., Olson, A.L. & Dohm, G.L. Exercise-induced transcription of the muscle glucose transporter (GLUT 4) gene. *Biochem Biophys Res. Commun.* **292**, 409-414 (2002).
178. Natsuizaka, M. *et al.* Synergistic up-regulation of Hexokinase-2, glucose transporters and angiogenic factors in pancreatic cancer cells by glucose deprivation and hypoxia. *Exp. Cell Res.* **313**, 3337-3348 (2007).
179. Ojuka, E.O., Nolte, L.A. & Holloszy, J.O. Increased expression of GLUT-4 and hexokinase in rat epitrochlearis muscles exposed to AICAR in vitro. *J Appl Physiol* **88**, 1072-1075 (2000).
180. Park, S. *et al.* Chronic elevated calcium blocks AMPK-induced GLUT-4 expression in skeletal muscle. *Am J Physiol Cell Physiol* **296**, C106-C115 (2009).
181. Walker, J. *et al.* 5-aminoimidazole-4-carboxamide riboside (AICAR) enhances GLUT2-dependent jejunal glucose transport: a possible role for AMPK. *Biochem J* **385**, 485-491 (2005).
182. Lei, B. *et al.* Exogenous nitric oxide reduces glucose transporters translocation and lactate production in ischemic myocardium in vivo. *Proc. Natl. Acad. Sci. U. S. A* **102**, 6966-6971 (2005).
183. Vadasz, I. *et al.* AMP-activated protein kinase regulates CO<sub>2</sub>-induced alveolar epithelial dysfunction in rats and human cells by promoting Na,K-ATPase endocytosis. *J. Clin. Invest* **118**, 752-762 (2008).
184. Woollhead, A.M., Scott, J.W., Hardie, D.G. & Baines, D.L. Phenformin and 5-aminoimidazole-4-carboxamide-1-beta-D-ribofuranoside (AICAR) activation of AMP-activated protein kinase inhibits transepithelial Na<sup>+</sup> transport across H441 lung cells. *J. Physiol* **566**, 781-792 (2005).

185. Woollhead, A.M. *et al.* Pharmacological activators of AMP-activated protein kinase have different effects on Na<sup>+</sup> transport processes across human lung epithelial cells. *Br. J. Pharmacol.* **151**, 1204-1215 (2007).
186. Grewer, C. *et al.* Glutamate forward and reverse transport: from molecular mechanism to transporter-mediated release after ischemia. *IUBMB Life* **60**, 609-619 (2008).
187. Hertz, L. Bioenergetics of cerebral ischemia: a cellular perspective. *Neuropharmacology* **55**, 289-309 (2008).
188. Amara, S.G. & Fontana, A.C. Excitatory amino acid transporters: keeping up with glutamate. *Neurochem Int.* **41**, 313-318 (2002).
189. Collin, M. *et al.* Plasma membrane and vesicular glutamate transporter mRNAs/proteins in hypothalamic neurons that regulate body weight. *Eur. J. Neurosci.* **18**, 1265-1278 (2003).
190. Furuta, A. *et al.* Expression of glutamate transporter subtypes during normal human corticogenesis and type II lissencephaly. *Brain Res. Dev. Brain Res.* **155**, 155-164 (2005).
191. Shashidharan, P. *et al.* Immunohistochemical localization of the neuron-specific glutamate transporter EAAC1 (EAAT3) in rat brain and spinal cord revealed by a novel monoclonal antibody. *Brain Res.* **773**, 139-148 (1997).
192. Schmitt, A. *et al.* Decreased gene expression of glial and neuronal glutamate transporters after chronic antipsychotic treatment in rat brain. *Neurosci. Lett.* **347**, 81-84 (2003).
193. Schniepp, R. *et al.* Retinal colocalization and in vitro interaction of the glutamate transporter EAAT3 and the serum- and glucocorticoid-inducible kinase SGK1 [correction]. *Invest Ophthalmol. Vis. Sci.* **45**, 1442-1449 (2004).
194. Maragakis, N.J. *et al.* Glutamate transporter expression and function in human glial progenitors. *Glia* **45**, 133-143 (2004).
195. van Landeghem, F.K., Weiss, T. & von Deimling, A. Expression of PACAP and glutamate transporter proteins in satellite oligodendrocytes of the human CNS. *Regul Pept.* **142**, 52-59 (2007).
196. Furuta, A., Rothstein, J.D. & Martin, L.J. Glutamate transporter protein subtypes are expressed differentially during rat CNS development. *J Neurosci.* **17**, 8363-8375 (1997).
197. Huerta, I., McCullumsmith, R.E., Haroutunian, V., Gimenez-Amaya, J.M. & Meador-Woodruff, J.H. Expression of excitatory amino acid transporter interacting protein transcripts in the thalamus in schizophrenia. *Synapse* **59**, 394-402 (2006).
198. Kim, J.H., Do, S.H., Kim, Y.L. & Zuo, Z. Effects of chronic exposure to ethanol on glutamate transporter EAAT3 expressed in *Xenopus* oocytes: evidence for protein kinase C involvement. *Alcohol Clin. Exp. Res.* **29**, 2046-2052 (2005).

199. Lang,U.E., Puls,I., Muller,D.J., Strutz-Seebohm,N. & Gallinat,J. Molecular mechanisms of schizophrenia. *Cell Physiol Biochem* **20**, 687-702 (2007).
200. McCullumsmith,R.E. & Meador-Woodruff,J.H. Striatal excitatory amino acid transporter transcript expression in schizophrenia, bipolar disorder, and major depressive disorder. *Neuropsychopharmacology* **26**, 368-375 (2002).
201. Nudmamud-Thanoi,S., Piyabhan,P., Harte,M.K., Cahir,M. & Reynolds,G.P. Deficits of neuronal glutamatergic markers in the caudate nucleus in schizophrenia. *J Neural Transm. Suppl* 281-285 (2007).
202. Smith,R.E., Haroutunian,V., Davis,K.L. & Meador-Woodruff,J.H. Expression of excitatory amino acid transporter transcripts in the thalamus of subjects with schizophrenia. *Am J Psychiatry* **158**, 1393-1399 (2001).
203. Crino,P.B. *et al.* Increased expression of the neuronal glutamate transporter (EAAT3/EAAC1) in hippocampal and neocortical epilepsy. *Epilepsia* **43**, 211-218 (2002).
204. Mathern,G.W. *et al.* Hippocampal GABA and glutamate transporter immunoreactivity in patients with temporal lobe epilepsy. *Neurology* **52**, 453-472 (1999).
205. Proper,E.A. *et al.* Distribution of glutamate transporters in the hippocampus of patients with pharmaco-resistant temporal lobe epilepsy. *Brain* **125**, 32-43 (2002).
206. Rakhade,S.N. & Loeb,J.A. Focal reduction of neuronal glutamate transporters in human neocortical epilepsy. *Epilepsia* **49**, 226-236 (2008).
207. Simantov,R. *et al.* Changes in expression of neuronal and glial glutamate transporters in rat hippocampus following kainate-induced seizure activity. *Brain Res. Mol Brain Res.* **65**, 112-123 (1999).
208. Chan,H., Zwingmann,C., Pannunzio,M. & Butterworth,R.F. Effects of ammonia on high affinity glutamate uptake and glutamate transporter EAAT3 expression in cultured rat cerebellar granule cells. *Neurochem Int.* **43**, 137-146 (2003).
209. Peghini,P., Janzen,J. & Stoffel,W. Glutamate transporter EAAC-1-deficient mice develop dicarboxylic aminoaciduria and behavioral abnormalities but no neurodegeneration. *EMBO J.* **16**, 3822-3832 (1997).
210. Huang,Y.H., Sinha,S.R., Tanaka,K., Rothstein,J.D. & Bergles,D.E. Astrocyte glutamate transporters regulate metabotropic glutamate receptor-mediated excitation of hippocampal interneurons. *J. Neurosci.* **24**, 4551-4559 (2004).
211. Horie,T. *et al.* Oxidative stress induces GLUT4 translocation by activation of PI3-K/Akt and dual AMPK kinase in cardiac myocytes. *J Cell Physiol* **215**, 733-742 (2008).

212. Kohno,D., Sone,H., Minokoshi,Y. & Yada,T. Ghrelin raises  $[Ca^{2+}]_i$  via AMPK in hypothalamic arcuate nucleus NPY neurons. *Biochem Biophys. Res Commun.* **366**, 388-392 (2008).
213. Crino,P.B. *et al.* Increased expression of the neuronal glutamate transporter (EAAT3/EAAC1) in hippocampal and neocortical epilepsy. *Epilepsia* **43**, 211-218 (2002).
214. Viollet,B. *et al.* Physiological role of AMP-activated protein kinase (AMPK): insights from knockout mouse models. *Biochem Soc Trans.* **31**, 216-219 (2003).
215. Andree,H.A. *et al.* Binding of vascular anticoagulant alpha (VAC alpha) to planar phospholipid bilayers. *J. Biol. Chem.* **265**, 4923-4928 (1990).
216. Seebohm,G. *et al.* Regulation of KCNQ4 potassium channel prepulse dependence and current amplitude by SGK1 in *Xenopus* oocytes. *Cell Physiol Biochem.* **16**, 255-262 (2005).
217. Wagner,C.A., Friedrich,B., Setiawan,I., Lang,F. & Broer,S. The use of *Xenopus laevis* oocytes for the functional characterization of heterologously expressed membrane proteins. *Cell Physiol Biochem.* **10**, 1-12 (2000).
218. Bohmer,C. *et al.* Stimulation of the EAAT4 glutamate transporter by SGK protein kinase isoforms and PKB. *Biochem Biophys Res. Commun.* **324**, 1242-1248 (2004).
219. Busch,A.E. *et al.* Properties of electrogenic Pi transport by a human renal brush border Na<sup>+</sup>/Pi transporter. *J. Am. Soc. Nephrol.* **6**, 1547-1551 (1995).
220. Dieter,M. *et al.* Regulation of glucose transporter SGLT1 by ubiquitin ligase Nedd4-2 and kinases SGK1, SGK3, and PKB. *Obes. Res* **12**, 862-870 (2004).
221. Fraser,S.A. *et al.* Regulation of the renal-specific Na<sup>+</sup>-K<sup>+</sup>-2Cl<sup>-</sup> co-transporter NKCC2 by AMP-activated protein kinase (AMPK). *Biochem J* **405**, 85-93 (2007).
222. Hamilton,S.R. *et al.* An activating mutation in the gamma1 subunit of the AMP-activated protein kinase. *FEBS Lett.* **500**, 163-168 (2001).
223. Hallows,K.R., Kobinger,G.P., Wilson,J.M., Witters,L.A. & Foskett,J.K. Physiological modulation of CFTR activity by AMP-activated protein kinase in polarized T84 cells. *Am. J. Physiol Cell Physiol* **284**, C1297-C1308 (2003).
224. Boehmer,C. *et al.* The peptide transporter PEPT2 is targeted by the protein kinase SGK1 and the scaffold protein NHERF2. *Cell Physiol Biochem* **22**, 705-714 (2008).
225. Boehmer,C. *et al.* Modulation of the voltage-gated potassium channel Kv1.5 by the SGK1 protein kinase involves inhibition of channel ubiquitination. *Cell Physiol Biochem* **22**, 591-600 (2008).

226. Dowd,L.A. & Robinson,M.B. Rapid stimulation of EAAC1-mediated Na<sup>+</sup>-dependent L-glutamate transport activity in C6 glioma cells by phorbol ester. *J Neurochem* **67**, 508-516 (1996).
227. Dowd,L.A., Coyle,A.J., Rothstein,J.D., Pritchett,D.B. & Robinson,M.B. Comparison of Na<sup>+</sup>-dependent glutamate transport activity in synaptosomes, C6 glioma, and *Xenopus* oocytes expressing excitatory amino acid carrier 1 (EAAC1). *Mol Pharmacol.* **49**, 465-473 (1996).
228. Boehmer,C. *et al.* Regulation of the glutamate transporter EAAT1 by the ubiquitin ligase Nedd4-2 and the serum and glucocorticoid-inducible kinase isoforms SGK1/3 and protein kinase B. *J. Neurochem.* **86**, 1181-1188 (2003).
229. Shigeri,Y. *et al.* Effects of threo-beta-hydroxyaspartate derivatives on excitatory amino acid transporters (EAAT4 and EAAT5). *J. Neurochem.* **79**, 297-302 (2001).
230. Gehring,E.M. *et al.* Regulation of the glutamate transporter EAAT2 by PIKfyve. *Cell Physiol Biochem* **24**, 361-368 (2009).
231. Klarl,B.A. *et al.* Protein kinase C mediates erythrocyte "programmed cell death" following glucose depletion. *Am J Physiol Cell Physiol* **290**, C244-C253 (2006).
232. Lira,V.A. *et al.* Nitric oxide increases GLUT4 expression and regulates AMPK signaling in skeletal muscle. *Am J Physiol Endocrinol. Metab* **293**, E1062-E1068 (2007).
233. Chuang,D.M. Neuroprotective and neurotrophic actions of the mood stabilizer lithium: can it be used to treat neurodegenerative diseases? *Crit Rev Neurobiol.* **16**, 83-90 (2004).
234. Gaskin,F.S., Kamada,K., Yusof,M. & Korthuis,R.J. 5'-AMP-activated protein kinase activation prevents postischemic leukocyte-endothelial cell adhesive interactions. *Am. J Physiol Heart Circ. Physiol* **292**, H326-H332 (2007).
235. Sell,H., Dietze-Schroeder,D., Eckardt,K. & Eckel,J. Cytokine secretion by human adipocytes is differentially regulated by adiponectin, AICAR, and troglitazone. *Biochem Biophys. Res Commun.* **343**, 700-706 (2006).
236. Torres-Salazar,D. & Fahlke,C. Neuronal glutamate transporters vary in substrate transport rate but not in unitary anion channel conductance. *J Biol Chem* **282**, 34719-34726 (2007).
237. Melzer,N., Biela,A. & Fahlke,C. Glutamate modifies ion conduction and voltage-dependent gating of excitatory amino acid transporter-associated anion channels. *J Biol Chem* **278**, 50112-50119 (2003).
238. Evans,A.M. *et al.* Does AMP-activated protein kinase couple inhibition of mitochondrial oxidative phosphorylation by hypoxia to calcium signaling in O<sub>2</sub>-sensing cells? *J Biol Chem.* **280**, 41504-41511 (2005).

239. Low,P.S., Rathinavelu,P. & Harrison,M.L. Regulation of glycolysis via reversible enzyme binding to the membrane protein, band 3. *J Biol Chem.* **268**, 14627-14631 (1993).
240. Zappulla,D. Environmental stress, erythrocyte dysfunctions, inflammation, and the metabolic syndrome: adaptations to CO<sub>2</sub> increases? *J Cardiometab. Syndr.* **3**, 30-34 (2008).
241. Nicolay,J.P. *et al.* Inhibition of suicidal erythrocyte death by nitric oxide. *Pflugers Arch* (2007).
242. Andrews,D.A. & Low,P.S. Role of red blood cells in thrombosis. *Curr. Opin Hematol.* **6**, 76-82 (1999).
243. Closse,C., Dachary-Prigent,J. & Boisseau,M.R. Phosphatidylserine-related adhesion of human erythrocytes to vascular endothelium. *Br. J Haematol.* **107**, 300-302 (1999).
244. Gallagher,P.G. *et al.* Altered erythrocyte endothelial adherence and membrane phospholipid asymmetry in hereditary hydrocytosis. *Blood* **101**, 4625-4627 (2003).
245. Pandolfi,A. *et al.* Mechanisms of uremic erythrocyte-induced adhesion of human monocytes to cultured endothelial cells. *J Cell Physiol* **213**, 699-709 (2007).
246. Wood,B.L., Gibson,D.F. & Tait,J.F. Increased erythrocyte phosphatidylserine exposure in sickle cell disease: flow-cytometric measurement and clinical associations. *Blood* **88**, 1873-1880 (1996).
247. Chung,S.M. *et al.* Lysophosphatidic acid induces thrombogenic activity through phosphatidylserine exposure and procoagulant microvesicle generation in human erythrocytes. *Arterioscler. Thromb. Vasc. Biol* **27**, 414-421 (2007).
248. Lang,K.S. *et al.* Inhibition of erythrocyte phosphatidylserine exposure by urea and Cl<sup>-</sup>. *Am J Physiol Renal Physiol* **286**, F1046-F1053 (2004).
249. Hirsch,J.R., Loo,D.D. & Wright,E.M. Regulation of Na<sup>+</sup>/glucose cotransporter expression by protein kinases in *Xenopus laevis* oocytes. *J Biol Chem* **271**, 14740-14746 (1996).
250. Subramanian,S., Glitz,P., Kipp,H., Kinne,R.K. & Castaneda,F. Protein kinase-A affects sorting and conformation of the sodium-dependent glucose co-transporter SGLT1. *J Cell Biochem* **106**, 444-452 (2009).
251. Lang,F. *et al.* Functional significance of cell volume regulatory mechanisms. *Physiol Rev.* **78**, 247-306 (1998).
252. Warden,S.M. *et al.* Post-translational modifications of the beta-1 subunit of AMP-activated protein kinase affect enzyme activity and cellular localization. *Biochem J* **354**, 275-283 (2001).

253. Weisova,P., Concannon,C.G., Devocelle,M., Prehn,J.H. & Ward,M.W. Regulation of glucose transporter 3 surface expression by the AMP-activated protein kinase mediates tolerance to glutamate excitation in neurons. *J Neurosci.* **29**, 2997-3008 (2009).
254. Giri,S., Khan,M., Nath,N., Singh,I. & Singh,A.K. The role of AMPK in psychosine mediated effects on oligodendrocytes and astrocytes: implication for Krabbe disease. *J Neurochem* **105**, 1820-1833 (2008).



## 9 Publications

1. Kempe, DS., Boini, K., Siraskar, B., Capuano, P., **Sopjani, M.**, Stange, G., Bhandaru, M., AckermannTF., Judenhofer, MS., Pichler, BJ., Biber, J., Alessi, DR., Föller, M., Wagner, CA., Lang, F. (2010). **Calciuria and phosphaturia in mice expressing PKB/SGK-resistant GSK3** (submitted).
2. Bhandaru, M., Kempe, DS., **Sopjani, M.**, Tyan, L., Rotte, A., Judenhofer, MS., Pichler, BJ., Pearce, D., Föller, M., Lang, F. (2010). **Phosphaturia of gene targeted mice lacking functional SGK3** (submitted).
3. Rexhepaj, R., Dërmaku-Sopjani, M., Gehring EM., **Sopjani, M.**, Kempe, DS., Föller, M., Lang, F. (2010). **Stimulation of electrogenic glucose transport by glycogen synthase kinase 3** (submitted).
4. **Sopjani, M.**, Alesutan, I., Dërmaku-Sopjani, M., Fraser, S., Kemp, BE., Föller, M., Lang, F. (2010). **Downregulation of Na<sup>+</sup>-coupled glutamate transporter EAAT3 and EAAT4 by AMP-activated protein kinase.** *Journal of Neurochemistry* (accepted).
5. Boehmer C., **Sopjani M.**, Klaus F., Lindner, R., Laufer J., Jeyaray, S., Lang, F., Palmada M., (2010). **The serum and glucocorticoid inducible kinases SGK1-3 stimulate neutral amino acid transporter SLC6A19.** *Cell Physiol Biochem* (accepted).
6. Kempe, DS., Dërmaku-Sopjani, M., Froehlich, H., **Sopjani, M.**, Umbach, A., Goverthan, P., Föller, M., Stübs, M., Weiss, F., Lang, F. (2010). **Rapamycin-induced phosphaturia.** *Nephrology Dialysis Transplantation* (accepted).
7. **Sopjani, M.**, Bhavsar, SK., Fraser, S., Kemp, BE., Föller, M., Lang, F. (2010). **Regulation of Na<sup>+</sup>-coupled glucose carrier SGLT1 by AMP-activated protein kinase.** *Molecular Membrane Biology* (accepted).

8. **Sopjani, M.**, Kunert, A., Czarkowski, K., Klaus, F., Laufer, J., Föller, M., Lang, F. (2010). **Regulation of the Ca<sup>2+</sup> channel TRPV6 by the kinases SGK1, PKB/Akt and PIKfyve.** *J. Membr. Biol.* **233**, 35-41.
9. Gehring EM., Zürn A., Klaus F., Laufer J., **Sopjani M.**, Lindner R., Strutz-Seebohm N., Tavaré JE., Boehmer C., Palmada M., Lang UE, Seebohm G., Lang F. (2009). **Regulation of the glutamate transporter EAAT2 by PIKfyve.** *Cell Physiol Biochem.* **24**, 361-368.
10. Rexhepaj, R., Rotte, A., Kempe, D. S., **Sopjani, M.**, Foller, M., Gehring, E. M., Bhandaru, M., Gruner, I., Mack, A. F., Rubio-Aliaga, I., Nassl, A. M., Daniel, H., Kuhl, D., & Lang, F. (2009). **Stimulation of electrogenic intestinal dipeptide transport by the glucocorticoid dexamethasone.** *Pflugers Arch.* **459**, 191-202.
11. Fedorenko, O., Tang, C., **Sopjani, M.**, Foller, M., Gehring, E. M., Strutz-Seebohm, N., Ureche, O. N., Ivanova, S., Semke, A., Lang, F., Seebohm, G., & Lang, U. E. (2009). **PIP5K2A-dependent regulation of excitatory amino acid transporter EAAT3.** *Psychopharmacology (Berl)* **206**, 429-435.
12. Foller, M., **Sopjani, M.**, Koka, S., Gu, S., Mahmud, H., Wang, K., Floride, E., Schleicher, E., Schulz, E., Munzel, T., & Lang, F. (2009). **Regulation of erythrocyte survival by AMP-activated protein kinase.** *FASEB J.* **23**, 1072-1080.
13. **Sopjani, M.**, Foller, M., Haendeler, J., Gotz, F., & Lang, F. (2009). **Silver ion-induced suicidal erythrocyte death.** *J.Appl.Toxicol.* **29**, 531-536.
14. Foller, M., **Sopjani, M.**, Schlemmer, H. P., Claussen, C. D., & Lang, F. (2009). **Triggering of suicidal erythrocyte death by radiocontrast agents.** *Eur.J.Clin.Invest* **39**, 576-583.

15. Sopi, RB., Bislimi,K., Halili, F., **Sopjani, M.**, Neziri, B., Jakupi, M. (2009). **Lead Acetate Induces Epithelium-Dependent Contraction of Airway Smooth Muscle.** *J. Int. Environ. Appl. & Sci.* 4(2):146-151.
16. **Sopjani,M.**, Foller,M., Gulbins,E. & Lang,F. (2008). **Suicidal death of erythrocytes due to selenium-compounds.** *Cell Physiol Biochem.* **22**, 387-394.
17. **Sopjani,M.**, Foller,M., Dreischer,P. & Lang,F. (2008). **Stimulation of eryptosis by cadmium ions.** *Cell Physiol Biochem.* **22**, 245-252.
18. Foller,M., **Sopjani,M.**, Mahmud,H. & Lang,F. (2008). **Vanadate-induced suicidal erythrocyte death.** *Kidney Blood Press Res.* **31**, 87-93.
19. **Sopjani,M.**, Foller,M. & Lang,F. (2008). **Gold stimulates Ca<sup>2+</sup> entry into and subsequent suicidal death of erythrocytes.** *Toxicology* **244**, 271-279.

## 10 Curriculum vitae



### Dr.rer.nat. **Mentor Sopjani**

E-mail: msopjani@yahoo.com  
 mensop@hotmail.com  
 mentor.sopjani@student.uni-tuebingen.de

Tel.: +377(0)44 604 944  
 +4917620496957

<b>Name</b>	<b>Mentor</b>
<b>Surname</b>	<b>SOPJANI</b>
<b>Birth date</b>	<b>08.08.1978</b>
<b>Country</b>	<b>KOSOVA</b>
<b>Birthplace</b>	<b>Harilaq, Fushë-Kosovë, KOSOVA</b>
<b>Languages</b>	<b>Albanian (native), English, Serbian, German (basics)</b>

### EDUCATION

- 2007-2010 **PhD Studies.** Faculty of Biology, University of Tübingen EBERHARD KARLS. Tübingen, Germany. Dissertation thesis subject: *“The AMP activated protein kinase in the regulation of sodium coupled transporters (SGLT1, EAAT3 & EAAT4) and eryptosis”*. (Magna cum laude).
- 2007 **Diplomarbeit** at the Institute of Physiology. Faculty of Biology, University of Tübingen, EBERHARD KARLS. Tübingen, Germany. Diploma thesis subject: *“Eryptosis induced by gold and by cadmium ions”*.
- 2005-2007 Post diploma-**Master studies**, branch: Physiology-Biochemistry, at the Biology Department; Faculty of Natural Sciences and Mathematics; University of Prishtina (average grade 9.94). Prishtinë, Kosova. Master thesis subject: *“Mechanisms of action of the lead acetate on the chicken ileum longitudinal smooth muscle and the NO role in those responses”*.
- 1997-2002 **University Studies**; Branch: Educational Biology, at the Biology Department; Faculty of Natural Sciences and Mathematics; University of Prishtina (average grade 9.33). Prishtinë, Kosova. Diploma thesis: *“Biometric characteristics of Fagus sylvatica leaves at different localities of the different regions of Kosova”*.
- 1993-1997 **High Medical School**, at high school “Dr. Ali Sokoli”; Prishtinë, Kosova.
- 1985-1993 **Elementary School** “Bajram Curri”, in Harilaq; Fushë-Kosovë, Kosova.

## **SCIENTIFIC EXPERIENCE**

Knowledge of	Physiology; Cell Biology; Molecular Biology; Genetics; Microbiology; Biochemistry.
Experienced on	Fluorescence Activated Cell Sorting (FACS) technique; Two Electrode Voltage Clamp (TEVC) technique; Fluorescence Microscopy; Luciferase measurement; cRNA generation; Animal operations, etc.
Familiar with	Western Blotting; polymerase chain reaction (PCR), Enzyme-Linked Immunosorbent Assay (ELISA); Immunofluorescence; Biotinylation; Immunohistochemistry; chemiluminescence.

## **WORKING EXPERIENCE**

03.03.2010-	Postdoctoral Researcher, Laboratory of Voltage Clamping and Molecular Biology, Institute of Physiology I, University of Tübingen, Tübingen, Germany.
2007-2010	Doctoral Researcher, Laboratory of Cell Biology and Lab. of Electrophysiology, Institute of Physiology I, University of Tübingen, Tübingen, Germany.
2004 -2010	Assistant for Biology and Human Genetics; Medicine Faculty; University of Prishtina (UP). Kosova.
2004-2006	Chief of the Sector for Forest Policy and Development; Department of Forestry; Ministry of Agriculture, Forestry and Rural Development; Kosova
2005	Engaged by the Ministry of Education Science and Technology for preparing the curriculums of the Biology course (for Agriculture High Schools). Kosova.
2004-2006	Member of different technical working groups for various documents preparation, as: <i>Strategy for Wildlife Management in Kosova</i> ; <i>Draft-Law for Hunting</i> ; <i>Draft-Law for Plant Health protection</i> , etc. Kosova.

## **AWARDS**

2002	By the Prishtina University awarded as “ <i>Student i Dalluar</i> “ (“ <i>Distinguished Student</i> “)
------	--

## **INTERNATIONAL WORKSHOPS AND STUDY VISITS**

2006	Participant in the international workshop:” <i>Agriculture and Environment in the Balkans and Turkey: Networking Regional Experience</i> ”. Gembloux, Belgium, 3-4 July, 2006.
2006	Study visits in the University Medical Center; University of Hamburg; Hamburg-Eppendorf, Germany; 13-18 November, 2006.

**SCIENTIFIC CONGRESS PARTICIPATIONS**

- 2009 Deutsche Physiologische Gesellschaft-Congress 2009. **M. Sopjani**, M. Föller, S. A. Fraser, F. Lang “*Stimulation of the Na-glucose cotransporter SGLT1 by AMP activated protein kinase*” (oral presentation). 22-25 March, 2009, Giessen. Germany.
- 2009 Deutsche Physiologische Gesellschaft-Congress 2009. M. Föller, **M. Sopjani**, S. Koka, S. Gu, H. Mahmud, K. Wang, E. Floride, E. Schleicher, E. Schulz, T. Münzel, F. Lang “*Regulation of erythrocyte survival by AMP-activated protein kinase*” (poster presentation). 22-25 March, 2009, Giessen. Germany.
- 2008 Deutsche Physiologische Gesellschaft-Congress 2008. “*Gold stimulates Ca<sup>2+</sup> entry into and subsequent suicidal death of erythrocytes*”, (poster presentation). 2-5 march, 2008, Köln. Germany.
- 2007 FASEB. Experimental biology annual meeting. 28.04-02.05.2007. Washington DC. **Sopjani, M.**, Ferizi, R., Jakupaj, M., Sopi, R., Bislimi, K., Halili, F. “*The role of extracellular Ca<sup>2+</sup> and NO on the ileum longitudinal smooth muscle (ILSM) in constrictive response to Pb-acetate*” (*The FASEB Journal*. 2007; 21:1b540) (poster presentation).

Tübingen

Date: 03.03.2010.